Scientific and Technical Information (STI) for Financial Assistance and Non-M&O/M&I

Final Technical Report

Reporting Period Start Date: 10/01/2004
Reporting Period End Date: 9/30/2011

Principal Authors: John LaGrandeur, Doug Crane

Submission Date: July 2, 2012

DOE Award Number: DE-FC26-04NT 42279

Submitting Organization:
BSST LLC (Amerigon Incorporated)
5462 Irwindale Avenue - Irwindale, CA 91706

Subcontractors/sub-recipients:
Ford Motor Company
2101 Village Rd – Dearborn, MI 48124
Faurecia
1050 Wilshire – Suite 200 – Troy, MI 48084
BMW AG
80788 Munich Germany

AMERIGON

5462 Irwindale Avenue
Irwindale, CA 91706

Disclaimer

Abstract

BSST (hereafter referred to as Amerigon) began work in November 2004 under a cost share contract [1] awarded by the U.S. Department of Energy Freedom Car Office to develop a high efficiency Thermoelectric Waste Energy Recovery System for passenger vehicle applications. The system increases fuel economy by partially replacing the electric power produced by the alternator with electric power produced by conversion of exhaust gas in a Thermoelectric Generator (TEG). Amerigon's team members included the BMW Group and Ford Motor Company, with both OEMs demonstrating the TEG system in their vehicles in the final program phase. Significant progress was made in modeling, building and testing the TEG system from the lowest subassembly levels through an entire vehicle system.

By the program's conclusion, the team had successfully overcome the challenges of integrating TE materials into an exhaust system component and evaluated the system behavior in bench and over the road testing for over six months.

1. Executive Summary

The conversion of heat to electric power using thermoelectric technology has been reliably used for niche applications including space vehicles and where low levels of power may be required off-grid. In the early years of the last decade, the existence of high performing, breakthrough thermoelectric (TE) materials was demonstrated, indicating that the technology may find broader utilization, including the possibility of helping solve the rising problem of greenhouse gas emissions and our accompanying dependence on fossil fuel.

In 2004 the DOE issued a solicitation [2] which included, amongst a broad portfolio of other fuel efficiency technologies, Topic Area 2 titled "Exhaust Energy Recovery". Amerigon and its partners including BMW and Ford were recipients of a program award. The motivations behind the program were several-fold. Internal Combustion Engines (ICE) are approximately 25% efficient, with $3/4^{th}$ of the fuel energy being rejected as heat via the exhaust system and powertrain coolant. When coupled with an 80% efficient alternator, it can be seen that for every watt of electric power used in the vehicle 5 watts of fuel energy is required. The combination of these factors, i.e. dramatic improvements in the performance of TE materials for power generation, low utilization level of exhaust waste heat, conversion efficiency of fuel energy to electric power coupled with the increasing electrification of vehicles indicated the potential for success of vehicular TE heat to power.

Significant technical and economic challenges confront the transfer of TE heat to power technology from the niche markets described to the high volume automotive market. These challenges include:

1. Design and construction of TE devices that operate between temperatures on the order of 600^0C and 100^0C across distances on the order of 3 mm;
2. Integration of the TE devices into an exhaust system, packaging for robustness and mitigation of exhaust gas back pressure, which opposes heat transfer effectiveness and can decrease fuel economy.
3. Developing and validating computer performance models from the TE device through a complete automotive system;
4. Establishing a path to commercialization recognizing the challenging cost-benefit required for the automotive market.

Amerigon introduced a nontraditional TE engine architecture prior to the program, in which the TE elements and substrates are arranged in a stack as opposed to the traditional planar configuration. As described in the body of this report, this architecture provides an effective means for addressing the high temperature differential across the closely spaced hot and cold heat source/sink, as well as reducing the amount of TE material required for a given power output. The Amerigon "stack design" TE engine was a fundamental building block utilized throughout the program.

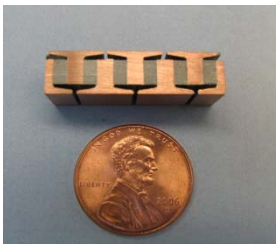

The development and refinement of a computer performance model in Matlab/Simulink guided the design of the TEG. The model integrates gas and liquid heat exchangers and their working fluid properties, thermoelectric elements, substrates and interfaces to provide performance prediction predict (i.e. the amount of electric power produced) as a function of working fluid mass flow, temperature and allowable pressure drop. The model was initially created and validated for steady state performance, and later was improved to transient performance, an important capability in that the first few minutes after key-on play a large part in contributing to fuel economy and emissions performance. The TEG model was stitched into more comprehensive vehicle bumper to bumper models, so that BMW

and Ford could predict FE performance as a function of different driving conditions and regulatory cycles.

The first full scale TEG prototype, based on a secondary heat transfer loop, was built and tested in Phase 2 and produced over 500 watts of electric power. This TEG was comprised of BiTe stacks, and was a proof of concept for a flat TEG architecture. Subsequently the secondary loop TEG system architecture was simplified to a direct flow-through design. Coincident with this change, higher temperature TE materials were designed into the TEG to enable higher temperature operation.

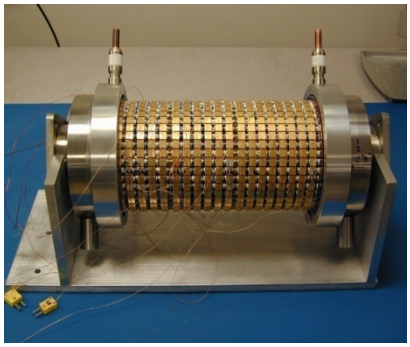

Initial testing of the flat, high temperature TEG indicated that the design would be difficult to manufacture, as extraordinary care had to be taken to effectively maintain heat transfer while managing thermal stress across the TE engines. A modification of the TEG architecture was made in Phase 4, retaining the stack design but arranging the TE engines around the circumference of a steel tube, approximately 4 inches in diameter and 15 inches in length. The cylindrical TEG with stack TE engines proved successful in bench tests and over 1 year of vehicle and dynamometer testing, and continues to operate today. In the final phase, Faurecia designed and integrated a proportional valve at the exhaust end of the TEG, which enabled bypass of exhaust gas in high load conditions through the coaxial bypass tube. The TEG produced over 700 watts of power in bench testing, and over 600 watts of power in over the road testing.

To summarize the program achievements;

- A TEG was built and tested that operates with a hot side temperature at the TE material interface in the range of exhaust gas temperatures, an important proof of concept previously not established. The TEG was operated over the road and in bench testing at Amerigon for over 12 months and continues to operate in extended rig and vehicle testing.
- Modeling tools have been developed and validated that are in use by vehicle designers to optimize system architectures for fuel economy benefit and trade studies. The tools have been invaluable in guiding the efforts of TEG design as well as vehicle systems.
- Fuel economy improvement in the initial prototype TEG/vehicle systems reached 1%-2% in over the road testing. Additional improvement is possible with further optimization of TEG and vehicle systems architectures.

A follow on program has begun, in which Amerigon and its partners BMW and Ford are preparing vehicular TEG systems for manufacturing readiness. Implementation of TEG systems into light-duty vehicles in the next decade is dependent on significant progress being made on the key technical and commercial attributes identified in this program.

Contents

2. Project accomplishments Vs stated goals and objectives

A summary of accomplishments versus the stated goals and objectives is provided below. The framework of objectives is taken from the program Statement of Project Objectives "Revised SOPO BP3 5[1], which is the final issue of the SOPO incorporating program objectives.

Phase I – Applied Research

The primary objectives in the Phase 1 program included developing an R&D path for success with requirements for technical and economic viability outlined. These objectives included developing system requirements and system concepts for the BMW engine, thermoelectric device subsystem modeling and analysis, TE material and parasitic loss reduction.

In the initial phase, the 2010 timeframe was used to establish requirements in preparation for technical and commercial readiness upon completion of the final phase of the program. Consequently, the system design accounted for anticipated improvements in engines, electronics and the results of increased vehicle electrification. This led to the selection of BMW's newest and most efficient engine, a 6-cylinder in line gasoline engine that is representative of the industry's state of the art in the period 2010 - 2015.

System architecture was optimized to maximize waste heat conversion efficiency throughout wide fluctuations in exhaust gas mass flow characteristic of city and highway drive cycles. Electrical power output was managed to balance the system power output against vehicle electrical demands. The Phase 1 system included a Primary Heat Exchanger (PHx) to transfer exhaust gas waste energy to the Thermoelectric Generator (TEG) via a closed liquid loop. It was thought that higher efficiency could be realized compared to direct attachment of Thermoelectric (TE) elements to the exhaust component through:

a. Improved thermal impedance match with exhaust gas
b. Direct control of heat flux which facilitates electrical load matching
c. Thermodynamic cycle optimization
d. The transfer of heat through a closed liquid loop to this TEG promotes a compact design and construction and facilitates hermetic enclosure and therefore easier recycling of the TEG materials.

TE material with ZT values ranging from 0.85 – 1.25 was used for modeling to reflect current and near-term available material systems.

Subsystems were individually modeled then integrated into the system simulation model by Amerigon using NREL's developed code: ADVISOR. The system architecture featuring a secondary loop is shown below:

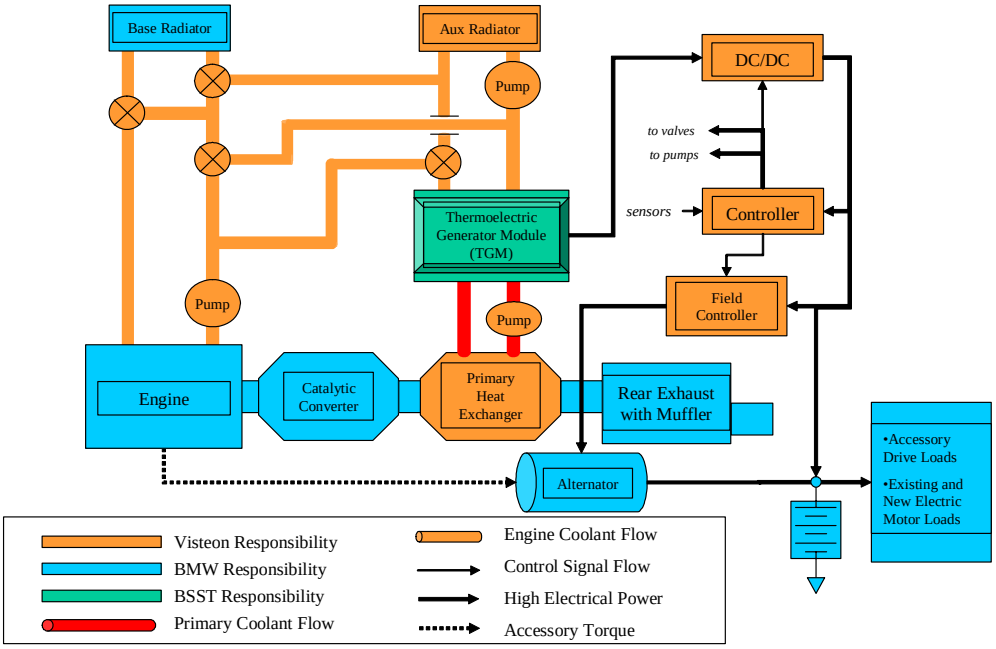

Figure 1: Block diagram showing TEG system integrated into the vehicle.

An initial FE performance prediction based on parametric variations in TE material effectiveness and other elements was made.

ADVISOR is a MATLAB-based numeric modeling tool developed by the U.S. DOE National Renewable Energy Resources Laboratory and subsequently commercialized by AVL. The model provides a basic framework for evaluating a wide range of vehicle performance parameters over fixed and user-programmable driving conditions and includes a library of generic functions as well as user definable features. ADVISOR has been extensively validated by independent assessors.

BMW platform/engine data and waste heat recovery subsystems (PHx, TEG and Power Control Electronics) were integrated into the basic ADVISOR model. The performance of the baseline ADVISOR model with BMW engine/platform characteristics demonstrated a 2% agreement to BMW tested fuel economy performance over FTP-75 and a 5% agreement to exhaust gas temperatures. PHx, TEG and Power Control subsystem models are based on existing validated models developed and used in many production programs by the contributing participants.

Key system factors were evaluated within ADVISOR to understand and configure system trade-offs in achieving 10% fuel economy improvement and to provide a basis for cost optimization in subsequent phases. They included:

- Average Alternator Load, Watts. The average alternator load was evaluated over a range from the baseline model (500 watts) to 2500 watts.
- PHx Number of Shells. The number of shells in the PHx shell and tube heat exchanger were varied between one and ten to evaluate pressure drop and heat exchanger effectiveness.
- Thermoelectric Material Effectiveness (ZT). ZT was varied between 0.85 and 1.25. Values of 0.85, 1.0 and 1.25 were used in the results section as they are values which the Team believes are current or near term within the scope of this program.
- Cold and Hot Side Coolant Temperatures. Cold side temperatures were varied from 30 to 110 degrees C. Hot side temperatures varied from 1050 to 650 degrees C (before and after the catalytic converter, respectively) Hot side temperature data was directly taken from BMW engine test data for the drive cycles used in ADVISOR.
- Power Converter Efficiency. TEG output power conversion efficiency ranged from 72% to 95% and was based on a two-stage converter (DC/DC conversion and load matching stages).

Results

Over-all results for phase 1 (fuel and emissions reduction percentages) are reported in the table below. These results were developed based on vehicle architecture assumptions made soley by Amerigon and are not based on analysis provided by BMW.

Representative city and highway drive cycles (FTP-75 and HWFET) were used to evaluate system performance. As shown in the Table, the system provides a range of fuel consumption reduction ranging from 8 to 12½ percent and decreases emissions accordingly.

	Present (2005) System Capability			Projected for Dyno Test, 2008			Target for Dyno Test, 2008		
Drive cycle	FTP-75	HWFET	combined (1)	FTP-75	HWFET	combined (1)	FTP-75	HWFET	combined (1)
Average alternator load (W)	1000	1000	1000	2000 (2)	2000 (2)	2000 (2)	2000 (2)	2000 (2)	2000 (2)
Average ZT	0.85	0.85	0.85	1.00	1.00	1.00	1.25	1.25	1.25
% improvement - mpg	8.36	8.25	8.28	9.60	10.50	10.03	11.64	12.61	12.10
% change - HC (3)	-1.67	0.19	-1.03	-2.19	0.58	-1.26	-2.77	0.58	-1.65
% change - CO (3)	-1.86	-1.75	-1.82	-2.07	-2.65	-2.27	-2.53	-3.16	-2.75
% change - NOx (3)	-2.99	-1.50	-2.53	-3.77	-1.48	-3.09	-4.25	-2.22	-3.64

(1) Combined drive cycle weighted 60% FTP-75 and 40% HWFET
(2) Increase in average alternator load is due to the estimated increase in electrification of vehicles by the year 2012
(3) Emissions results do NOT included significant reduction in emissions due to faster coolant warm-up

Figure 2: System Performance Results

The performance predictions were made to analyze what conditions would be required in order to achieve a 10% FE gain. As the program progressed, these parameters and the overall system architecture would be re-evaluated and redefined to provide better alignment with the automotive market's technical and economic factors.

Phase II – Exploratory Development

Based on the design requirements developed in the first phase, the Primary heat Exchanger (PHx), secondary loop pump, a fractional 20-watt Thermoelectric Generator (TEG) and Power Control System (PCS) were designed, built and tested. The results of the tests were successful in that the equipment met their designated requirements.

The system model responsibility was transferred to BMW who used GT Cool as a modeling platform. The baseline characterization of the vehicle and engine was more accurately represented in the new model platform, as BMW had previously established a number of the subsystems in GT Cool. This led to an improvement in system modeling in Phase 2 that was carried forward in subsequent phases. The fuel efficiency improvement predicted by the model ranged from -0.5% to 8.5% based on the driving condition evaluated. As in Phase 1, the average thermoelectric material effectiveness, or ZT, was held within the range of 0.85 to 1.25. A number of assumptions were modified from the Phase 1 model in Phase 2 to reflect characteristics and restraints posed by vehicle installation requirements judged as practical for a TEG system to be installed in an existing vehicle configuration by BMW.

Specific recommendations to further improve system and subsystem equipment recommendations included:

1. The use of existing thermoelectric materials shows compliance with the overall program objectives. The contact metallization must be improved however to fully realize the benefit of high density packaging with the objective of lowering the material cost (reducing the amount of material required).
2. The continued development of subsystem equipment to fully optimize performance at subsystem and system levels is a high priority and a necessary step to rapid commercialization. Specific areas for improvement include:
    a. A reduction in size, weight and power consumption of the secondary loop pump;
    b. Further consolidation of the PCS converters and load matching electronics to reduce size and weight.
    c. Early in Phase 3 the development of hot-side heat exchangers and their integration within the TEG to effectively transfer thermal power must be addressed.

Phase 2 objectives were met through completion of design, build and test of the following key subsystem equipment that demonstrated compliance to design requirements:

- Primary Heat Exchanger and Pump
- Fractional Thermoelectric Generator
- Power Control System

Phase 2 key accomplishments are listed below:

1. A full scale BiTe TEG was built and tested that produced over 500 watts of electric power.
2. A fractional high temperature TEG was built using PbTe/TAGS that produced 20 watts electric power.
3. A fractional high temperature TEG was built using PbTe/TAGS/BiTe that demonstrated net 10% conversion efficiency.

An objective, added during Phase 2, updating the system model, was completed with performance predictions revised to reflect subsystem test results. Best fuel efficiency improvement is achieved in higher speed driving where thermal power and electrical load demands are highest.

Phase III - Advanced Development

Phase 3 objectives were targeted at simplifying the system architecture to reduce system complexity and cost. TEGs were built and tested using BiTe and high temperature PbTe/TAGS materials. A key Phase 3 result was the modification of the system architecture to eliminate the secondary loop in favor of a direct heat transfer of thermal power from the exhaust gas to the TEG hot side heat exchanger as shown below:

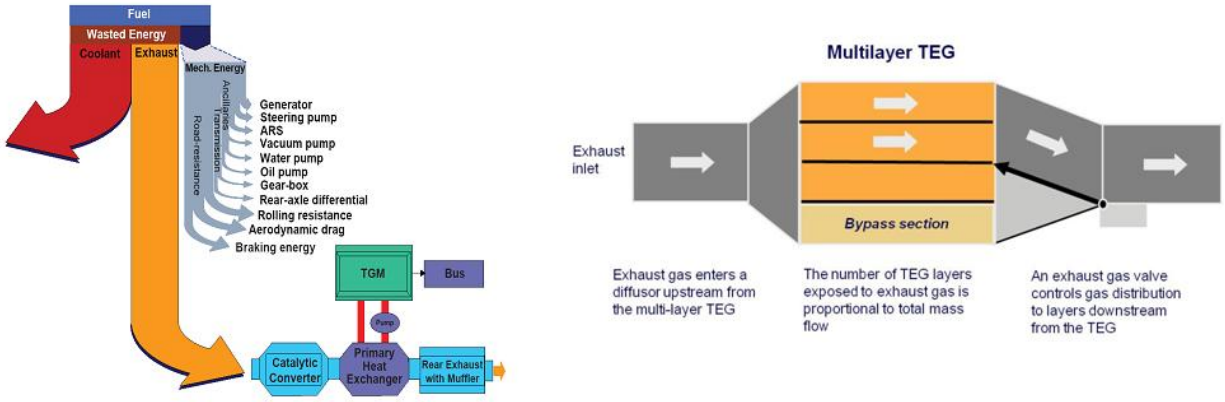

Figure 3. Energy flow and TEG system diagram and multi-layer TEG device

Phase 3 key accomplishments are listed below::

1. The system model was updated to predict transient performance and was used to evaluate system performance over a variety of driving conditions including engine start up.
2. A simplified architecture was modeled and preliminary results generated.

While the Amerigon team achieved a number of successful outcomes in developing, building and testing TEG components and systems, concerns arose over the anticipated difficulty in manufacturing a planar TEG in high volume. Using the patented stack engine design showed favorable results, however the manufacturing tolerances required to achieve effective heat transfer over large, flat surfaces proved difficult in the prototype build and a clear path to manufacturing implementation was not apparent. For these reasons the team began to focus on solutions to manufacturability at the close of phase 3 and the start of phase 4.

In Phase 3 Ford Motor Company joined the Program and began to actively model and analyze TEG technology for future vehicle potential applications. Their role would grow over the next two phases culminating in Ford vehicle tests using Phase 5 TEG technology.

Phase IV – Engineering Development

The primary objective for Phase 4 was to install and evaluate a TEG in conjunction with a BMW engine. This did not occur in Phase 4, as the team needed to address the fundamental issues relating to the manufacturability of a flat TEG.

In Phase 4, Amerigon modeled, designed, built and tested a new, cylindrical TEG with internal, coaxial bypass. The cylindrical TEG arranged TE engines between copper rings fixed to the outer circumference of a stainless steel gas tubular heat exchanger. This design also conserved system volume, as the bypass of exhaust gas was accomplished internally through a closed tube inside the gas heat exchanger.

At the conclusion of Phase 4, the cylindrical design concept had been proven in the form of a full scale, high temperature compliant TEG, although it was not ready for dynamometer testing due to the need to improve prototype assembly tools and subcomponent parts.

Phase V – Vehicle Installation and Performance Evaluation

The Phase 5 SOPO key objectives included integration and test of full scale, high temperature compliant TEGs in Ford and BMW vehicles. This objective was achieved, and the TEGs, which operated with TE material interface surface temperatures on the order of 500C, produced over 700 watts electric power in bench testing at Amerigon and over 600 watts in road testing. The two TEGs, put into service in July 2011, continue to operate with essentially unchanged performance at the time of this report, June 2012.

Additionally, the TEG was tested with a BMW engine on an engine dynamometer at NREL in Golden Colorado. These results are discussed in detail in following sections of this report.

This accomplishment demonstrates the technical capability of using thermoelectric engines to convert waste heat to electric power in passenger vehicles. While the technology has met the expectations of the team, fuel efficiency improvement on the order of 1% to 2% was calculated using the TEG performance and vehicle computer models as well as from measured vehicle data. It is anticipated that with optimization of the vehicle architecture and tighter integration of the TEG subsystem higher levels of fuel economy improvement will be achieved. These areas are the focus of the follow-on program awarded to Amerigon which began in October, 2011.

3. Project activities summary

a. Amerigon TEG development

Introduction

The following report summarizes Amerigon TEG activities under DOE award # DE-FC26-04NT42279, a project that began in Oct. 2004. The history of the program, Phases 1 – 4, will be summarized followed by a more extensive discussion of the activities in Phase 5. Modeling of the TEG led design and development activities and was used to extensively optimize TEG performance. A discussion of computer modeling follows the description of hardware design and development.

Program History – Phase 1 – 4

In Phase 1 of the program, the boundaries of the problem were defined along with the system architecture. The team analyzed system tradeoffs including whether the TEG should be installed in the coolant or exhaust system. The coolant system, despite having large amounts of waste heat, is not a good choice for thermoelectric waste heat recovery at this time due to the lower temperatures available. The team also looked at the tradeoffs in the location of the TEG in the exhaust line as well as whether an auxiliary or main radiator should be used for the waste side of the generator.

An initial system architecture was developed that is shown in Figure 1. This system has the TEG in a secondary loop. Heat is extracted from the exhaust with a primary heat exchanger (PHx) and dissipated into a secondary loop. This secondary loop requires a suitable heat transfer fluid. It also necessitates a dedicated pump. The system included both a base radiator and an auxiliary radiator. The auxiliary radiator would provide lower cold side or waste temperatures once the engine was warm while the base radiator would be used during warm-up so that the TEG waste heat could be used to heat the engine up faster. This faster warm-up would help to reduce emissions and improve fuel economy.

Methods for handling the power output of the TEG were also considered. This included peak power tracking (PPT) technology along with boost/buck conversion in a DC/DC converter**.**

In Phase 1, an initial model was created for the TEG along with a model for the PHx. These models were then utilized in a system model to provide an estimate for fuel economy improvement over a drive cycle. The software platform used for this system-level model was ADVISOR, a MATLAB based tool originally developed at NREL.

In Phase 2, the responsibility for the system-level modeling transitioned from Visteon, the original Tier 1 partner of the program to BMW who transitioned the system model to Gamma Technologies “GT Cool” from ADVISOR that was used in Phase 1. GT Cool is used by the powertrain development department at BMW, and a thermal vehicle model was present that was modified to the special needs of the TEG project. The motivation for changing modeling platforms in Phase 2 was to take advantage of the knowledge and expertise held by BMW in modeling powertrains using their simulation tools.

Prototype build and test

In Phase 2, a small-scale generator was designed. The goal for this fractional generator was to produce at least 20W of power at high temperatures (> 400C) and in a relatively compact size. The TE materials used in the 20W device were TAGS for the p-type material and PbTe for the n-type material. Figure 4 shows the final assembled 20W generator.

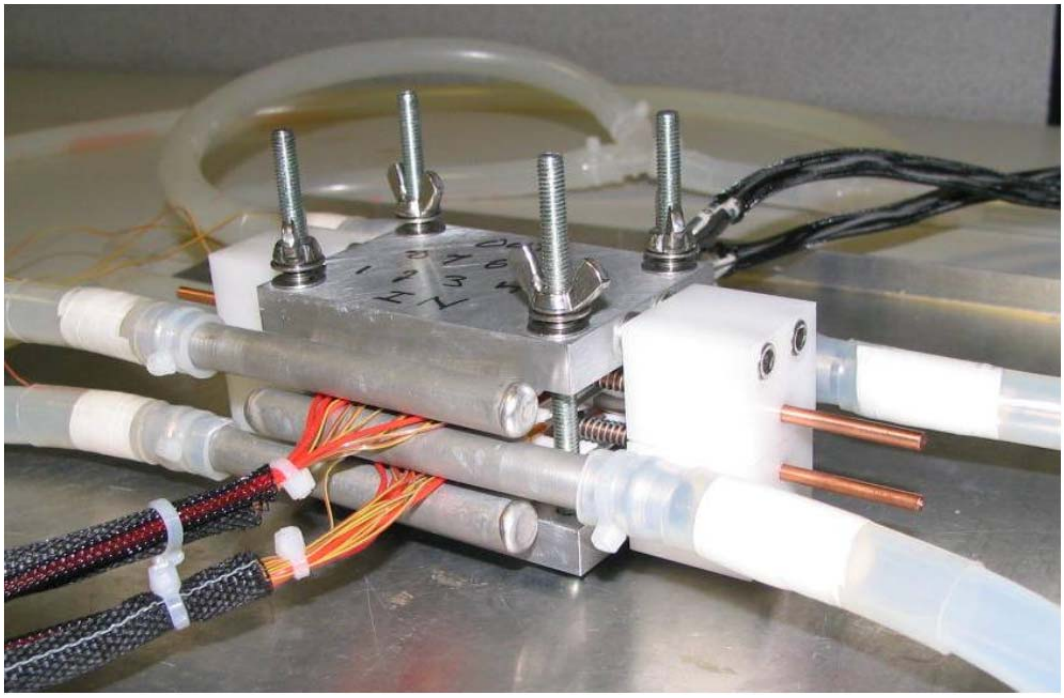

Figure 4: Final assembled 20W device, plumbed and ready for test.

Figure 5 shows the results of the testing for the 20W generator. The device was tested at heater temperature settings ranging from 150C to 475C with a cold bath temperature setting of 20C. In both sets of tests, the device generated over 21W for this condition. The demonstrated repeatability of these tests gave the team confidence that the device performance could be duplicated.

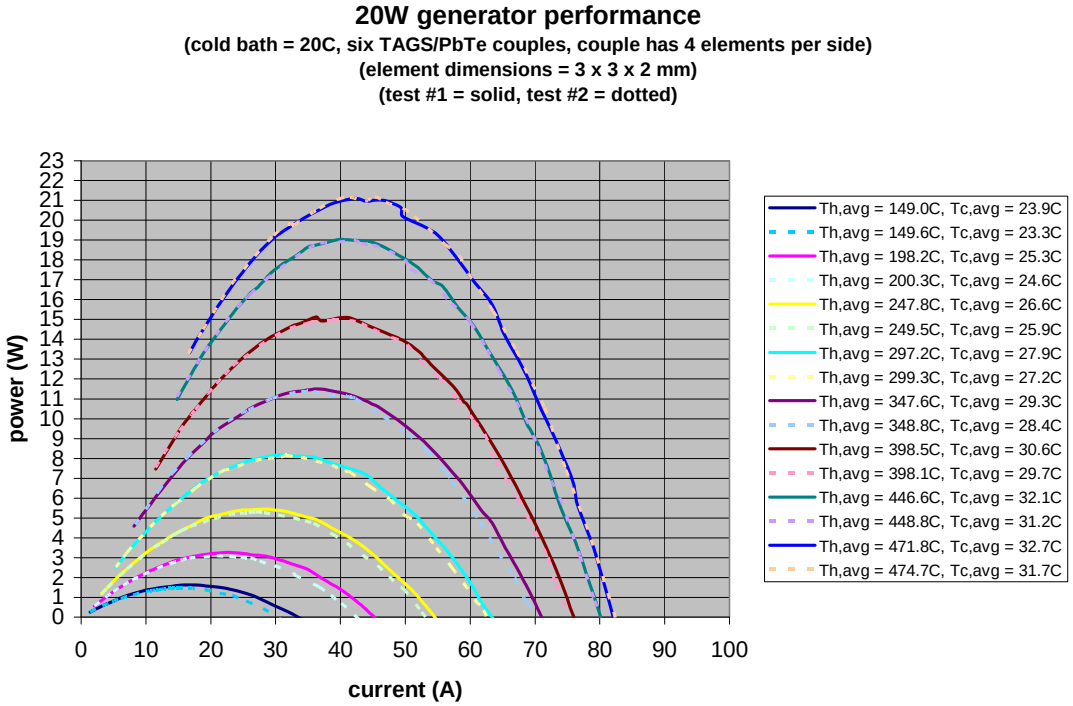

Figure 5: Test results for the 20W generator.

The next goal was to scale the 20W generator into a full-scale generator. With limited availability of effective high temperature materials in the size and shapes desired in time to complete Phase 2, the team set out to build and test a full-scale generator using lower temperature, more readily available, Bi_2Te_3 materials. This design uses "Y"-shaped TE connectors. The differences between the traditional configuration and the high power density configuration which uses the "Y" or "T" shaped shunts can be seen in Figure 6. The "T" shunt design has a shorter electrical path between p- and n- legs and provides more design flexibility in matching the thermal and electrical impedance between p- and n- elements. The "T" design also allows p- and n- elements of differing thermal expansion coefficients to be used without more complex accommodations such as springs. It allows the thermal and electrical paths to run perpendicular to each other potentially allowing the compressive force to be different and more appropriate for each. These aspects allow for potentially lower stress on the parts, allowing thinner TE elements to be used, reducing the amount of overall TE material. The negative of the "T" design is potentially in its assembly and that the thermal path from the heat source/sink to TE element is potentially longer, increasing the thermal resistance.

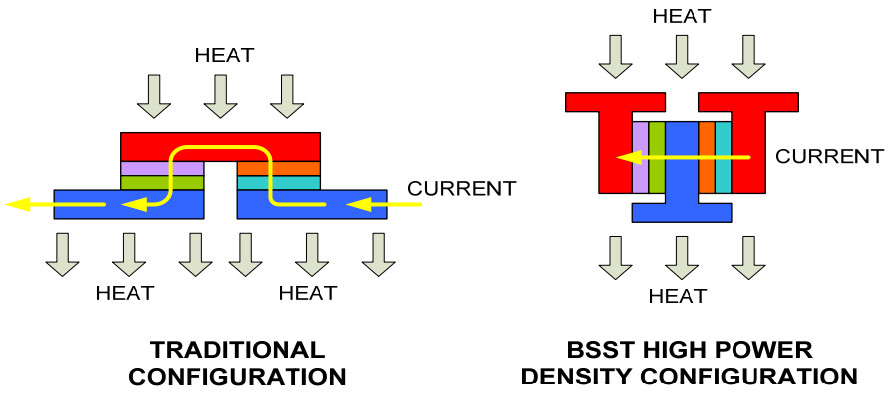

Figure 6: Alternative TE couple configurations.

An example of a "Y" shunt part is shown in Figure 7. Figure 8 shows the completed low temperature (BiTe) generator made of "Y" shaped shunt TE engines. This TEG was a liquid/liquid generator, using hot oil for the high temperature heat transfer and water or water/glycol as the low temperature heat transfer medium. The TE engines were sandwiched between the flat heat exchanger plates.

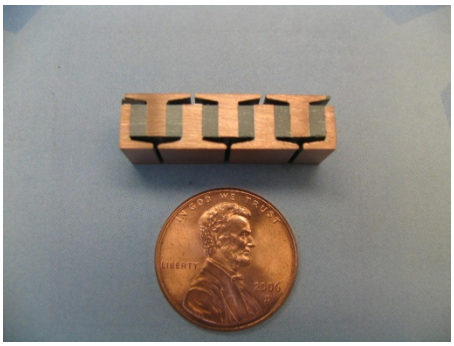

Figure 7: TE engine using "Y" shunt design configuration.

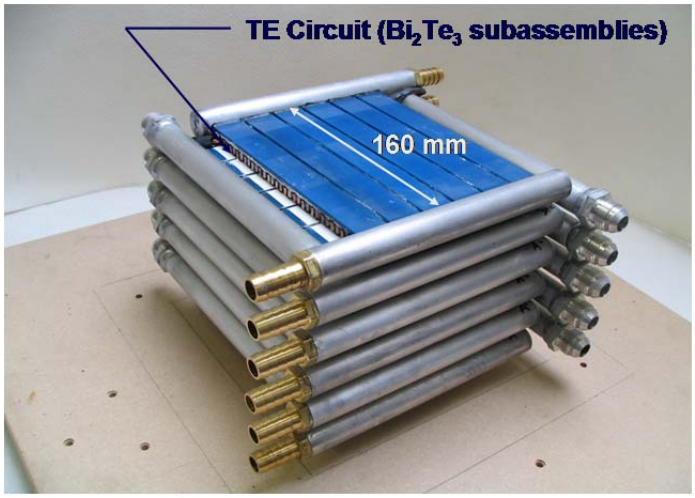

Figure 8: Liquid/liquid Bi2Te3 TEG using "Y" shunt design TE engines

Test results for this generator are shown in Figure 9. Over 500W was generated at a temperature difference of ~200C. Figure 10 shows the PHx prototypes as built by Visteon.

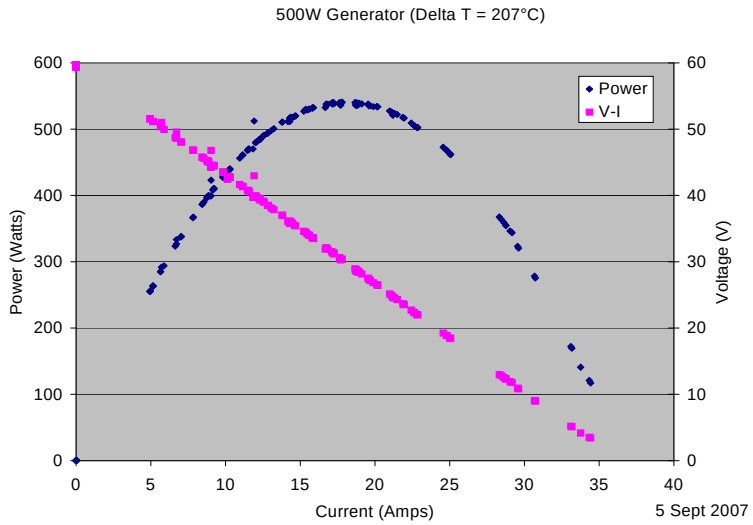

Figure 9: Test results for the Bi2Te3 TEG.

(a) Prior to tube section insertion in to shell

(b) Complete assemblies

Figure 10: Phase 2 PHX prototype

Within Phase 2 and throughout the remainder of the program, the team began testing the TE engines long term robustness. Figure 11 is an example of one of these cycling tests. A TE engine similar to the one shown in Figure 7 had its hot side cycled between 50C – 190C while the water bath temperature was maintained at 20C. The electrical load on the device during this cycling remained constant. The figure shows how the peak power output of the engine varied over these temperature cycles. There was less than 5% variation in power output for over 1000 cycles for this engine. Other higher temperature engines were also tested. These engines were tested up to 500C will little to no degradation shown for over 100 cycles.

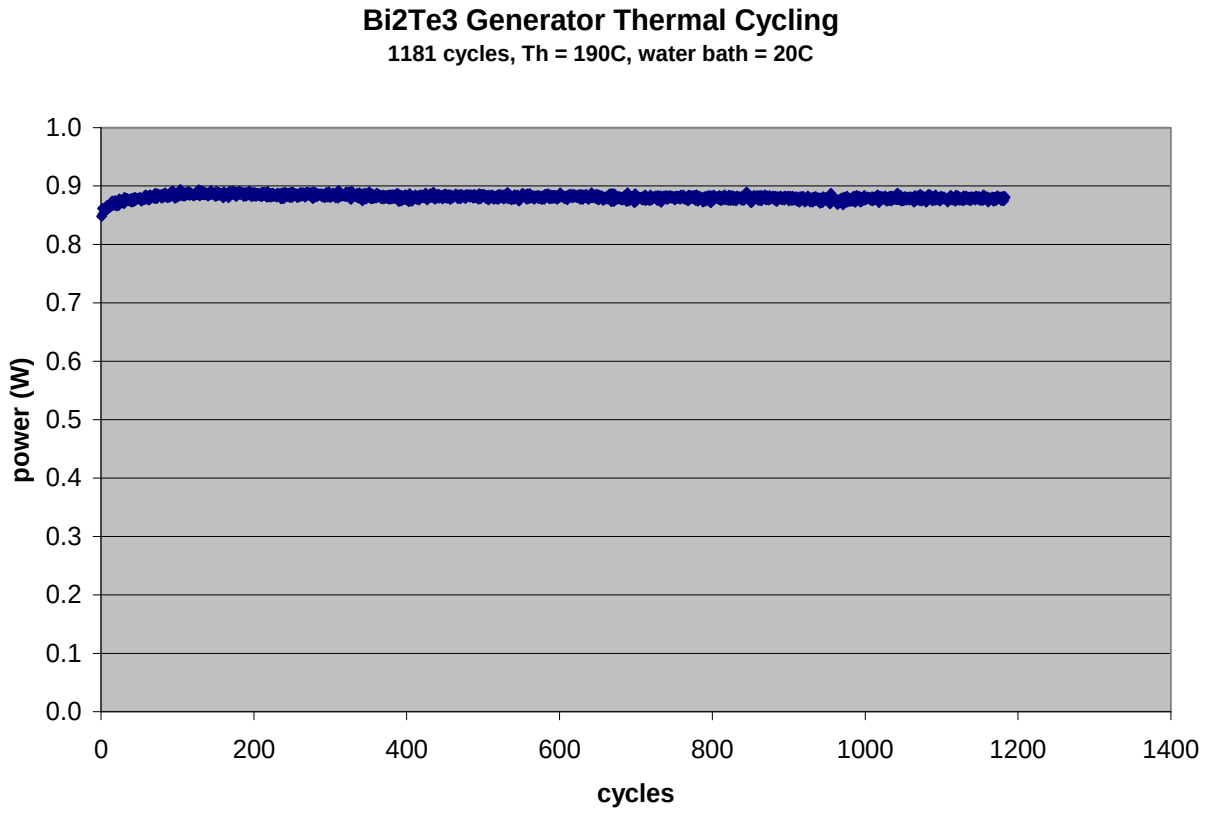

Figure 11: Thermal cycling test results for a Bi2Te3 TE engine.

In Phase 3 of the program, the focus moved to building a generator with TE elements that could withstand temperatures up to 500C and gas temperatures potentially over 600C. For such configurations, the exhaust gas temperature drop through the TEG often exceeds 300C. Thus, the temperature differences in the TEG can be greater than 400C near the inlet of the TEG and due to the thermal power extracted from the gas closer to 100C near the outlet. The heat flux through the TE elements from the hot to cold side of the TEG can also vary greatly from the inlet to the outlet of the TEG. To ideally compensate for these differences, the TEG was made of TE elements of varying shapes and materials along the length of the TEG in the direction of gas flow. Instead of varying each successive row of TE elements in the direction of flow, the team decided on a compromise of three different banks of TE elements. This can be seen in Figure 12.

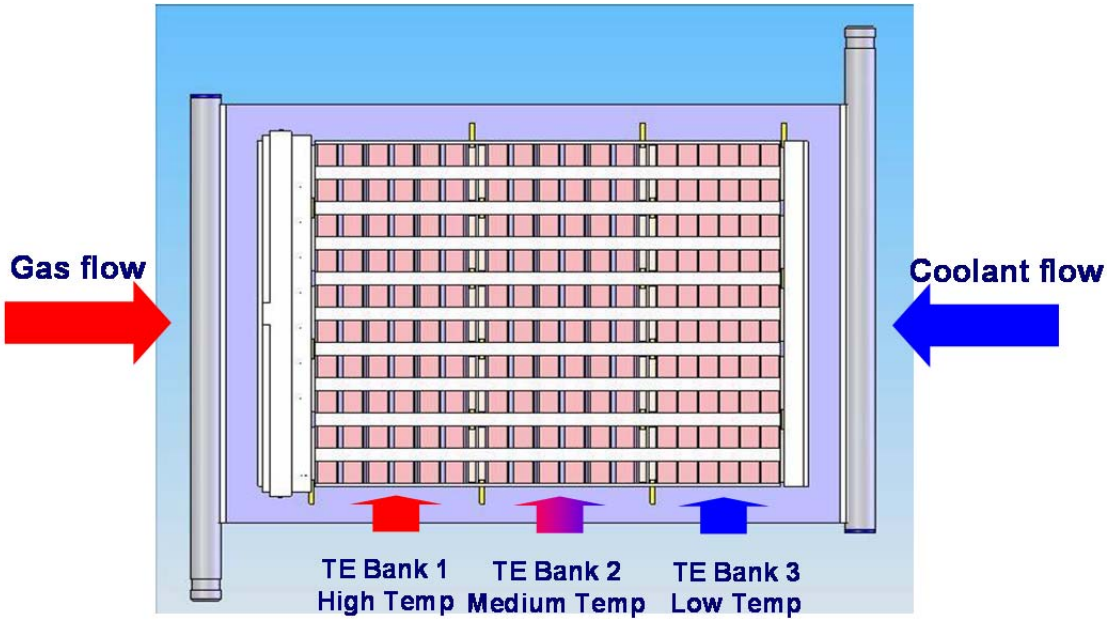

Figure 12: TE engine layout showing different banks of TE engines tailored for different heat flux and temperature regions.

The high and medium temperature banks were made of segmented TE elements (half Heulser for the hot end and Bi2Te3 for the cold end). The high temperature bank had thicker TE elements than the medium temperature bank. The low temperature bank was made of Bi2Te3 only TE elements. Also, these TE elements were thinner than the TE elements in the medium temperature bank.

The device was designed to make over 100W for a single plate. The device is shown in Figure 13. The hot side gas heat exchanger is shown on the right with the TE elements on the cold side heat exchanger shown on the left. Again, the flat plate heat exchangers sandwiched the TE engines.

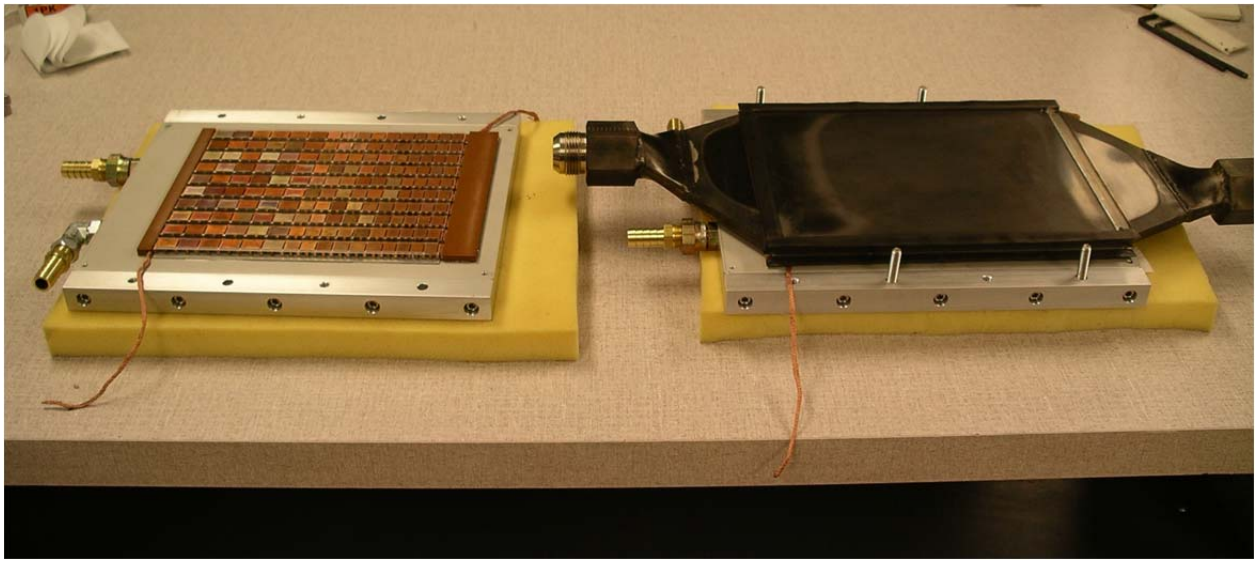

Figure 13: Higher temperature gas/liquid TEG made of segmented TE elements.

Figure 14 shows the test results for this device, which achieved 125W at an air inlet temperature of 600C and a water inlet temperature of 25C.

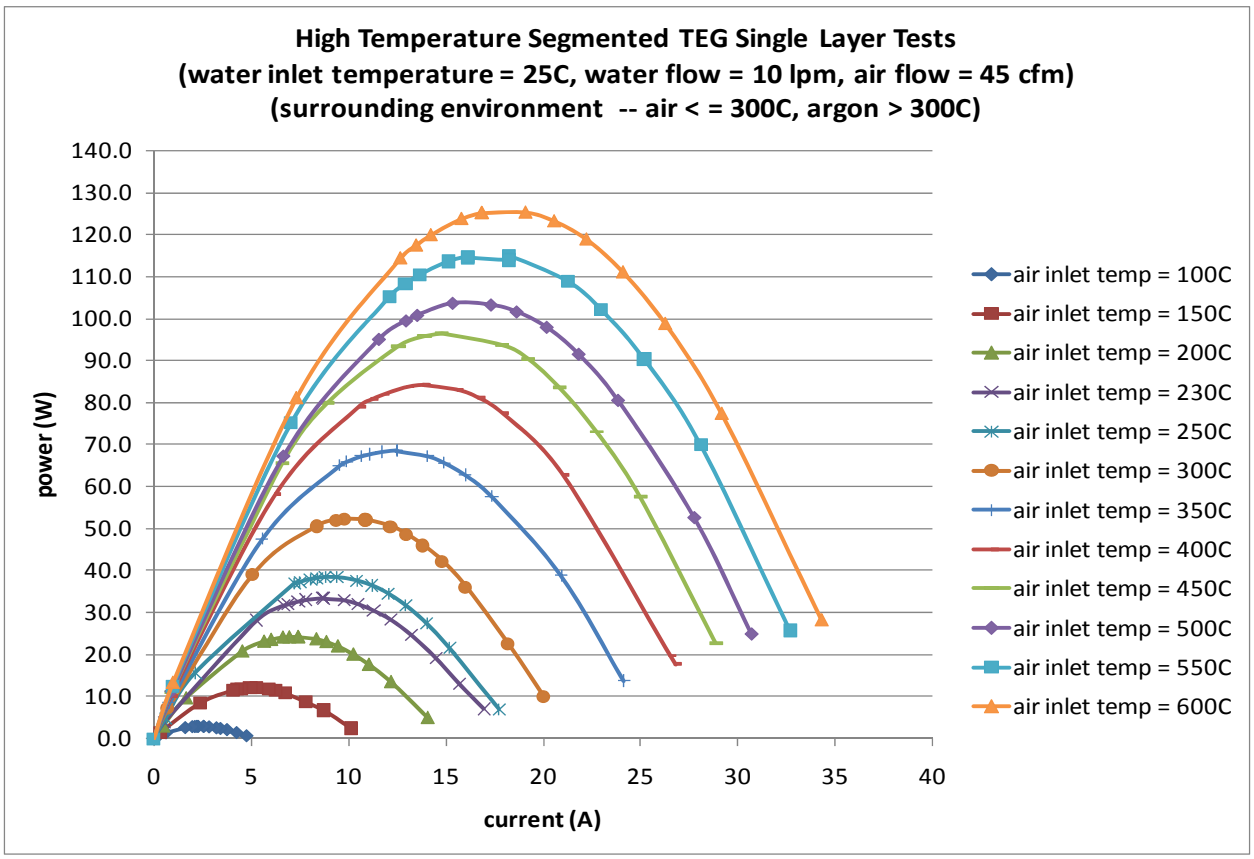

Figure 14: Test results for higher temperature gas/liquid TEG.

In addition to the work done on the TEG itself, team members Visteon and Virgina Tech created power conditioning systems for the TEG power output. These systems provided boost/buck capabilities at greater than 95% efficiency. The Visteon converter is shown in Figure 15 along with a set of headlamps that allowed the converter to vary the electrical load on the TEG.

Figure 15: Power converter.

In the course of Phase 3, the team decided that the secondary loop system architecture was too complex to be initially cost effective. The intermediate loop was eliminated from the system, effectively eliminating the PHx and the additional pump as well. The TEG would be incorporated directly into the exhaust gas stream. An update of this system architecture can be seen in Figure 16.

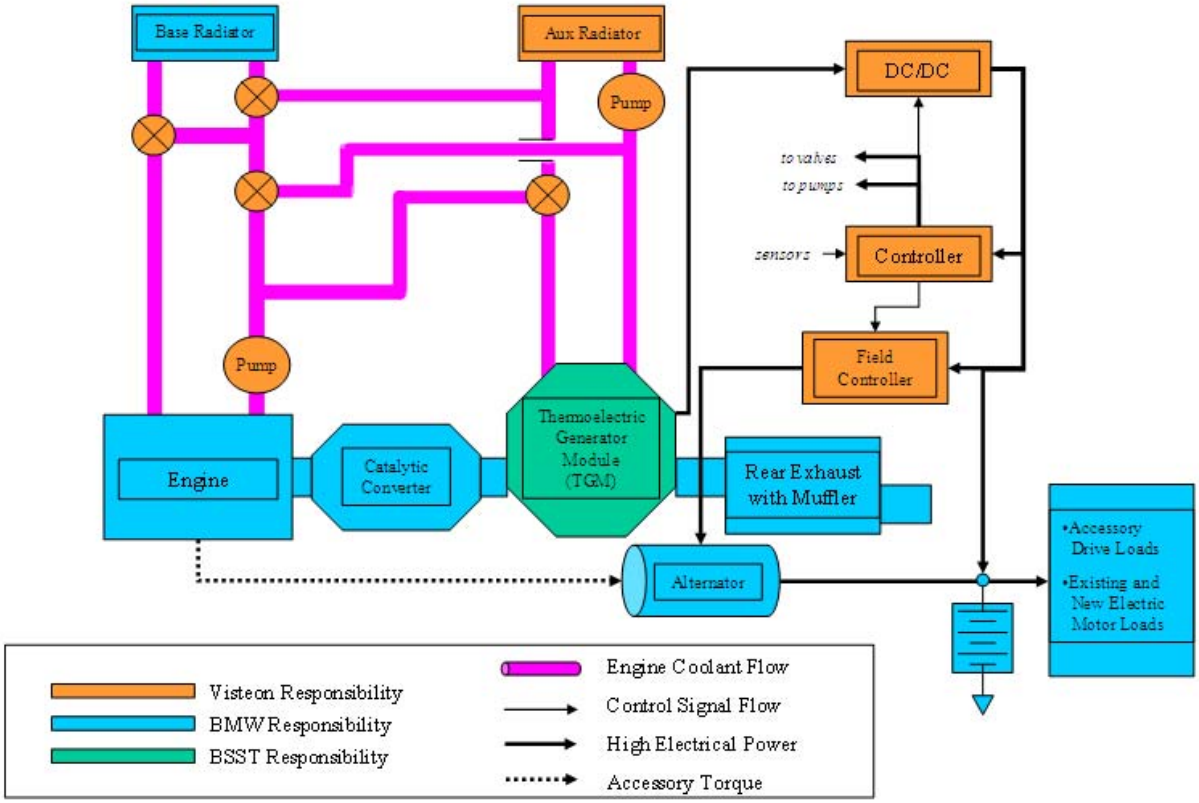

Figure 16: Modified TEG system architecture.

Phase 3 had successes, including making over 100W with a high temperature TEG made of segmented TE elements, but it also had difficulties. In the flat plate TEG design used in Phase 2 and 3, it was difficult to keep the TE engines in good thermal contact to the hot and cold heat exchangers over large surface areas. Testing showed that some of the TE engines were in good thermal contact while others were not. It was difficult to put enough pressure over the entire surface area of the TEG to maintain good thermal contact without crushing the TE engines in certain places. To try to aid in this process, the team had each TE engine plus the hot and cold heat exchanger surfaces lapped. This was a costly process that also often damaged the TE engines. How could we eliminate the excessive pressures and the costly extra machining processes and still maintain excellent thermal contact? How could we take advantage of the thermal expansion inherent in the system?

In Phase 4, the team embarked on a radical change to the TEG design. The design went from a flat plate to cylindrical design. The new cylindrical design could take advantage of the inherent thermal expansion in the device and allow the hot heat exchanger to expand into the hot shunts, eliminating any need for any additional pressure being applied to the device. The cold shunt design changed as well where the cold heat exchanger tubes were placed inside cold shunt sleeves. Again, no additional pressure was needed for thermal contact. A bypass was needed for the system to allow for excessive flows and temperatures to bypass the TEG to avoid excessive backpressure for the engine and prevent overheating of the temperature sensitive TEG components. In the new cylindrical design, the bypass was placed

inside the TEG, conserving precious system volume and allowing some additional power to be generated during bypass situations. The first cylindrical TEG is shown in Figure 17 with the test results for the device shown in Figure 18. Over 200W of power output were achieved with this device made of similar banks of TE elements used in Phase 3.

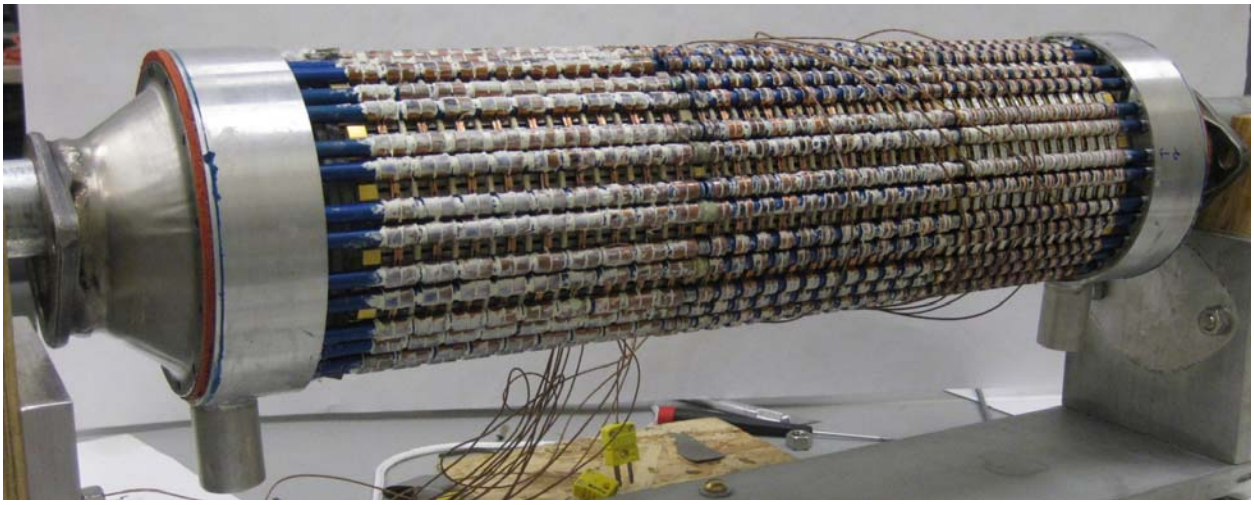

Figure 17: Gas/liquid cylindrical TEG made of segmented TE elements.

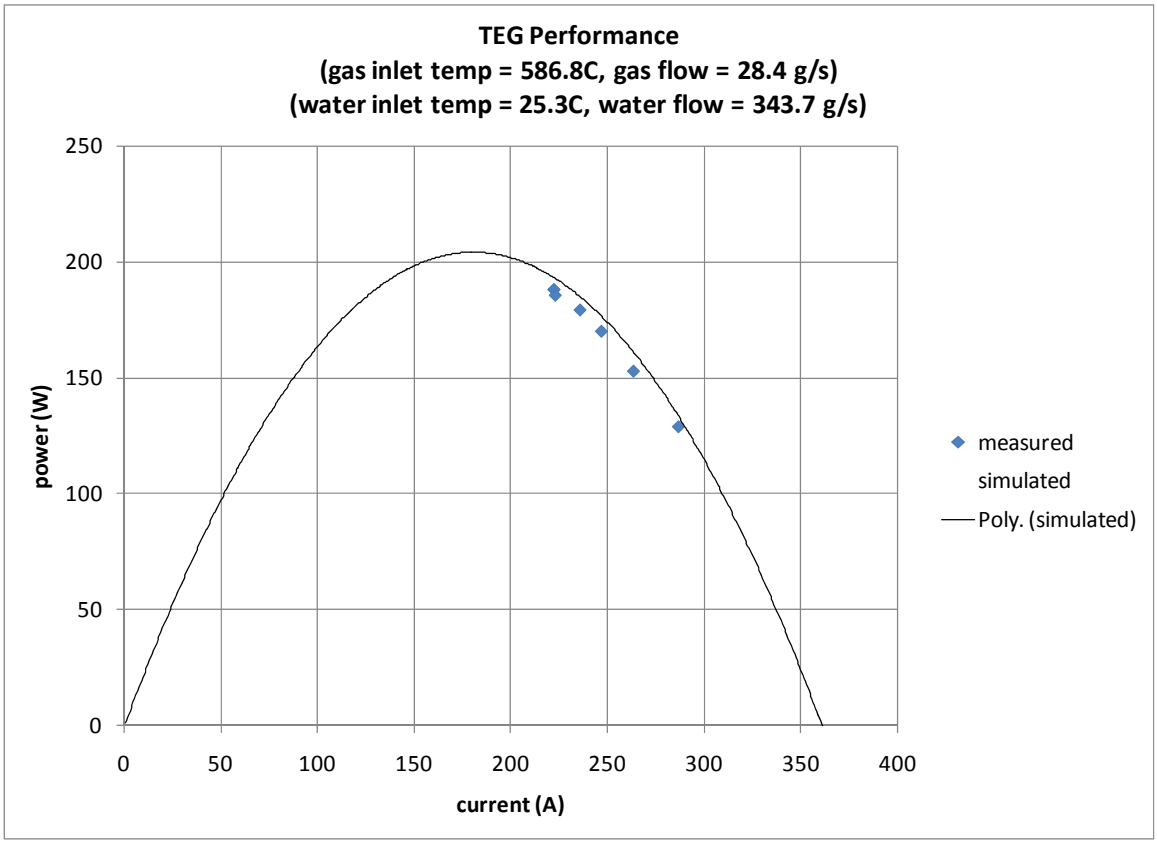

Figure 18: Test results for cylindrical TEG.

Although the cylindrical TEG was successful in that it was the first higher temperature, gas/liquid TEG that the team made that produced over 200W, it had been designed to produce over 500W at the nominal design condition.

Phase 5

The objective of Phase 5 of this program was to successfully design and build two TEGs and install and test them in both BMW and Ford vehicles. It was also inherent in the Phase 5 design objective to fix the design issues with the cylindrical TEG that prevented it from reaching its full potential.

To better understand what caused the problems with the Phase 4 TEG, the team set out to do a thorough analysis of how the TEG performed vs. how it was expected to perform based on the extensive models that had been developed during the course of the project. These models will be more thoroughly discussed in an upcoming section.

It was determined that the TE electrical contact resistance had by far the largest impact on the degradation in TEG performance. Sensitivity analyses were done on the TE electrical contact resistance along with the thermal contact resistance between the hot shunt and the hot heat exchanger and the cold shunt and the cold tube. These graphs can be seen in Figures 19-21.

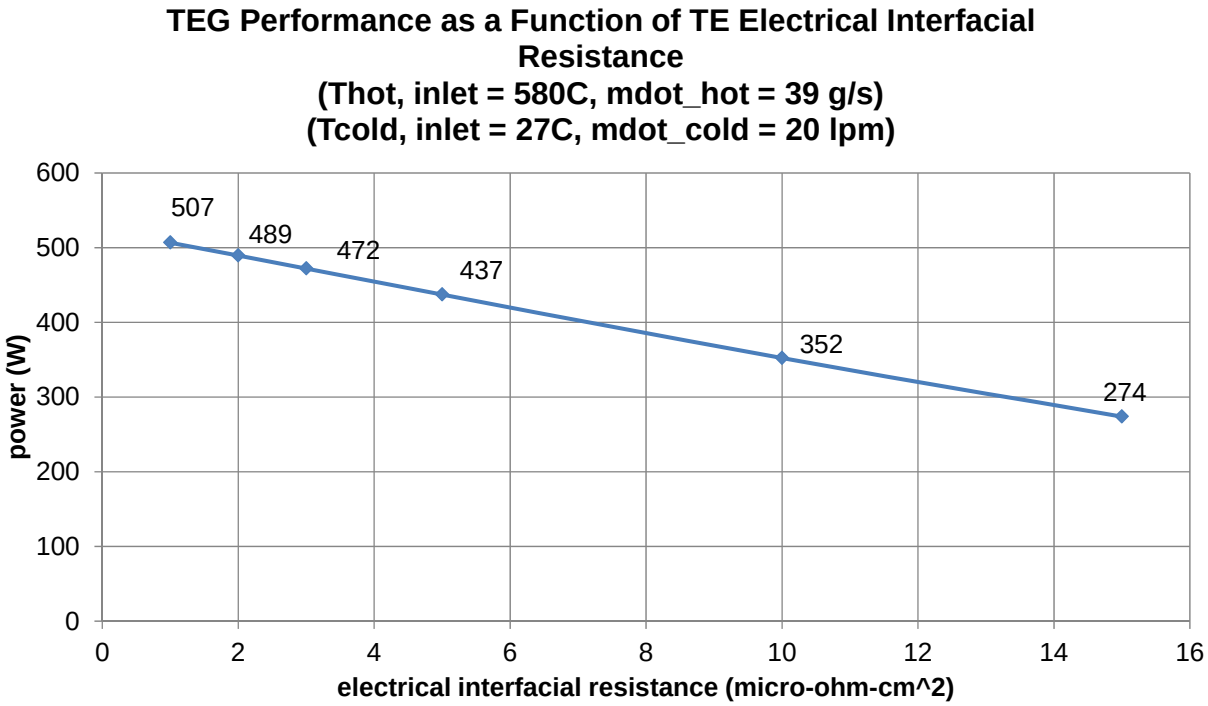

Figure 19: Performance degradation as a function of electrical interfacial resistance.

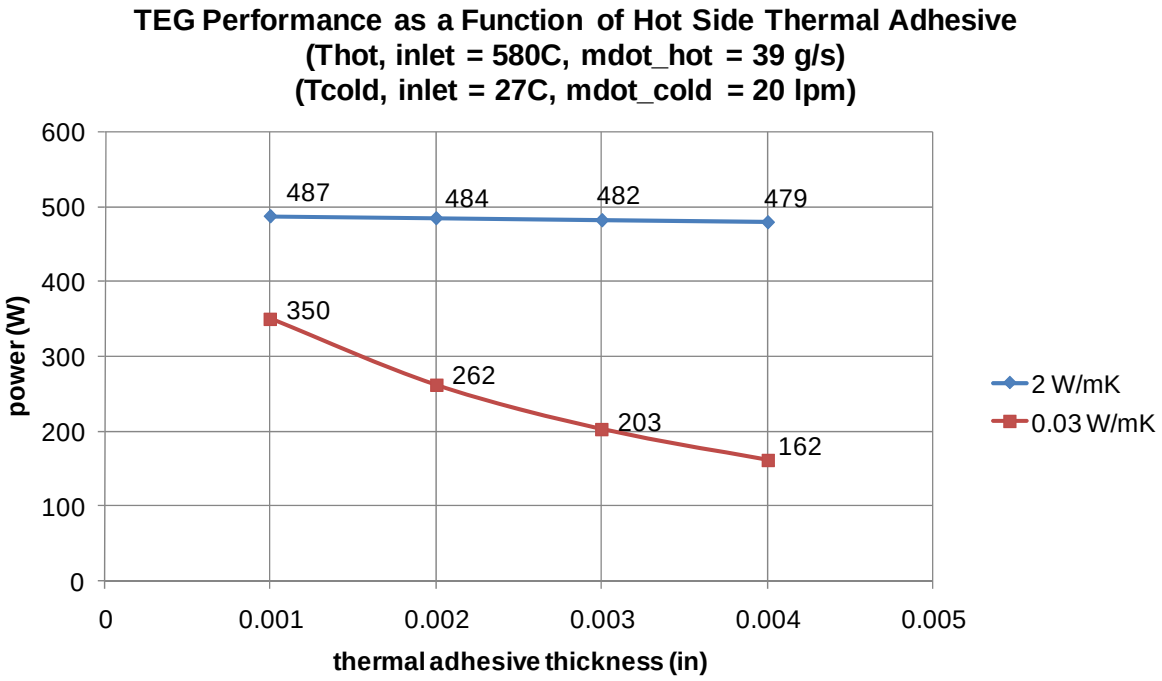

Figure 20: Performance degradation as a function of hot side thermal interfacial resistance.

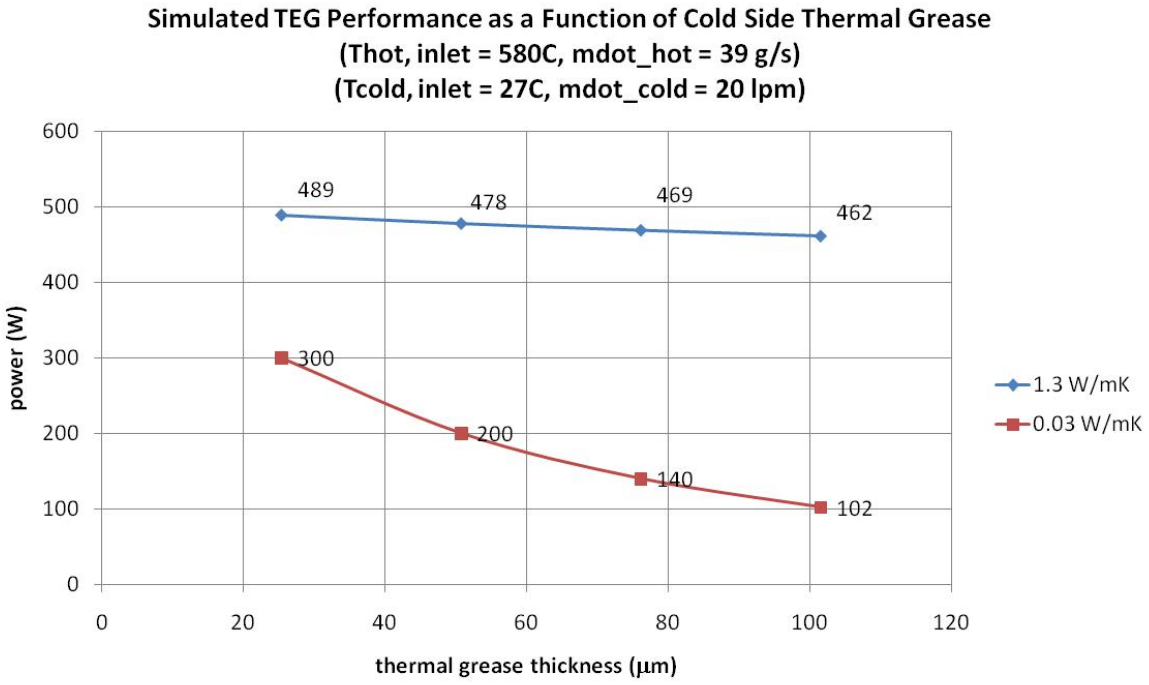

Figure 21: Performance degradation as a function of cold side thermal interfacial resistance.

Having identified the problems, the team embarked on fixing them. Several of the most important improvements included the following:

1. Providing a better means to place thermal grease between the cold shunt and cold tube.
2. Create a more uniform and robust electrical isolation layer between the hot shunt and hot heat exchanger.
3. Create a more effective cold shunt subassembly that would provide the flexibility to accommodate for the thermal expansion of the device while still providing low electrical resistance.
4. Use improved assembly fixtures and methods. This had the largest impact on reducing the excessive electrical contact resistance in the system

With these design flaws identified and design and assembly changes underway, new TEGs were built. The first new cylindrical TEG built was made of Bi2Te3 TE material only and was meant to be tested at low temperatures (<450C gas temperatures) on the Amerigon test bench. A picture of this device can be seen in Figure 22.

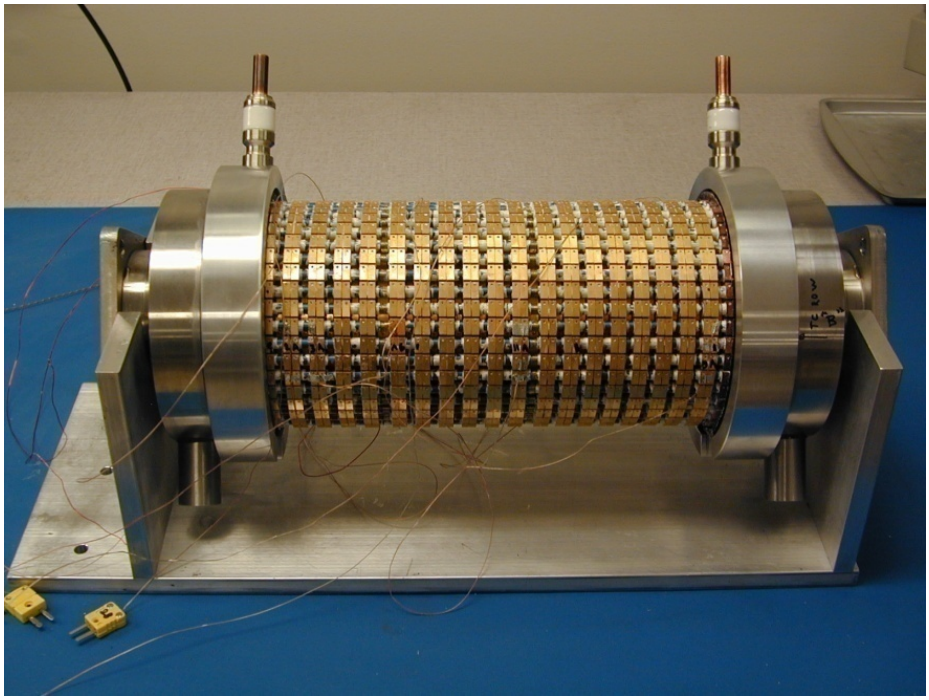

Figure 22: Bi2Te3 gas/liquid cylindrical TEG.

Test setup

The test bench at the Amerigon facility is shown in Figure 23. The bench includes a blower, a pair of gas heaters, and a control panel used to simulate the hot exhaust gas that would be provided by an internal combustion engine. The bench can provide gas temperatures in excess of 600C at flow rates exceeding 45 g/s. Air flow is measured downstream of the blower, but upstream of the gas heaters. Three thermocouples per flange are used to measure the inlet and outlet temperatures of the air. An average of these thermocouples can then be used to obtain the inlet and outlet temperature of the TEG.

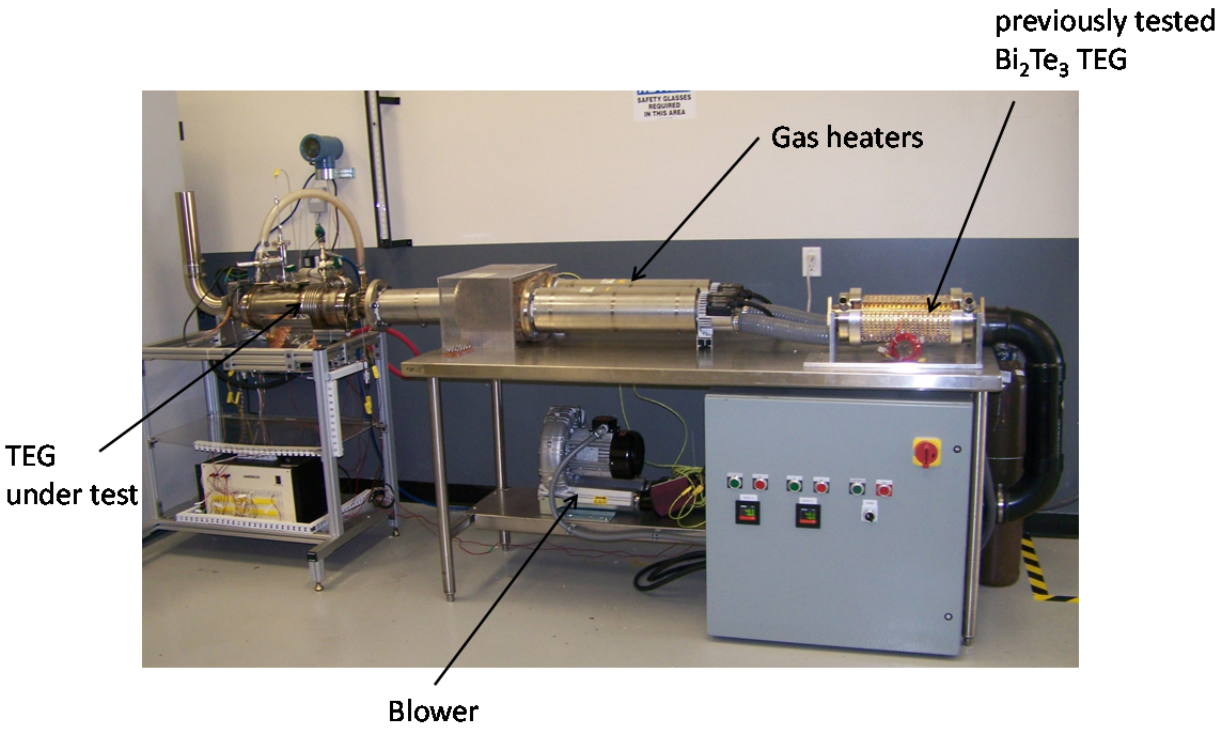

Figure 23: TEG test bench setup.

On the cold side of the TEG, cold water is provided by a high capacity chiller. The chiller can provide temperature control up to 40C with cooling capacities up to 40 kW. A Coriolis mass flow meter was used to measure water flow and thermistors were used to measure the water inlet and outlet temperatures of the TEG.

In addition to the system inputs, the TEG was instrumented with 5 thermocouples embedded in hot shunts and 5 thermocouples attached to cold shunts. These thermocouples were at different axial and radial locations on the TEG to determine how the temperatures of the TEG changed in the direction of air and water flow. Voltages were also measured for 3 different sections of the device plus the total voltage.

A variable electrical load was used to create as much of the voltage vs. current curve as possible. A shunt resistor was used to measure the output current of the device. A picture of one of the higher temperature TEGs under test is shown in Figure 25.

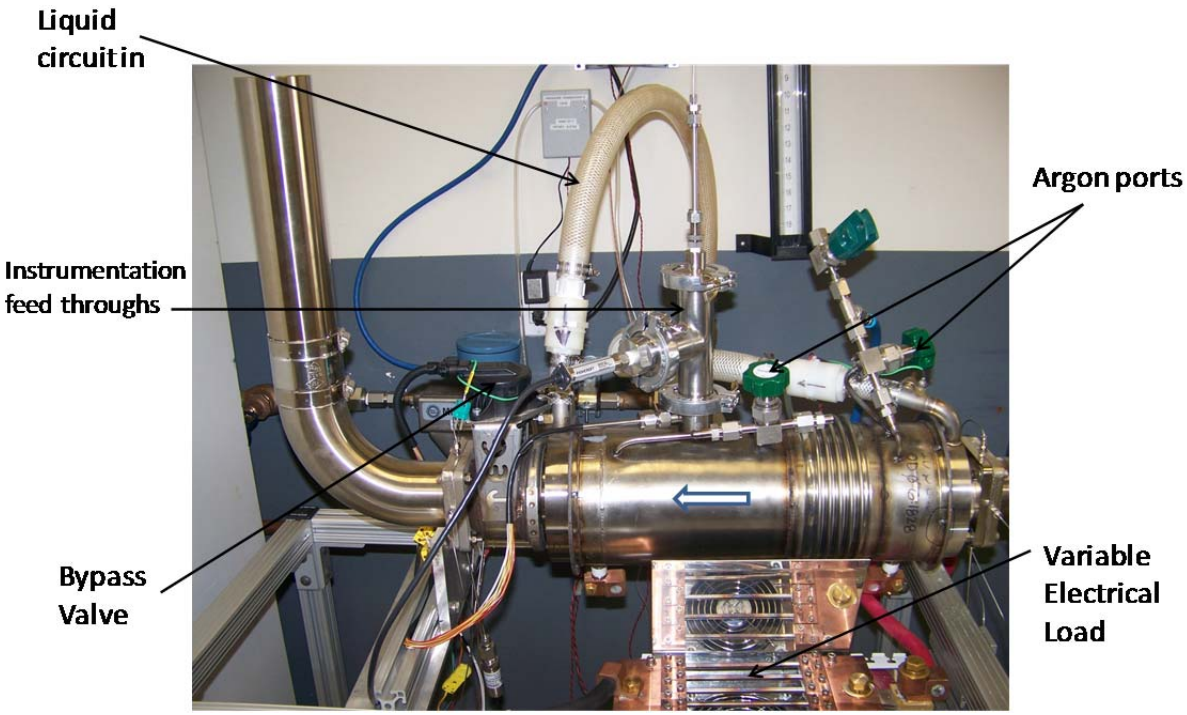

Figure 24: Higher temperature TEG on the test bench.

Test Results and Modeling Analyses

With much of the test results for the Phase 5 TEGs discussed in the context of how they compare to the performance models, it is appropriate at this time to introduce and describe these extensive models in order to put into context the bench test results of the TEGs.

Previously introduced in Crane et al.[3, 4], the equations used to model the TE elements were defined in Snyder[5]. Looking at the TE element in the direction of heat flow, a temperature gradient across the element is predefined. This temperature gradient is then subdivided into smaller equal temperature steps. The three basic thermoelectric material properties, Seebeck coefficient, electrical resistivity, and thermal conductivity, which are defined as functions of temperature, are calculated at each of these temperature steps across the entire temperature gradient. The reduced current density, which is the ratio of the electric current density to the conduction-driven heat flux[5] is calculated at each temperature step using the calculated TE material properties.

An initial reduced current density is defined as

$$u_1 = \frac{I}{Q_h - \alpha_1 I T_1}$$

Equation 1

This equation is negative if an n-type material is being evaluated. The temperature variation along the length of the element is then calculated as a function of the reduced current density, with the sum being equal to the current density times element length[5].

Using these now defined equations, the model makes initial assumptions for heat flow and current. Using the optimization function, FMINCON, in MATLAB, the model iteratively solves for the heat flow and current that maximizes TE element efficiency. A constraint for the optimization is that the TE

elements must match a predefined element length. Another input to the model is the electrical resistance at the TE element interfaces. This resistance has been indirectly measured in validated TE heating and cooling experiments and is similar to those reported in the literature[6]. The thermal interfacial resistance is related to this electrical contact resistance using the Wiedmann-Franz law [7]. A reduced current density is also evaluated at the temperature step created by the electrical contact resistance and the temperature drop caused by the thermal contact resistance. In this way, the metallization and other interfacial attributes of the elements are evaluated. To model segmented or multi-material elements, more interfaces were added, but the evaluation method remained the same. Validation of this model was described for both single material and segmented material TE elements in Crane et al.[4]. This element and couple-level model was adjusted to fit into a larger model that integrated these TE elements into a TE device, including shunts, heat exchangers, and fluid flows.

Building on previous work of validated TE numerical simulation[8], a MATLAB-based, numerical, steady-state model was created, comprised of simultaneously solved, non-linear, energy balance equations. These energy balance equations simulate the high-power density, segmented element TE assemblies discussed above. The numerical model of the TE heat exchanger uses a finite volume approach with discretization in the axial direction of both hot and cold flows. A first-order upwind differencing scheme is implemented for the convective derivatives. Downwind differencing can also be chosen as an option. Transverse or radial heat transfer is modeled using standard conduction equations that incorporate central differencing discretization for the gradients. Each segment of the fluid-carrying channel is separated into four control volumes. Since the temperature gradients across each segment and from one segment to another are small, this level of discretization was determined to be adequate. Differential algebraic equations model the energy balances for each control volume.

Convective heat transfer coefficient and pressure drop correlations were derived from experimental and simulation[9] data. The thermal resistances of the device are rigorously modeled. These resistances include thermal contact resistances at each TE element interface, including between different material segments of a segmented element as well as the interfacial resistance between the TE element and the shunts on both the hot and cold side of the elements. The metallization layer(s) on the elements are lumped into this contact resistance both thermally and electrically. The thermal contact resistance is also simulated between the shunts and the heat exchangers. Temperature drops are also calculated from the fluid through the fins to the wall of the heat exchanger. These drops continue through the heat exchanger wall and through any interface materials, which can include electrically insulating coatings such as anodize and thermal grease. The thermal resistance of the shunts, based on geometry and material, are then accounted for culminating in a surface temperature at the metallization layer of the TE.

Heat loss factors are also rigorously accounted for in the model. Convective, conductive, and radiative heat losses are considered. Heat can be lost to the outside environment or it can be transferred from a hot surface to a cold surface within the device or system. The geometry of the components is considered when determining where the heat is being transferred to. Different environments can be modeled, including air, argon, xenon, or vacuum. Different insulations can also be modeled, such as microporous insulation and aerogel. The emissivity and absorbtivity of the exposed surfaces is also accounted for.

Different fin correlations can be chosen for the fluid channels. The choices include straight, offset, wavy, annular, as well as other more specialized correlations. The shape of the fluid channels can also be specified as square (rectangular), hexangonal, or circular. Radiation heat transfer is also computed with the convective heat transfer coefficient within the fluid channels. Temperature dependent fluid properties for many different fluids are also part of the model. The user can choose from air, water,

glycol/water, helium/xenon, oil, exhaust gas, CO2, argon, as well as other specialized fluids. The temperature dependent properties modeled include density, thermal conductivity, specific heat, and dynamic viscosity.

Many different TE materials can be chosen for simulation, including Bi2Te3, PbTe, TAGS, half heusler, and skutterudite. These materials can be chosen as single material or as a part of segmented TE elements. Material properties, Seebeck coefficient, electrical resistivity, and thermal conductivity, as a function of temperature are taken from measured data or are supplier-provided. To simulate improved TE materials, base TE material properties can be scaled to a desired ZTavg. The model allows the user to choose how this will occur, either by changing the Seebeck coefficient, electrical resistivity, or thermal conductivity.

The other materials of the device can also be chosen. This includes the materials for the fluid channel structures, the connectors, and the fins, which may be different from the fluid channel. Material choices for these components include copper, aluminum, different grades of SST, molybdenum, clad materials, and various ceramic materials. For many of these materials, thermal and electrical conductivity are modeled as a function of temperature.

The TE device can be broken up into multiple temperature banks in the direction of fluid flow. Each temperature bank can have a separate set of TE elements. These elements can have different area to length aspect ratios, be segmented differently with different TE materials, or not be segmented at all. Each temperature bank can operate on its own electrical circuit or one electrical circuit can be used for all of the temperature banks. The temperature banks can be of different lengths to better match the temperature gradients and heat flows in the direction of fluid flow. In addition, each temperature bank can be modeled as having different hot side fin densities. This can be used to better match the heat fluxes and temperatures seen in a particular bank. It also can help reduce the pressure drop and weight of the fluid channel if lower density fins can be more advantageously used in different banks of the TEG.

Electrical load resistance affects the operating current and power output of the TEG at a particular set of temperature and heat flow conditions. Equation 2 shows how load resistance relates to operating current[10].

$$\boldsymbol{I = \frac{\alpha \Delta T_{TE}}{R_{TE}+R_{load}}}$$

Equation 2

When designing the TEG for a particular set of temperature and heat flow conditions, the user will typically want to maximize the power output of the TEG. This condition occurs when the load resistance is equal to the internal resistance of the TEG. The model will also allow the user to run the model in off nominal conditions where the load resistance can be varied. This can be valuable in some designs since changing the current also affects the heat flow through the TE elements as can be seen in Equation 8.

To compute how all of the above attributes affect TEG operation, a set of energy balance equations have been defined.

$$Q_{h1} + \frac{1}{2} I^2 R_{conn,h} - UA_{TE-conn}(T_{cen,h} - T_{h1}) = 0$$

Equation 3

$$Q_{h2} + \frac{1}{2} I^2 R_{conn,h} - UA_{TE-conn}(T_{cen,h} - T_{h2}) = 0$$

Equation 4

$$UA_{TE-conn}(T_{cen,h}-T_{h1})+UA_{TE-conn}(T_{cen,h}-T_{h2})-UA_{cross,conn}(T_{sh2}-T_{cen,h})=0$$

Equation 5

$$hA_h(T_{fh}-T_{sh2})-UA_{cross,conn}(T_{sh2}-T_{cen,h})-hA_{nat}(T_{sh2}-T_\infty)$$
$$+UA_{cross,ch,h,1-2}(\Delta T_{sh1})-UA_{cross,ch,h,2-3}(\Delta T_{sh2})=0$$

Equation 6

$$\dot{m}Cp_h\Delta T_{fh}-hA_h(T_{fh}-T_{sh2})=0$$

Equation 7

Where

$$Q_h=\alpha IT_h+K\Delta T_{TE}-\frac{1}{2}I^2(R_{TE}+2R_{int})$$

Equation 8

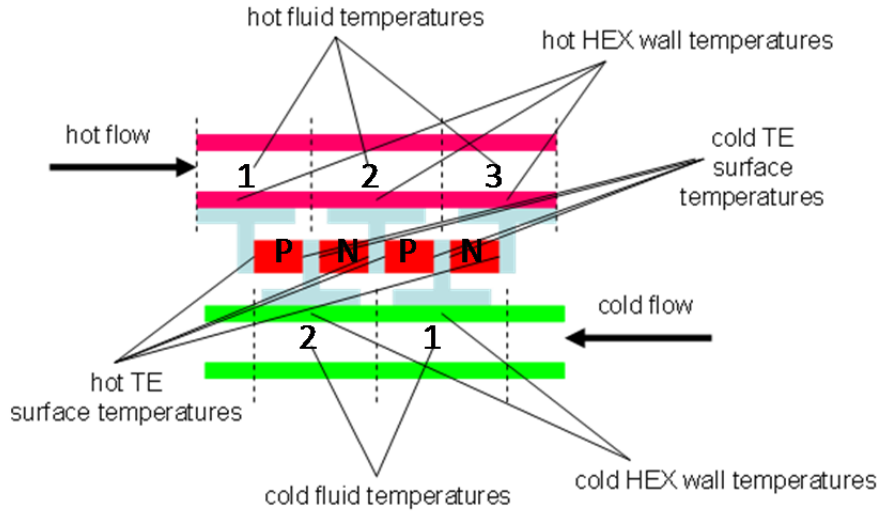

Figure 25: Schematic of TE subassembly with heat exchangers (HEX) showing temperature locations in the model.

Equation 3 and 4 are energy balance equations for conductive heat transfer from the TE elements into the connectors. Equation 5 and 6 are energy balance equations for conductive heat transfer from the connector through the fluid-carrying channel wall through the fins to fluid convective heat transfer. They include the losses due to natural convection, radiation, and Joule heating of the boxes. Equation 7 is an energy balance equation for the convective heat transfer into the fluid. Equation 8 is the basic equation for thermoelectric heat flow in power generation.

The model solves these governing equations simultaneously for steady-state temperatures at each node in the direction of flow using the FMINCON function in MATLAB. The number of simultaneous equations varies with the number of TE elements in the direction of fluid flow.

Outputs for the model include power output, efficiency, hot and cold outlet temperatures, hot and cold pressure drops, total mass and volume, and many others. Auxiliary power of pumps and/or fans is also computed based on the pressure drops. This output can be used to calculate a net power output instead of gross power.

Optimization

Advanced multi-parameter optimization can be used on the steady state model for better understanding of the interactions between various design variables and parameters and to further improve the performance of the design. The TEG design problem, an example of a constrained, non-linear, minimization problem, is solved using the MATLAB function FMINCON, which uses a gradient-based optimization scheme.

A design engineer can choose to optimize from greater than 20 different design variables, including fin and TE dimensions and include dozens of different design parameters. A variety of different constraints can also be chosen, including minimum power density, maximum hot- and cold-side pressure drops, maximum total mass, and minimum output power. Constraints can also be placed on maximum TE surface temperatures and maximum temperature gradients across the TE elements to help improve design robustness. The objective function of the analysis can also be chosen. Choices include maximum gross or net power, maximum efficiency, and maximum gross or net power density, which can be based on either total mass or TE mass. Once the design variables, parameters, constraints, and objective function have been chosen, an optimization analysis can be conducted. The result is a nominal design that can now be used in an operating model where the design conditions can vary.

Transient model

The steady state model gives an effective means to choose a nominal design point and optimize the design for this set of operating conditions. However, a thermoelectric generator often may see a wide array of operating conditions, and these conditions may change frequently as a function of time. This is certainly the case when the TEG is integrated into a car or truck. The thermal time constants of the exhaust system and of the TEG itself can have a large effect on how the TEG performs in this cycle.

In order to model the TEG in different cycles as well as other non-steady state operating conditions, the steady state models for TE couples and devices were adapted into transient models. To do this, the energy balance equations defined above were setup as differential equations based on Equation 9 and integrated into the S- Function template of MATLAB/Simulink..

$$\boldsymbol{mC_p \frac{dT}{dt} = Q_1 - Q_2}$$

Equation 9

The mC_p term in Equation 9 is the thermal mass of each control volume that the equation represents. This could be a fluid, heat exchanger, connector, or TE thermal mass depending on the control volume. It is important to determine the direction of heat flow to make sure that the signs for Q_1 and Q_2 are correct. Otherwise, the differential equations will not be able to be solved correctly.

When using Simulink to solve ordinary differential equations, there is a choice of solvers made available to the user. Due to the potential rapid variation in the solution of the differential equations, the transient TEG problem is considered stiff. Ode15s, specifically designed to handle stiff problems, is the solver that most successfully solved the set of differential equations for the transient TEG problem.

A transient model was first setup for the TE couple. A validation experiment was conducted using segmented elements on a heater housing, cooled between two small cold plates. The heater housing holds a cartridge heater, which was used to provide heat to the couple. This couple setup was similar to that described in Crane et al.[4] for the 10% efficient generator. The segmented elements were made up of TAGS/PbTe and Bi2Te3. Graphs of the test results can be seen in the figure below.

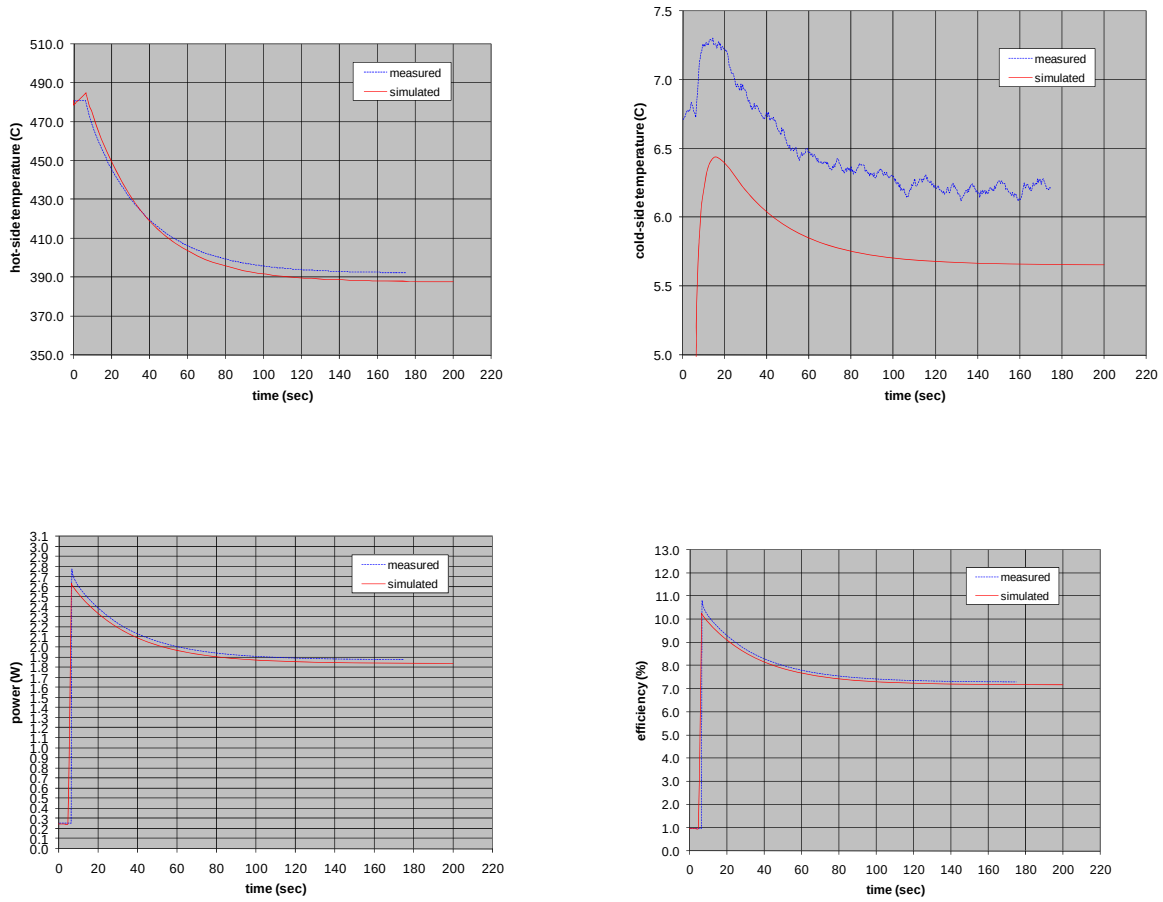

Figure 26: Transient experimental and simulated performance of a TE couple.

The test was setup where the cartridge heater was held at a constant heat input of 35W. The hot side temperature of the TE elements was 500C and the cold water bath was set at 0C. The electrical load resistance was initially infinite making the initial current zero by Equation 2. Then the electrical load resistance was instantly changed to 30A. The electrical time constants of the couple were much faster than the thermal time constants. Thus, spikes in power and efficiency can be seen in the graphs before the thermal time constants catch up to the electrical time constants.

By adjusting the electrical load resistance, the electrical current is instantly increased. This increases the effective thermal conductivity of the elements by Equation 8. The original temperature differences of the couple no longer balance the steady state equations. The time it takes to balance these temperature differences with the new effective thermal conductance of the couple is based on the thermal mass of the elements and their connectors. This can clearly be seen in the graphs. Greater power output and efficiency are achieved initially due to the couple operating at higher temperature differences at the same heat flow. The higher temperature differences increase open circuit voltage and subsequently power output. They also increase the Carnot term of the TEG efficiency. However, these temperature differences are not sustainable in steady state, and thus the power output and efficiency eventually come down.

The cold side temperature initially increases due to the sudden increase in effective thermal conductance, transferring more heat from the hot to cold side of the TE elements. This is also what causes the hot side temperature to decrease. As the system balances, it stabilizes at a more in-between

temperature in this example. The figures show excellent correlation between the measured and simulated data, where differences are <5%.

With this validation, a transient model was created of the TEG itself, TE couples integrated directly into the heat exchangers. The optimized design from the steady state model is used as a baseline. Inputs for the model are similar to those of the steady state model. Operating condition inputs include the hot and cold side inlet temperatures and flows and the electrical load resistance. The electrical load resistance can be set to be always equal to the internal resistance of the TEG or it can be set at a particular constant load. A controller simulator can be attached to the model as an additional Simulink block in order to simulate the effects of a varying electrical load that is not necessarily optimal. Outputs for the model are again similar to those of the steady state model.

The model can be operated as is in a stand-alone mode or the S-function can be cut and pasted into a larger systems-level model. Both BMW and Ford have cut and pasted versions of this model into their larger systems-level models[11]. The model can be run using single hot-side inlet flow and temperature conditions or using the hot-side inlet flow and temperature conditions for a drive cycle.

Additional systems level attributes have been added to the transient model to aid in its use as a part of a larger system. A maximum hot inlet temperature can be defined to prevent the overheating of the TE elements or any other part of the TEG device. A maximum hot flow can be defined to prevent excessive backpressure in the system. This excessive backpressure can reduce engine performance if the TEG is integrated into the exhaust system of a vehicle. In addition, to better match the thermal impedance of a dynamic thermal system as defined in Crane and Bell[12], the TEG can be broken into a number of TE sections. Having multiple TE sections can allow the TEG to operate better at low flows when the design has been optimized for higher flow rates.

Model validation

Table 1 shows the list of tests run on the Bi_2Te_3 cylindrical TEG device. These conditions were meant to test the unit over a range of air and water inlet temperatures and flow rates. Tfh,in and Tfc,in represent hot and cold inlet temperatures respectively, while vdot,h and vdot,c represent hot and cold volume flows.

Test	2	3	4	5	6	7	8	9	10	11	12	13
Tfh,in (°C)	200	300	400	435	435	435	435	435	435	400	300	200
Tfc,in (°C)	35	35	35	35	20	20	20	20	20	20	20	20
vdot,h (cfm)	47	47	47	47	47	70	47	47	30	30	30	30
vdot,c (lpm)	15	15	15	15	15	15	10	20	15	15	15	15
max power output (W)	28.3	73.5	130	148	165	205	158	163	116	102	55.5	22.7

Note: Test 1 is not listed because it was only a water-side pressure drop test.

Table 1. Test conditions for Bi_2Te_3 cylindrical TEG

Data from these twelve tests was then used to make modifications to the model to better simulate the actual TEG device. Despite previous component level testing, there is still uncertainty in many variables, particularly as they are scaled from the subassembly to the full scale level.

The interface between the hot side heat exchanger and the hot shunt/ring was studied previously. However, it was still uncertain how this interface would perform when its thermal resistance was averaged over many rings. It was also uncertain how this interface would perform when subjected to higher temperatures compared to the component level tests. The interface between the cold side heat exchanger (cold tube) and the cold shunt subassembly had similar uncertainty relating to how uniformly the thermal grease was applied across many cold shunts.

Uncertainty also existed in the average value of electrical interfacial resistance for the TE element to hot and cold shunt. When stacking multiple TE subassemblies in series and in parallel, it is difficult to obtain the electrical interfacial resistance that can be obtained for a single TE subassembly. Although it is a goal to accurately measure the thermal interface resistance directly, as discussed in Crane [13], the thermal interfacial resistance is calculated using the Wiedmann-Franz law. It became apparent from our component level and initial device level testing that this relationship does not hold for all situations, particularly as electrical contact resistance increases. Thus, an additional Lorentz factor was included as a variable to be multiplied against the Lorentz number in the Wiedmann-Franz law.

$$\lambda = \frac{L_{fact} LT}{\rho} \qquad \text{Equation 10}$$

where L, the Lorentz number, is 2.45 x 10^{-8} ($W\Omega/K^2$), T is the interface temperature (K), ρ is the electrical interfacial resistivity (Ω-m), λ is the thermal interfacial conductivity (W/mK), and L_{fact} is the Lorentz factor.

In an effort to reduce the number of variables, an overall average emissivity was used to predict radiation heat transfer from each surface within the TEG. Emissivity is a material property that indicates the ability to emit heat radiatively from one surface to another compared to an ideal radiator. With so many different surfaces and surface finishes inside the TEG from the hot shunt to cold shunt to TE material, an average emissivity is difficult to predict. The emissivity of different materials can vary from low values at 0.05 up to values near unity depending on whether the surface has been oxidized or polished. Due to this uncertainty, average emissivity became another variable for which to solve. Included in this emissivity value is any uncertainty in view factor. In radiation heat transfer, view factor defines the amount of radiation that leaves one surface and intercepts another surface. Surfaces that are not in a direct line of sight to the emitting surface may not see all of the emitted heat. For parallel plates, it is easy to determine the view factor or amount of radiation heat possible to transfer from one parallel surface to another. The surfaces in the TEG device are not all parallel. Thus, there is some uncertainty to the amount of heat that is emitted by one surface and received by another. This value has been included in the overall average emissivity. In the future, these terms can be broken down into more distinct variables to provide further simulation accuracy.

Finally, multipliers were included for four different heat transfer coefficients. Each coefficient is based on either general textbook correlations or empirical data for a similar component but not specific to the particular parts being tested. The heat transfer coefficients (W/m^2K) included the hot heat exchanger convection coefficient, h_{hot}, the cold heat exchanger convection coefficient, h_{cold}, free convection between the device and the environment, $h_{free,1}$, and free convection between the hot and cold sides of the device, $h_{free,2}$. The multipliers were used to adjust these correlations to better match the component performance in the actual device, see equations 11-14.

$$Q_{conv,hot} = h_{hot} h_{mult,hot} A_{hot} (T_{f,hot} - T_{s,hot}) \qquad \text{Equation 11}$$

$$Q_{conv,cold} = h_{cold} h_{mult,cold} A_{cold} (T_{s,cold} - T_{f,cold}) \qquad \text{Equation 12}$$

$$Q_{free,1} = h_{free,1} h_{mult,free,1} A_s (T_{s,hot} - T_{\infty}) \qquad \text{Equation 13}$$

$$Q_{free,2} = h_{free,2} h_{mult,free,2} A_s (T_{s,hot} - T_{s,cold}) \qquad \text{Equation 14}$$

where Q is heat flow (W), h is heat transfer coefficient (W/m^2K), h_{mult} is the heat transfer coefficient multiplier, A is the heat transfer surface area (m^2), T is temperature (K), subscript conv is convective, subscript hot is for hot side, subscript cold is for cold side, subscript f is for fluid, subscript s is for surface, subscript free is for free convection, and subscript ∞ is for the environment.

Simulations were then run using these variables and allowing them to vary to create a least squares or best fit to the data. Table 2 lists the variables along with the values that provided the best fit to the data. All of these values are reasonable and not outside the range that is physically possible.

Variable	Value
hot interface heat transfer coefficient (W/m^2K)	6562
cold interface heat transfer coefficient (W/m^2K)	68898
electrical interfacial resistance ($\mu\Omega cm^2$)	65
Lorentz factor	65
emissivity	0.4
hot convection heat transfer coefficient multiplier	1.2
cold convection heat transfer coefficient multiplier	1
free convection multiplier 1	0.5
free convection multiplier 2	1

Table 2. Variable values used to provide least squares fit to empirical test data.

Figure 27 shows the empirical test results of tests 2 – 13 compared to simulated test results for air and water pressure drop and outlet temperatures. The difference between the measured and simulated values is less than 5%. For the air outlet temperature, the difference is slightly higher, but in this case there is also some uncertainty in the air temperature measurements due to stratification of temperature within the air flow within the pipe. Three thermocouples were used to try to measure the outlet air temperature in different parts of the air stream. Using more thermocouples and/or a temperature integrator would potentially further reduce the error between measured and simulated data for air outlet temperature.

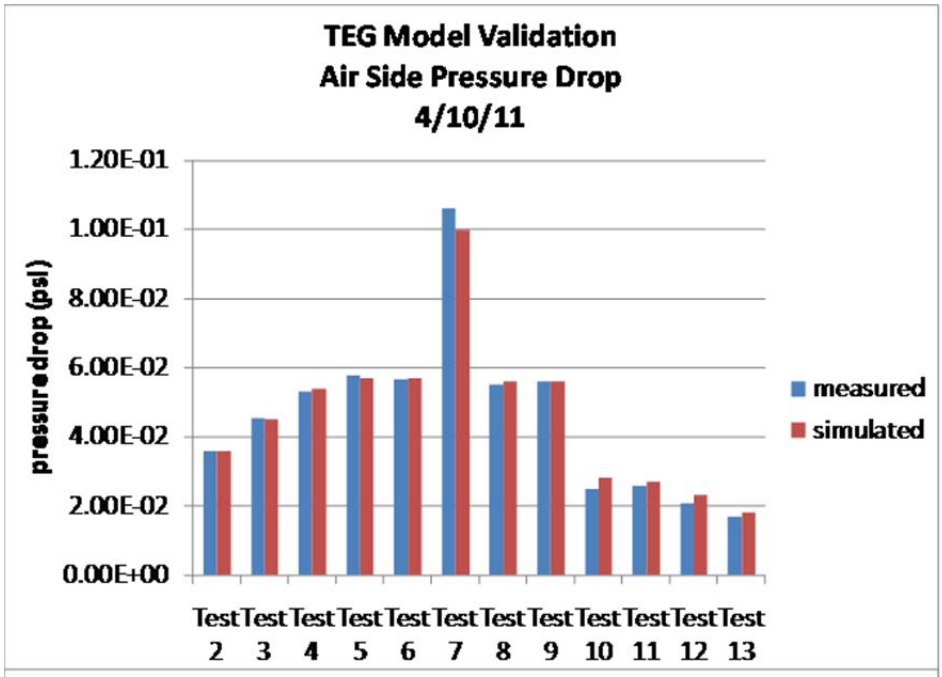
TEG Model Validation
Air Side Pressure Drop
4/10/11
pressure drop (psi)
1.20E-01
1.00E-01
8.00E-02
6.00E-02
4.00E-02
2.00E-02
0.00E+00
Test 2
Test 3
Test 4
Test 5
Test 6
Test 7
Test 8
Test 9
Test 10
Test 11
Test 12
Test 13
measured
simulated

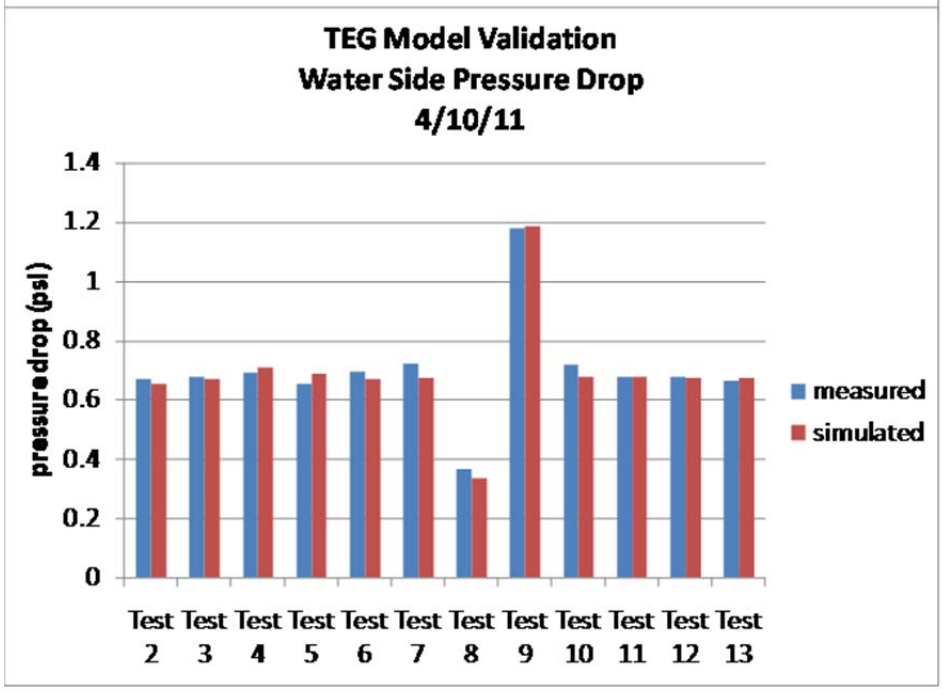
TEG Model Validation
Water Side Pressure Drop
4/10/11
pressure drop (psi)
1.4
1.2
1
0.8
0.6
0.4
0.2
0
Test 2
Test 3
Test 4
Test 5
Test 6
Test 7
Test 8
Test 9
Test 10
Test 11
Test 12
Test 13
measured
simulated

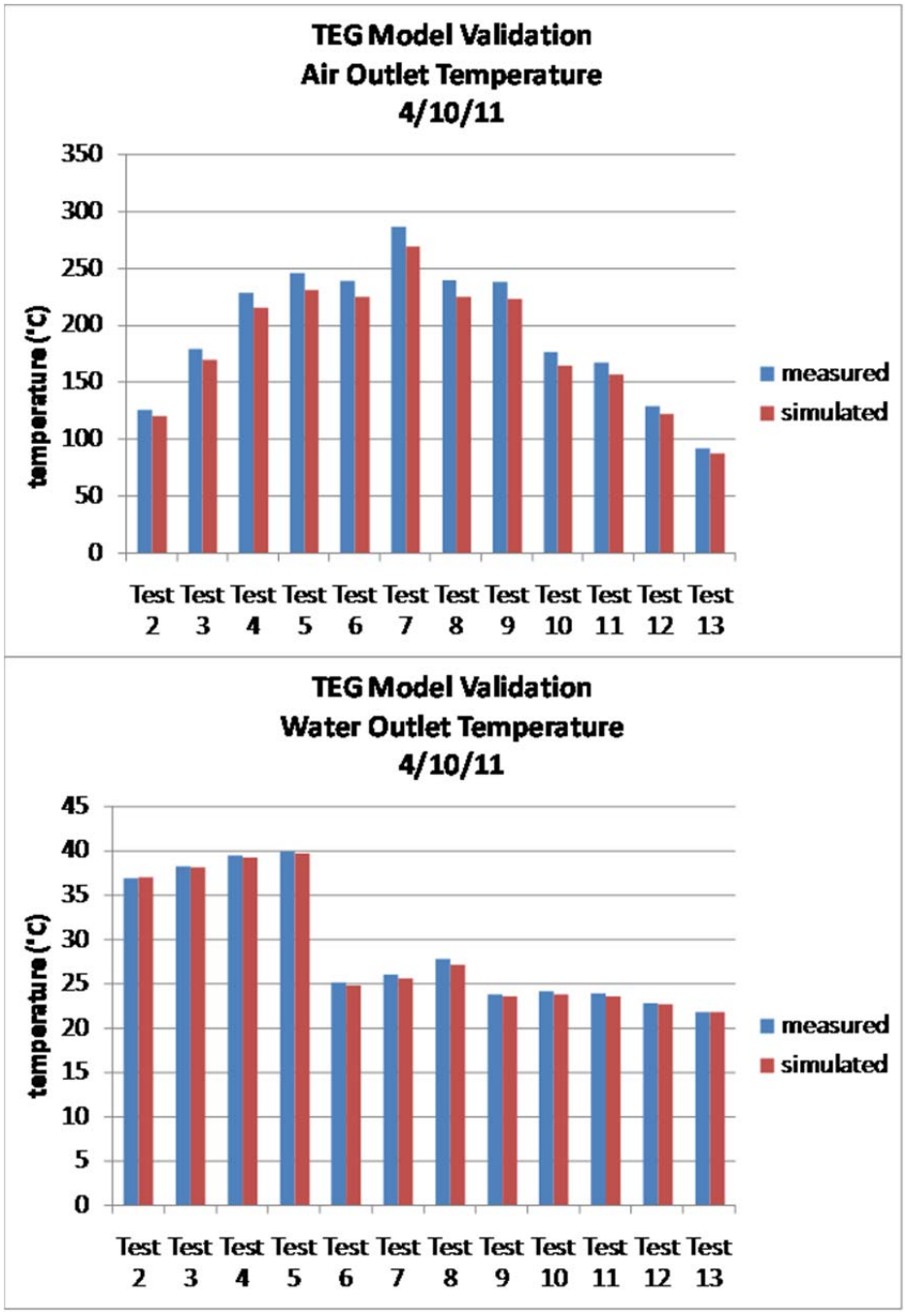

Figure 27: Bi_2Te_3 cylindrical TEG bench test results compared to simulated test results for TEG air and water pressure drops and outlet temperatures.

Figure 29 shows a comparison between measured and simulated data for hot and cold shunt temperatures in the TEG for Test 5. Similar graphs were achieved for all of the different test conditions. Again, there is an excellent correlation between the simulated and measured results down the axial length of the TEG (from hot ring 1 to 19, from hot air inlet to outlet).

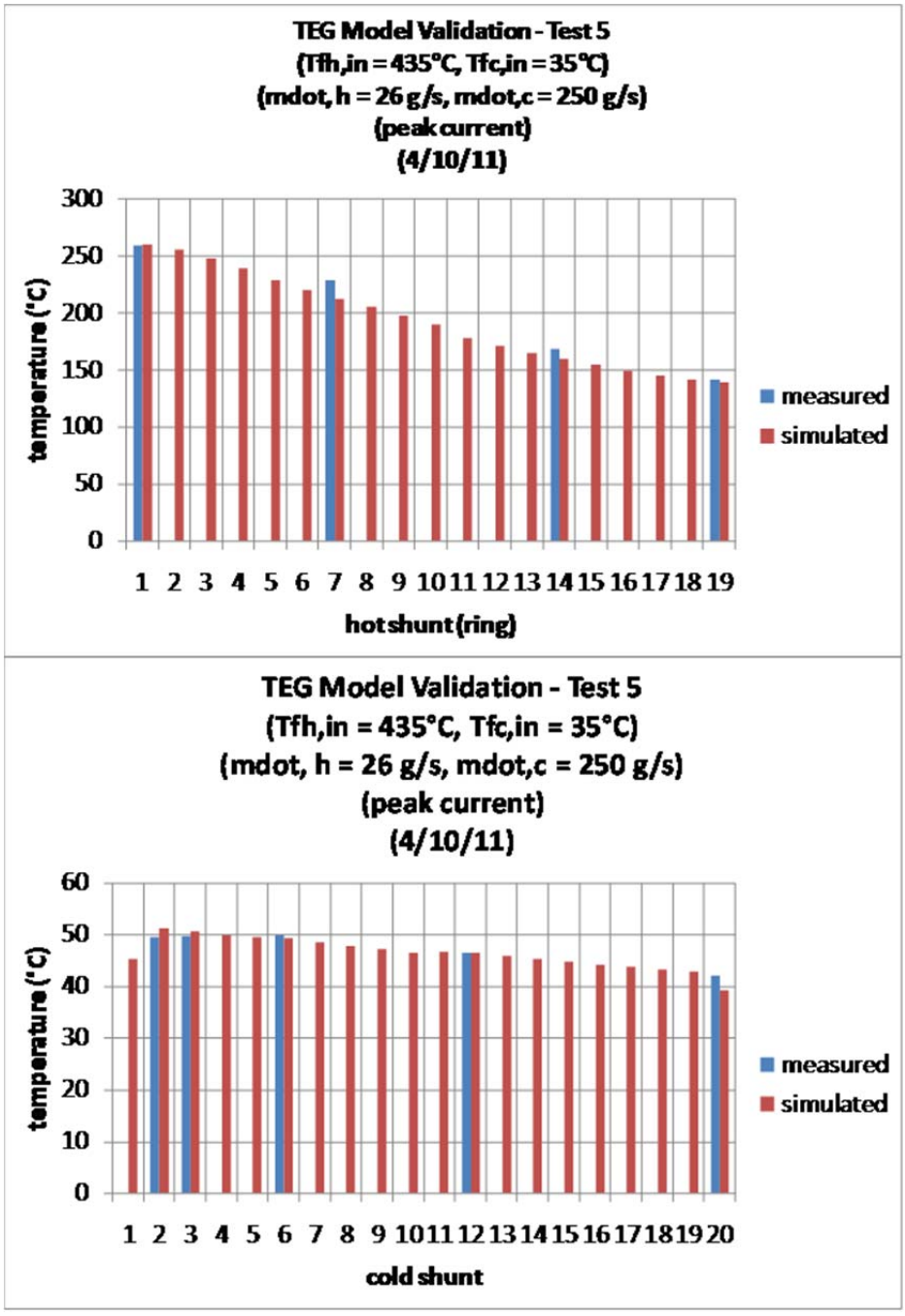

Figure 28: Bi_2Te_3 cylindrical TEG bench test results compared to simulated test results for TEG hot and cold shunt temperatures.

Figure 30 shows the measured vs. simulated voltage and power output for tests 7 and 13. Similar graphs were achieved for all of the different test conditions. Again, we can see excellent correlation between measured and simulated data. The difference between the measured and simulated data is less than 5% across the range of electrical currents for both test conditions.

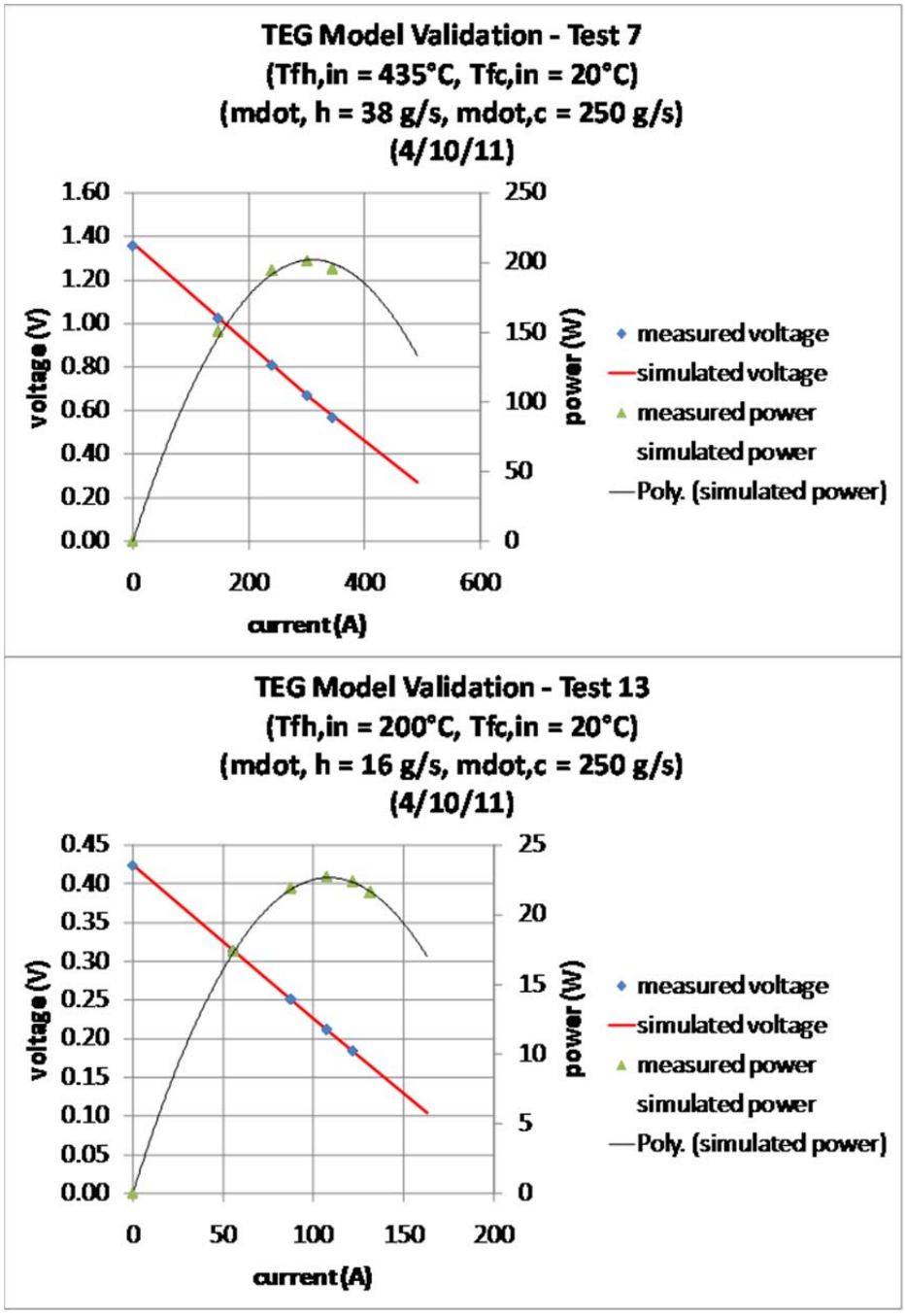

Figure 29: Bi_2Te_3 cylindrical TEG bench test results compared to simulated test results for TEG voltage and power output.

In addition to the low temperature cylindrical TEG, two higher temperature gas/liquid cylindrical TEGs were built and tested as shown on the test bench in Figure 24. These devices differed from the low temperature TEG. They were made of segmented TE material, half-Heusler and Bi_2Te_3. They were also operated at higher temperatures requiring them to operate in an inert environment (argon) to prevent oxidation of the TE elements and the hot shunts. To ensure the inert environment, an outer shell was added to the devices as can be seen in Figure 24. The figure also shows the argon ports used to establish the inert environment and the instrumentation feedthroughs. A bypass valve, shown in the figure, is also a part of this construction to allow high temperature and high flow gas to bypass the TEG.

Similarly to the low temperature TEG, Table 3 shows the list of tests run on the higher temperature cylindrical TEG devices. These conditions were again meant to test the units over a range of air and water inlet temperatures and flow rates.

Test	1	2	3	4	5	6	7	8	9	10	11	12
Tfh,in (°C)	390	390	390	425	425	425	510	510	510	620	620	620
Tfc,in (°C)	20	20	20	20	20	20	20	20	20	20	20	20
mdot,h (g/s)	13.5	13.5	13.5	20.5	20.5	20.5	30.1	30.1	30.1	45	45	45
mdot,c (g/s)	170	250	330	170	250	330	170	250	330	170	250	330
max power output (W)	56.1	56.5	57.6	119	121	122	261	270	272	495	580	595

Test	13	14	15	16	17	18	19	20	21	22	23	24	25
Tfh,in (°C)	390	390	390	425	425	425	510	510	510	620	620	620	620
Tfc,in (°C)	40	40	40	40	40	40	40	40	40	40	40	40	20
mdot,h (g/s)	13.5	13.5	13.5	20.5	20.5	20.5	30.1	30.1	30.1	45	45	45	48
mdot,c (g/s)	170	250	330	170	250	330	170	250	330	170	250	330	330
max power output (W)	49.3	49.2	49.6	103	104	106	228	237	241	436	461	N/A	608

Note: Test 24 not completed due to the chiller overheating.

Table 3. Test conditions for the higher temperature cylindrical TEGs made of segmented TE material

Run repeatability was tested as well. An example of this is shown in Figure 30 for Test 11. Three runs of Test 11 were performed over a two week period (over 25 hours of testing) and show good repeatability. There is a 9% decrease in electrical resistance from run 1 to run 2 due to “settling in” of the device interfaces. This reduction in electrical resistance caused a 5% increase in peak power output.

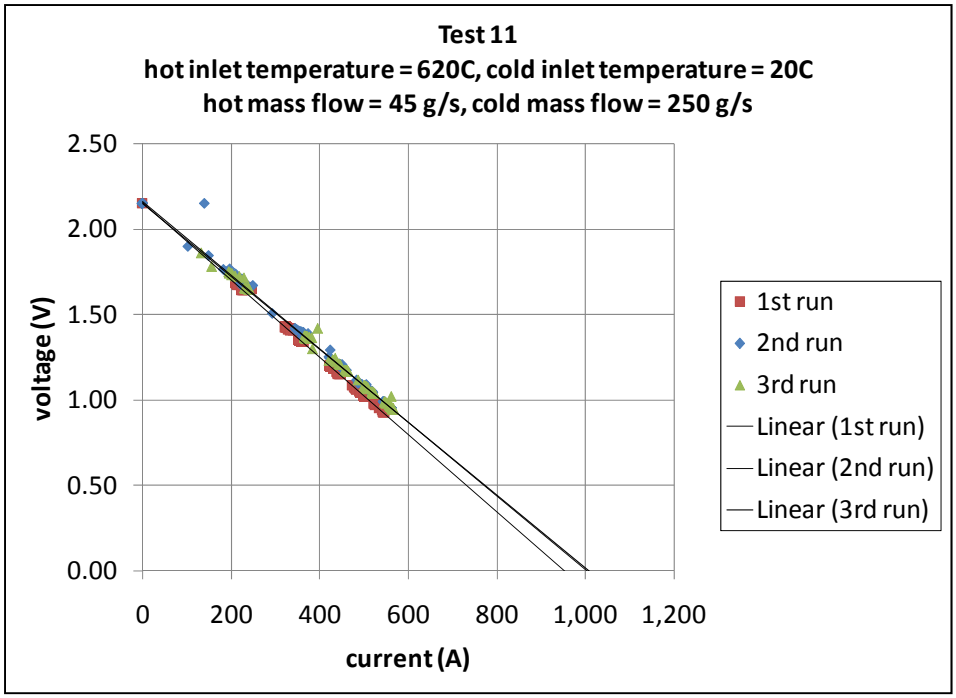

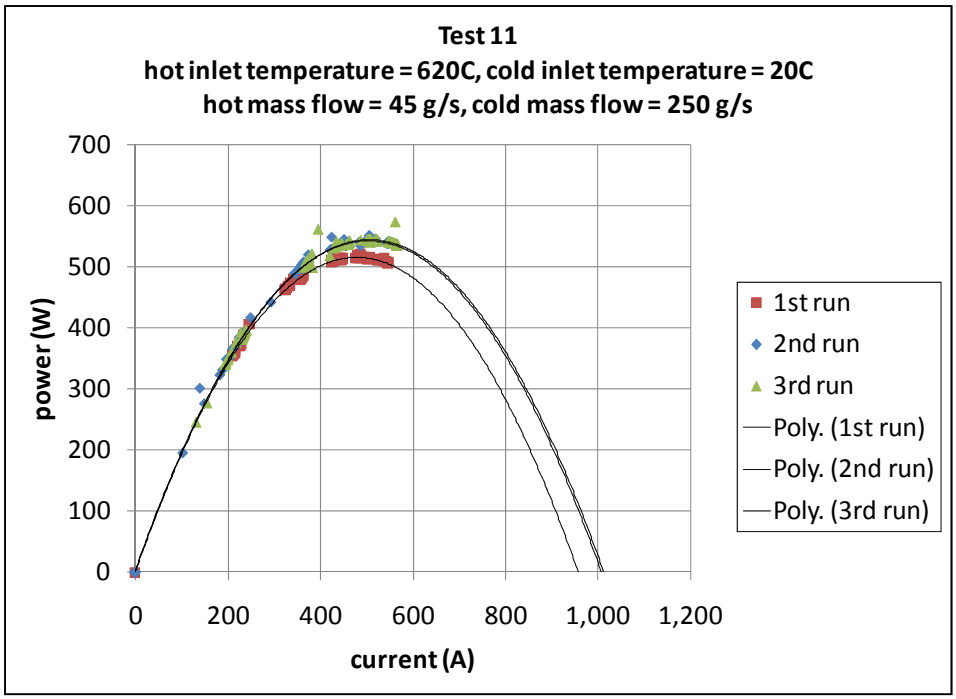

Figure 30: Run repeatability for higher temperature TEG.

The results of the Bi_2Te_3 TEG testing became inputs for the segmented TE material device. The hot and cold convection heat transfer coefficient multipliers were fixed to the values for the Bi_2Te_3 TEG and were no longer used as variables for the least squares fit of data. Table 4 lists the best fit values for the first higher temperature TEG.

Variable	Value
hot interface heat transfer coefficient (W/m^2K)	20997
cold interface heat transfer coefficient (W/m^2K)	39370
electrical interfacial resistance ($\mu\Omega cm^2$)	25.0, 17.5, 13.5
Lorentz factor	25.0, 17.5, 13.5
emissivity	0.58
free convection multiplier 1	1.75
free convection multiplier 2	1.75

Table 4. Variable values used to provide least squares fit to empirical test data.

The emissivity and free convection multipliers changed as the materials changed from the Bi_2Te_3 to the higher temperature TEG. The addition of the outer shell also affected these parameters. The hot interfacial resistance became lower because the interfacial resistance is a function of the hoop stress between the metal shunt/ring and the stainless steel (SST) heat exchanger. The hoop stress increases as a function of temperature. The cold interface became worse due to variations in manufacturing tolerances. The electrical interfacial resistance and Lorentz factors improved over the Bi_2Te_3 unit due to differences in TE materials and TE material interfaces. These variables also decreased as the device was tested further. This is thought to be caused by an annealing effect on the interfaces that results from thermal cycling. This has also been seen in thermal cycling results at the TE subassembly level. The electrical interfacial resistance went from $25\mu\Omega cm^2$ to $17.5\mu\Omega cm^2$ after the device was taken to 620°C air inlet temperature. The electrical interfacial resistance went from $17.5\mu\Omega cm^2$ to $13.5\mu\Omega cm^2$ after the chiller overheated and shutdown, causing the cold shunt temperatures to increase to over 120°C.

Figure 32 shows the empirical test results of tests 1 – 24 compared to simulated test results for air pressure drop and water outlet temperatures. The difference between the measured and simulated values is less than 5%. Again for air outlet temperature (not shown), the difference is greater than 10%, but this measured value has significant error itself due to stratification of temperature within the air flow, which is a function of air inlet temperature and air flow.

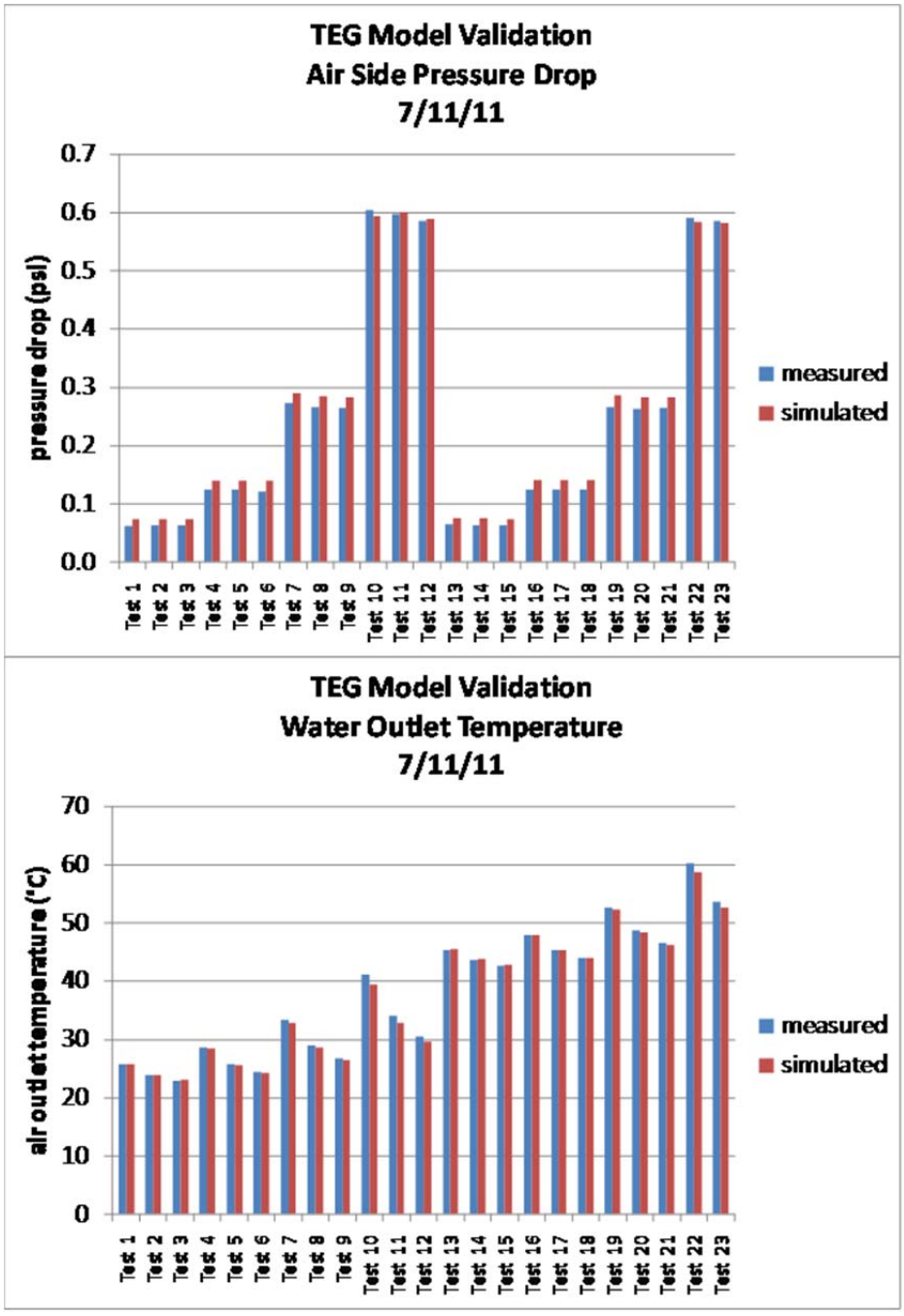

Figure 31: Higher temperature cylindrical TEG bench test results compared to simulated test results for TEG air pressure drop and water outlet temperature.

Figure 33 shows a comparison between measured and simulated data for hot and cold shunt temperatures in the TEG for Test 11. Similar graphs were achieved for all of the different test conditions. There is slightly more error in these results than the error shown in the previous results for the Bi_2Te_3 TEG. This is due to error in surface contact temperature measurements.

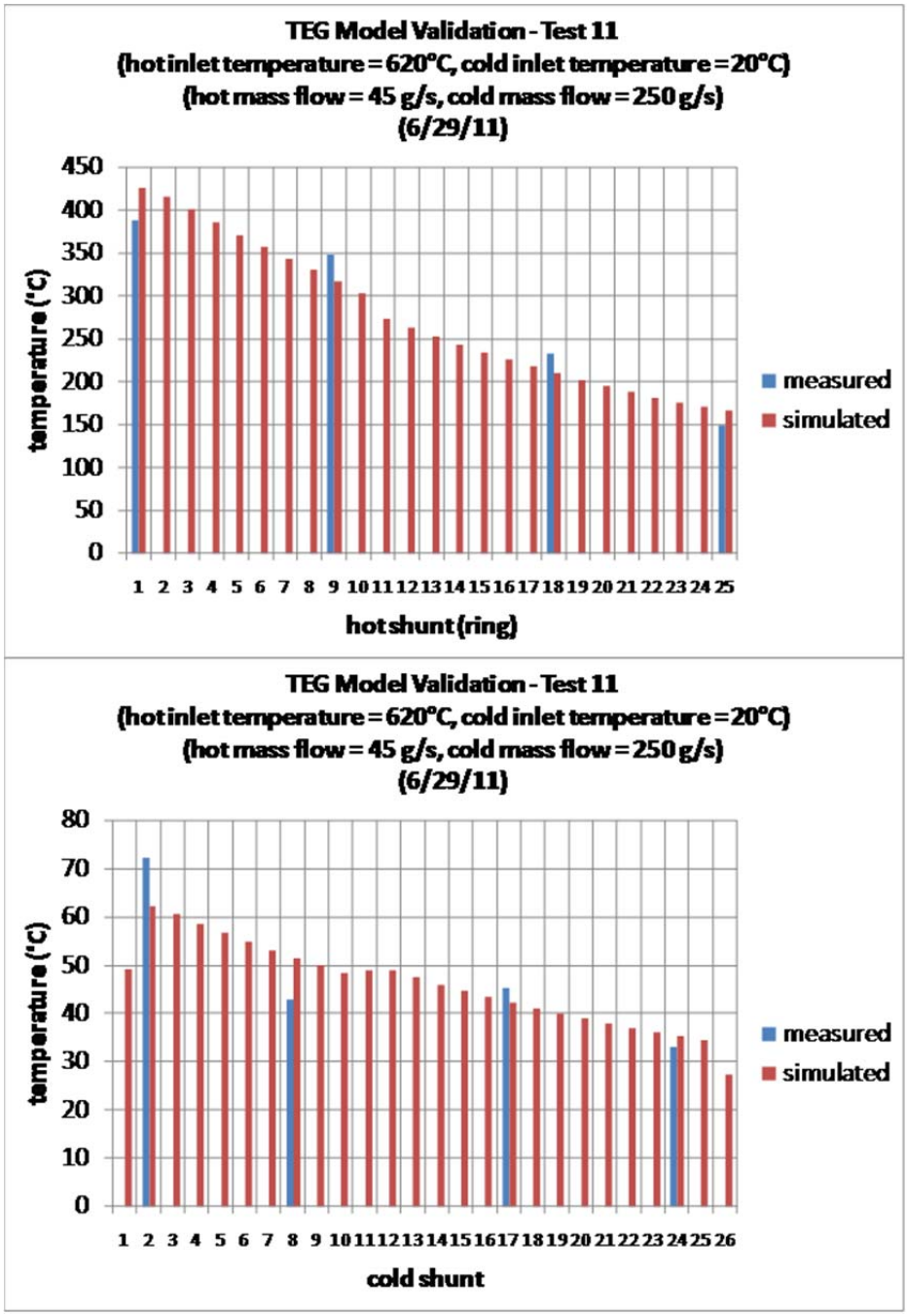

Figure 32: Higher temperature cylindrical TEG bench test results compared to simulated test results for TEG hot and cold shunt temperatures.

Figure 34 shows the measured vs. simulated voltage and power output for tests 11 and 19. Similar graphs were, again, achieved for all of the different test conditions. Error between measured and simulated data is less than 5% across the range of currents for both test conditions.

Maximum power achieved on the test bench for this TEG was 608W at Test 25 as shown in Table 3. This corresponds to a power density of 42W/L (based on flange to flange dimension including outer shell and internal bypass) and 1100 W/kg of TE material used.

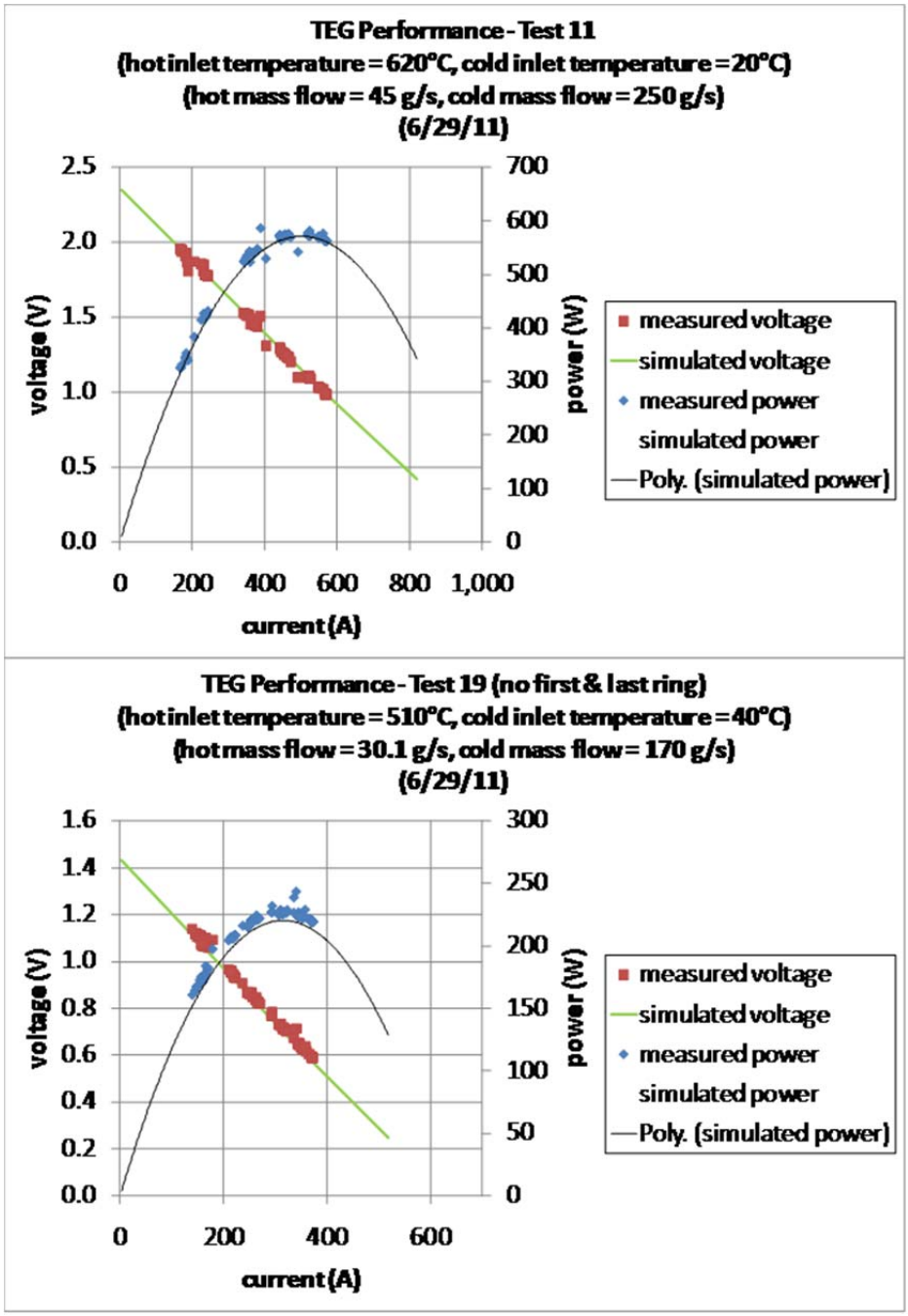

Figure 33: Higher temperature cylindrical TEG bench test results compared to simulated test results for TEG voltage and power output.

Additional tests were run on the second higher temperature TEG. These test results are shown in Figure 34. Despite the fact that this was a different TEG, the model was able to effectively predict performance for it as well.

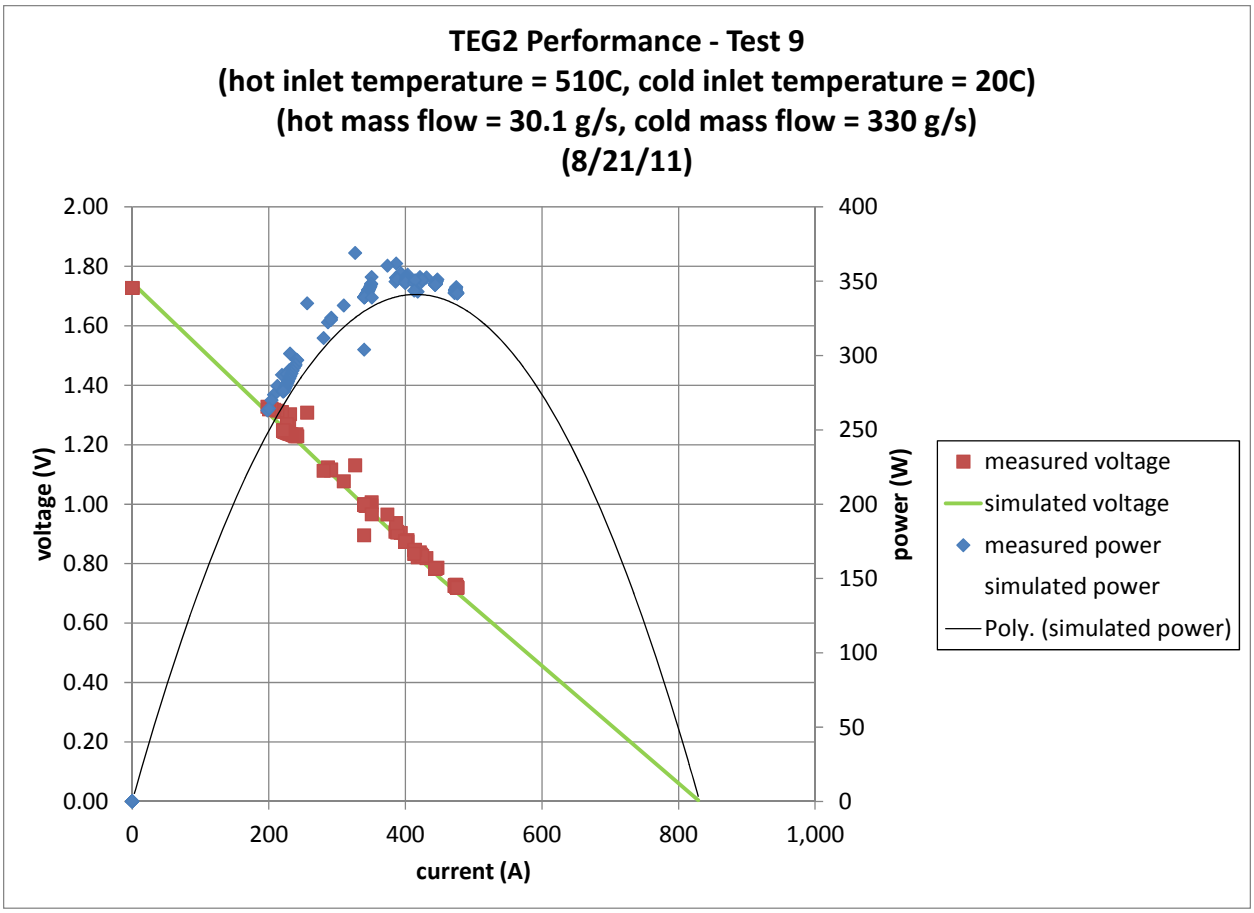
TEG2 Performance - Test 9
(hot inlet temperature = 510C, cold inlet temperature = 20C)
(hot mass flow = 30.1 g/s, cold mass flow = 330 g/s)
(8/21/11)
voltage (V)
power (W)
current (A)
2.00
1.80
1.60
1.40
1.20
1.00
0.80
0.60
0.40
0.20
0.00
400
350
300
250
200
150
100
50
0
0
200
400
600
800
1,000
measured voltage
simulated voltage
measured power
simulated power
Poly. (simulated power)

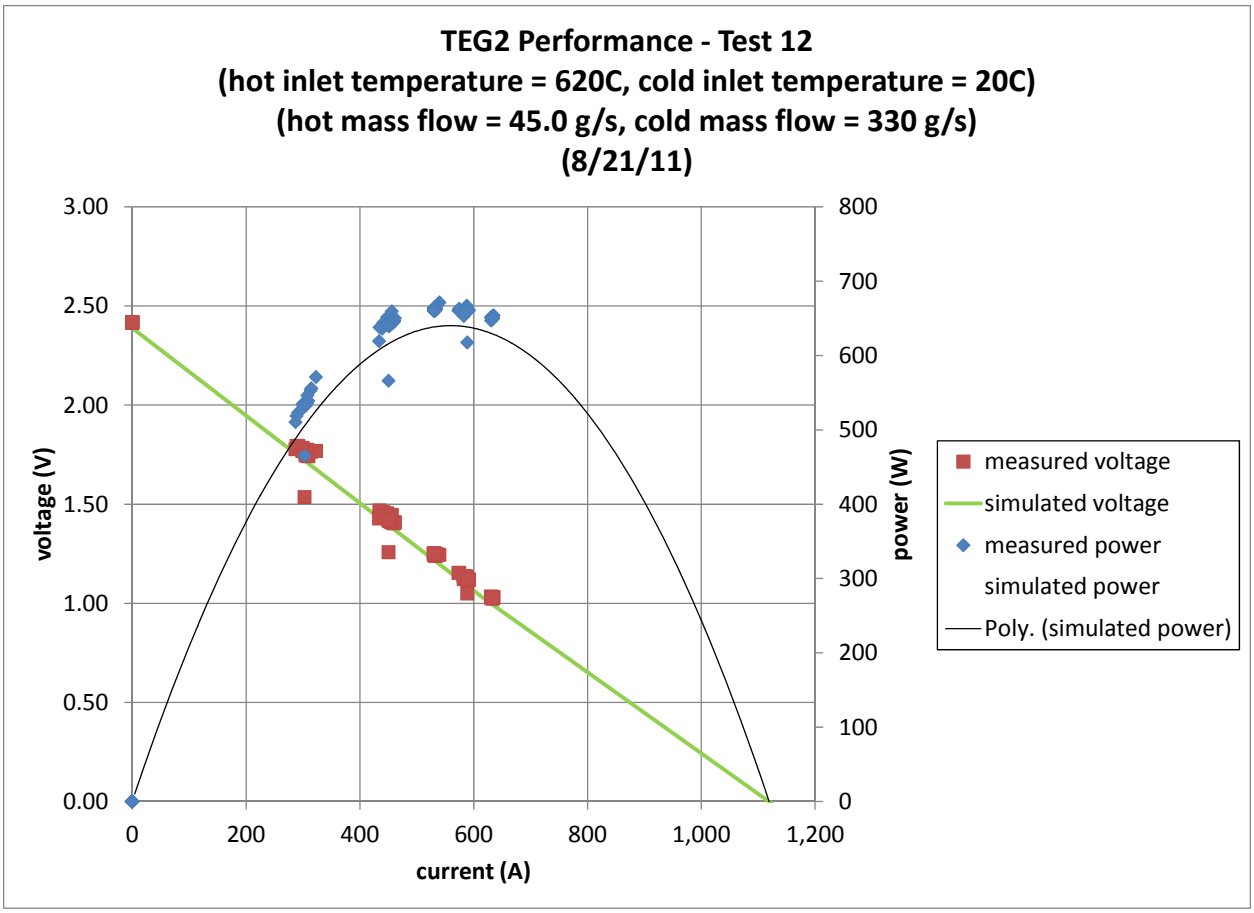

Figure 34: TEG bench test results for the second higher temperature cylindrical TEG compared to simulated test results for TEG voltage and power output.

This second TEG produced a maximum power output on the test bench of 712W for the test conditions as shown in Figure 35. This improvement over the first higher temperature TEG is due to lower interfacial resistances.

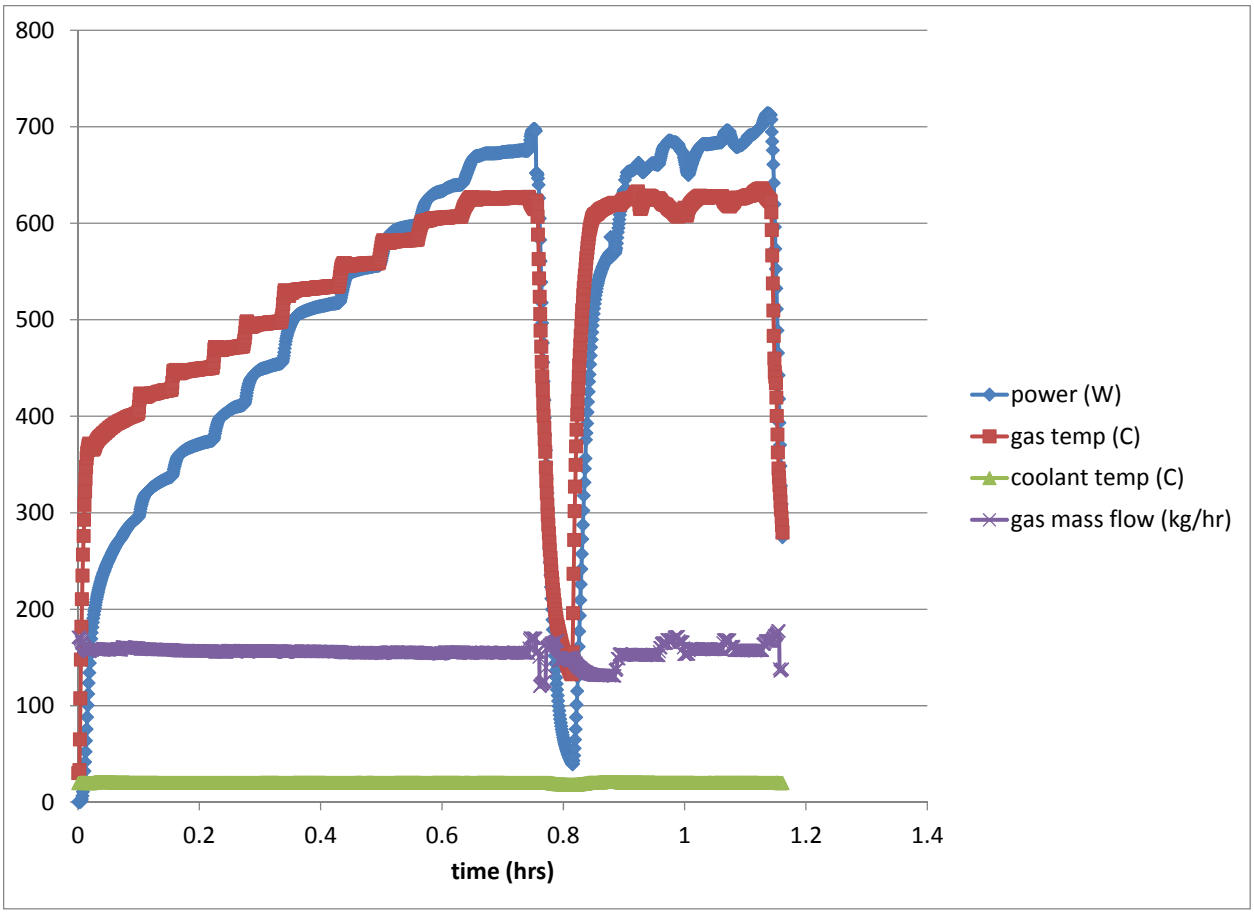

Figure 35: Second higher temperature TEG producing over 700W of power.

With the steady state device level model validated for a range of conditions and designs, this model can now be used as the starting point for the transient device level model validation. Additional component level tests were not conducted with the exception of the transient TE couple tests described in Crane [13]. The good agreement in these transient couple tests in response to a sudden change in electrical load resistance is another important building block towards the transient device level model. Transient response of the cold tubes and the hot side heat exchanger could have been tested and would certainly have helped in the validation process.

Figure 36 shows the measured and simulated transient response of the Bi_2Te_3 TEG. The first graph shows the transient response of the TEG as the hot and cold side temperatures and flows vary. The slight difference in this graph is due to the error in the steady state model.

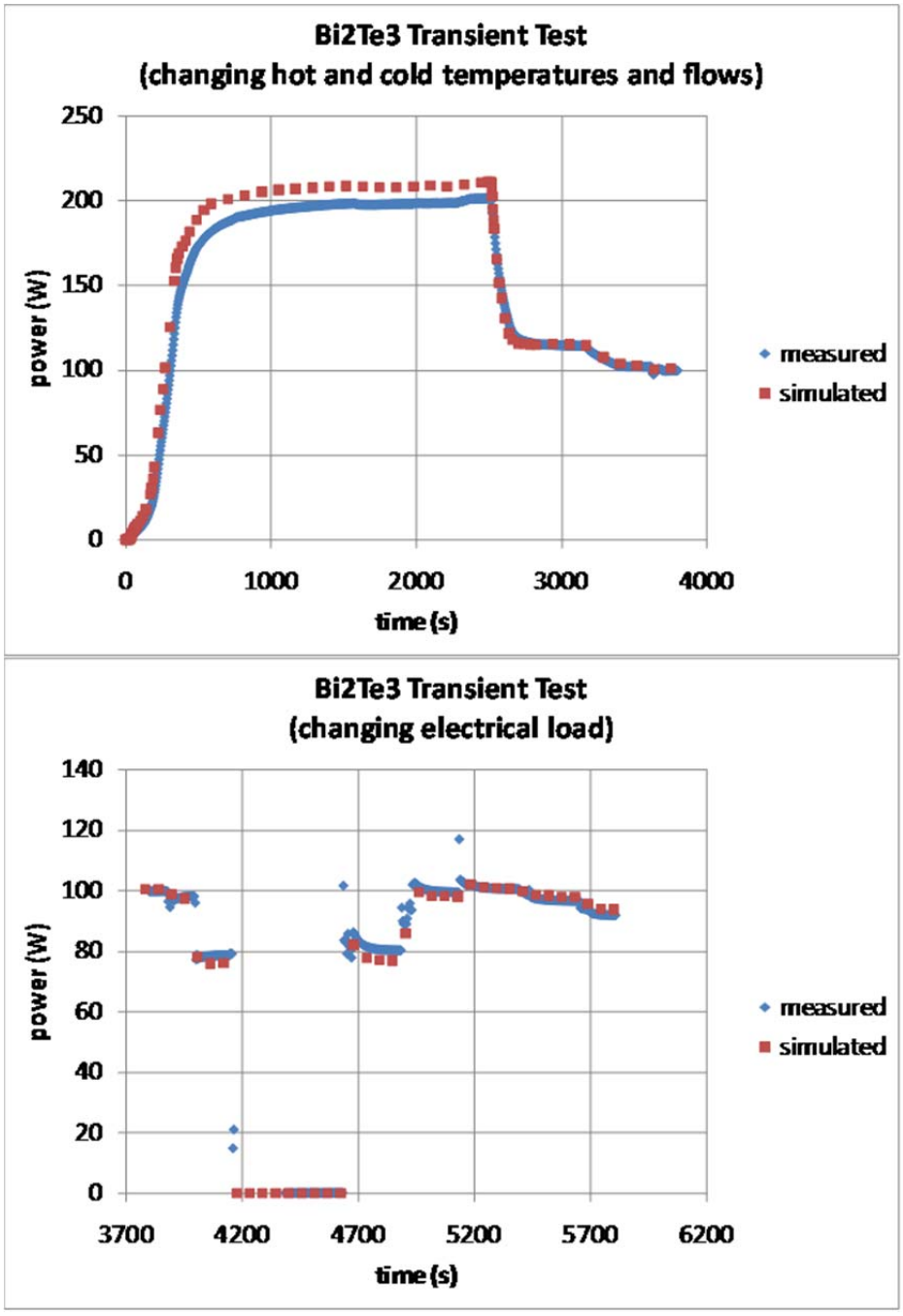

Figure 36: Transient test results for Bi_2Te_3 cylindrical TEG compared to simulated transient results

The second graph shows the transient response to changes in electrical load resistance on the TEG. This load resistance goes from open circuit to other resistances including the load resistance at peak power. All of the other operating conditions were held constant for this graph. It can be seen from these graphs that agreement between the measured and simulated data is very good. The model captures the sudden changes in temperature, flow, and load resistance. Figure 37 shows similar graphs for the medium temperature TEG.

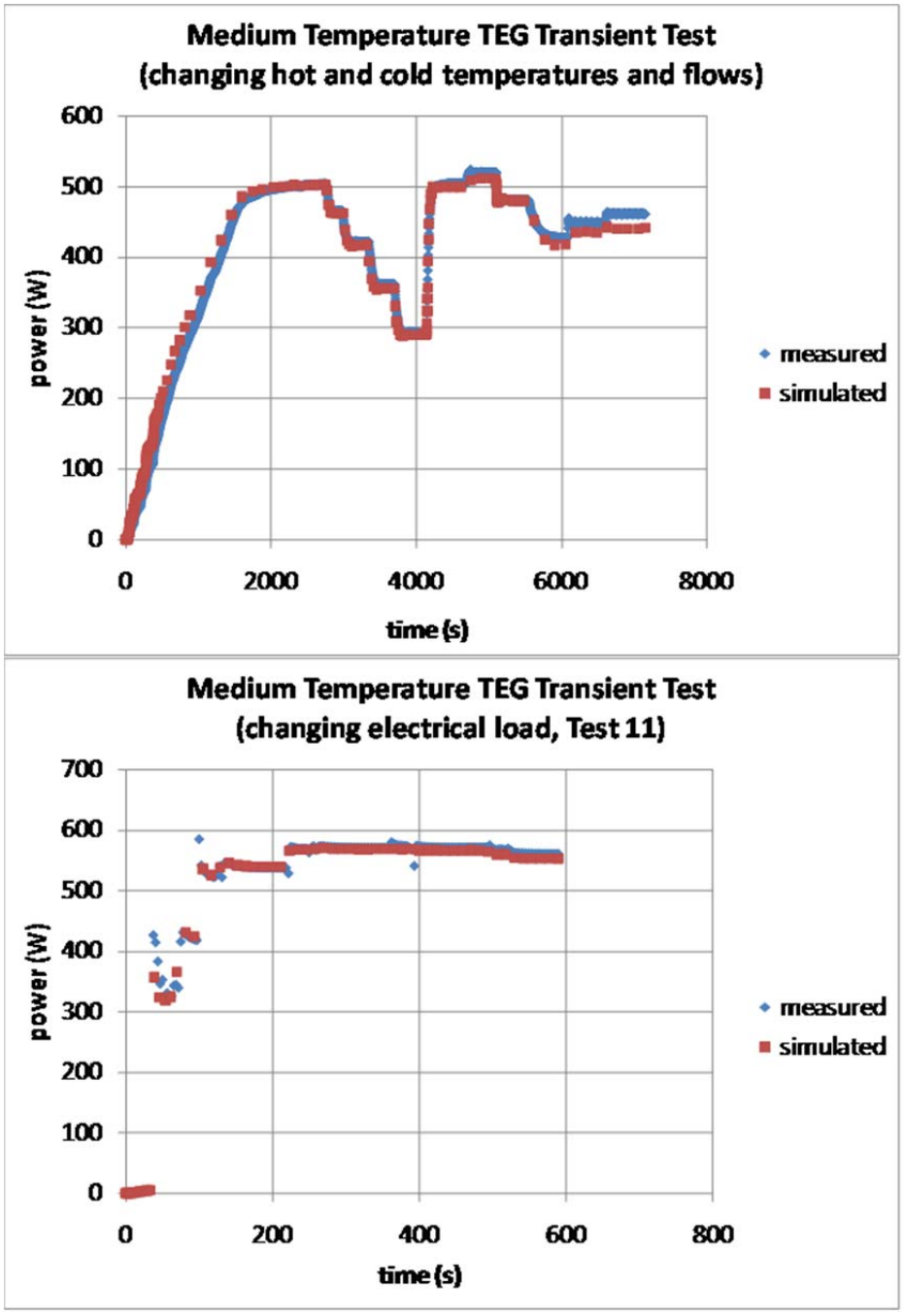

Figure 37: Transient test results for the higher temperature cylindrical TEG compared to simulated transient results

The exhaust temperature as well as the exhaust mass flow rate is rising with increased load on the engine. Hence the exhaust enthalpy is strongly dependant on the vehicle speed. However the utilized exhaust stream has to be restricted at higher speeds due to two primary aspects:

- The temperature limits of the thermoelectric material.
- The exhaust backpressure of the TEG results in negative effects on the combustion process.

In summary this leads to a peak in electric power for the so-called design point that was chosen for this specific prototype vehicle at 125 kph (78 mph). Additionally the highest power output is reached for constant driving conditions due to the thermal inertia of the TEG component.

In summary, computer performance modeling guided the design and development of thermoelectric engines and the TE Generator, from initial planar designs into a compact and robust cylindrical form with the key building block, a stack designed n and p couple, maintained throughout the evolution.

Faurecia exhaust system development-

Exhaust System Bypass Valve

A bypass valve was used to control temperature into the thermoelectric engines. A maximum temperature limit was programmed into the valve so that it would close or partially close to protect the thermoelectric engines from thermal overload. The bypass would redirect exhaust flow from the thermoelectric generator around the periphery of the bypass exhaust tube to an open bypass tube in the center of the assembly.

The following inputs were considered for controlling the valve angle;

1) Engine RPM, 2) Mass Air Flow, 3)Engine Oil Temperature, 4)Gas Pedal Position, 5)Exhaust Manifold Pressure, 6)Exhaust Gas Temperature, 7)Heat Exchanger Surface Temperature

Three operation condition methods were used, 1) Warm-up phase, 2) Full engine power phase, and 3) Full heat recovery phase.

The warm-up phase uses the following conditions to determine open or closed bypass valve;

- Triggers by-pass condition (determined by whether valve is open or closed)
- Exclusively determined by “cold” engine conditions i.e. when the engine oil temperature is below a pre-determined threshold
- This condition is to aid warm up of post TEG catalytic converter for emissions reasons

The full power phase uses the following conditions to determine open or closed bypass valve.

- Triggers by-pass condition (determined by whether valve is open or closed)
- Determined by gas pedal position sensor[1]

This condition is to reduce backpressure of TEG system by reducing the maximum gas flow through the TEG.

The full heat recovery phase uses the following conditions to determine open or closed bypass valve.

- Valve position determined by map (temperature vs. air mass flow > valve opening)
- Valve will be used as a throttling device to deliver heat into the heat exchanger
- Valve will also be used in this mode to prevent overheating of the TEG modules during high engine operating conditions
- Within the controller will be a closed loop feature which will maintain a set operating temperature of the heat extractor by varying the valve angle

[1] gas pedal position sensor may not be exclusively used to determine this condition – it could be throttle rate application, calculated throttle demand, etc

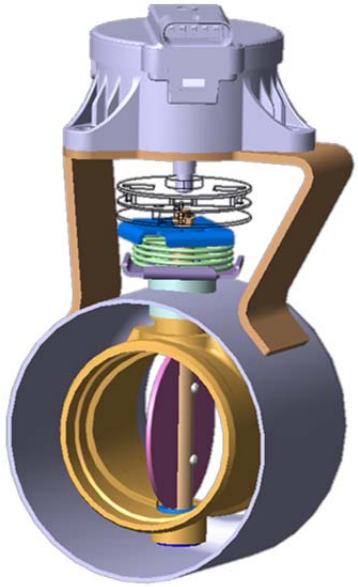

Figure 38: Bypass Valve

Outer Shell- Faurecia

The purpose of the outer shell was to protect all thermoelectric generator internals, and to make the assembly leak free. Shell thickness was 0.9mm using 316L stainless steel. This grade of material was chosen because it contains low carbon which resists carbide precipitation during welding.

The shell started as a blank, was rolled and then seam welded to create the round tube. A stringent zero leak rate was a requirement. To accomplish this, first the shell was assembled to the thermoelectric generator and TIG welded. Second the full assembly was coated with a proprietary coating from Praxair to fully make the assembly leak proof. The entire outer surface of the shell was coated.

Zero leak requirement was needed so that the thermo electric engines would not be exposed to oxygen from the atmosphere which leads to corrosion on the thermo electric engines and negatively affects the interfacial contact which contributes to reduced voltage output.

The TEG assembly was leak checked with the vessel pressurized at 104 kPa with helium.

All valves and ports (see Figure 39) were Metal Inert Gas (MIG) welded to the outer shell.

Two valves were used to add an inert atmosphere to the internal of the assembly. Argon was chosen to protect the thermoelectric engines. An instrumentation port was also welded to the outer shell. The purpose of the port was so that thermocouples could monitor internal temperatures. Electrical interface connections were welded to the shell so that the voltage output of the TEG assembly could flow to the vehicle electrical system.

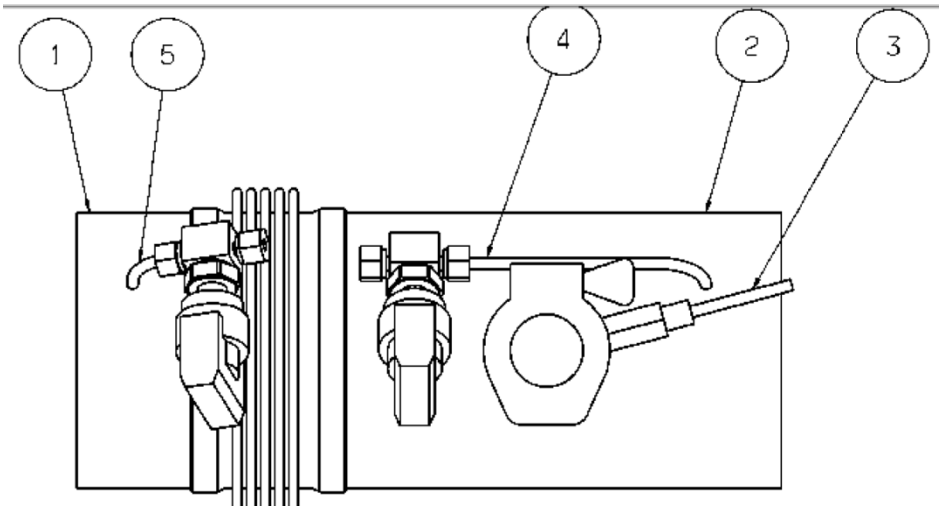

Figure 39: Isometric view of the assembled shell and bellows.

Component #1 and #2 (not shown) – Electrical Connections (positive and negative)

Component #3 – Instrumentation port

Component #4 and #5 – Fill and purge valves for inert gas

Vehicle development and testing

Engine Dynamometer testing at NREL

One of the two higher temperature TEGs was sent to ETC (supervised by NREL) for performance testing on an engine dynamometer. The test setup included a BMW 6 cylinder engine and a Boysen exhaust component, including the catalytic converters. The TEG was mounted downstream of the catalytic converters and tested over a range of steady state engine conditions at different coolant temperatures and flow rates. The TEG was also tested over the New European Drive Cycle (NEDC) and US06 drive cycles. Test results from these tests are shown in Figures 41-44.

Figure 40 shows steady state test results for engine conditions that ranged from 1300 – 3000 RPM and 50 – 105 Nm. Coolant temperatures ranged from 30C – 80C, and coolant flow rates ranged from 10 – 20 lpm. Expected trends can be seen from this data as TEG power output increased with engine RPM and torque. TEG power output was also higher at lower coolant temperatures and higher coolant flow rates.

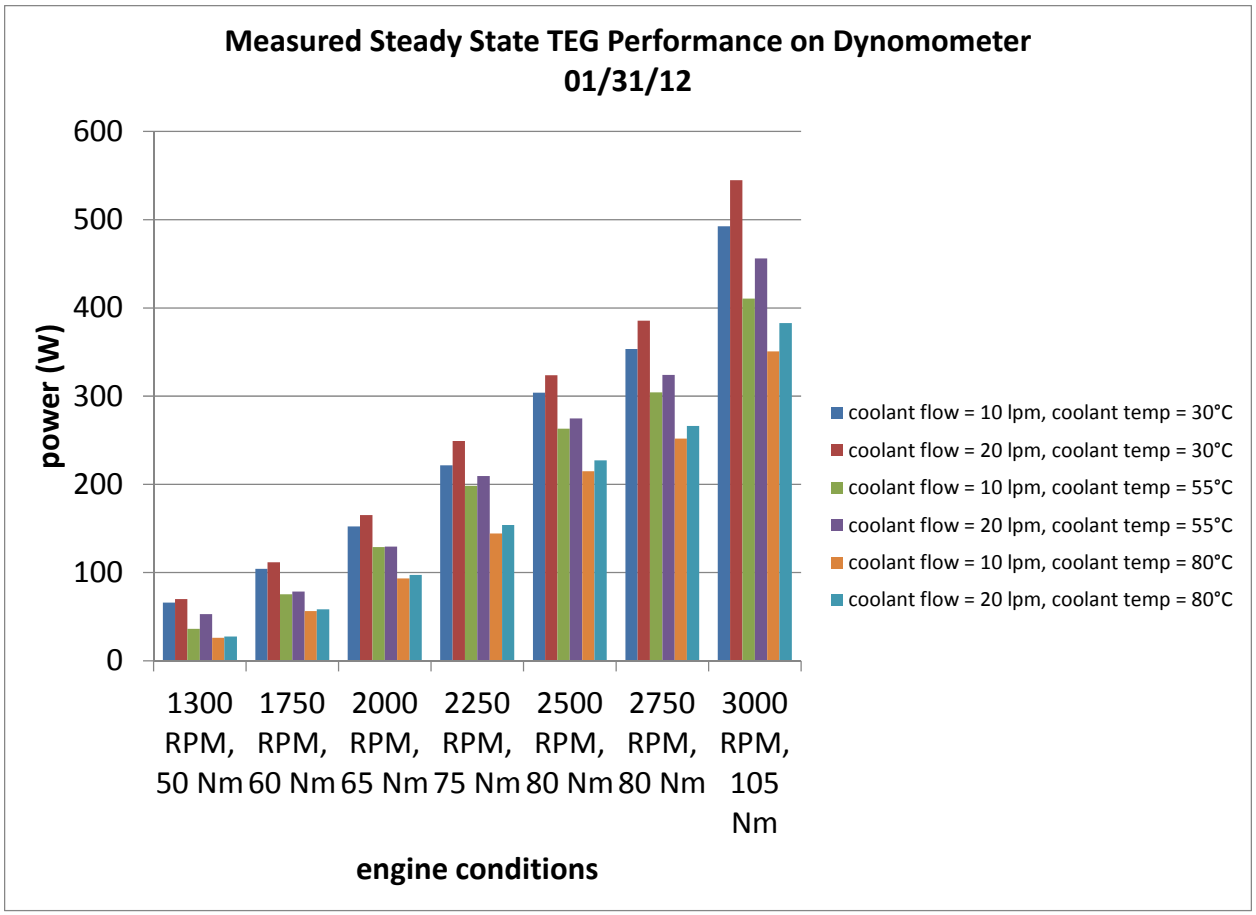

Figure 40: Measured steady-state TEG performance on the engine dynamometer at various RPM, torque, and coolant temperature and flow.

Figure 41 shows the repeatability of 4 tests done before and after the transient engine tests were performed. It can be seen from the figure that the power output was repeatable for these tests. If anything, performance improved slightly for 3 of the 4 conditions. Differences in performance could be due to the tests not being fully at steady state, interfacial resistances continuing to improve, or thermal inertia being higher in the later tests.

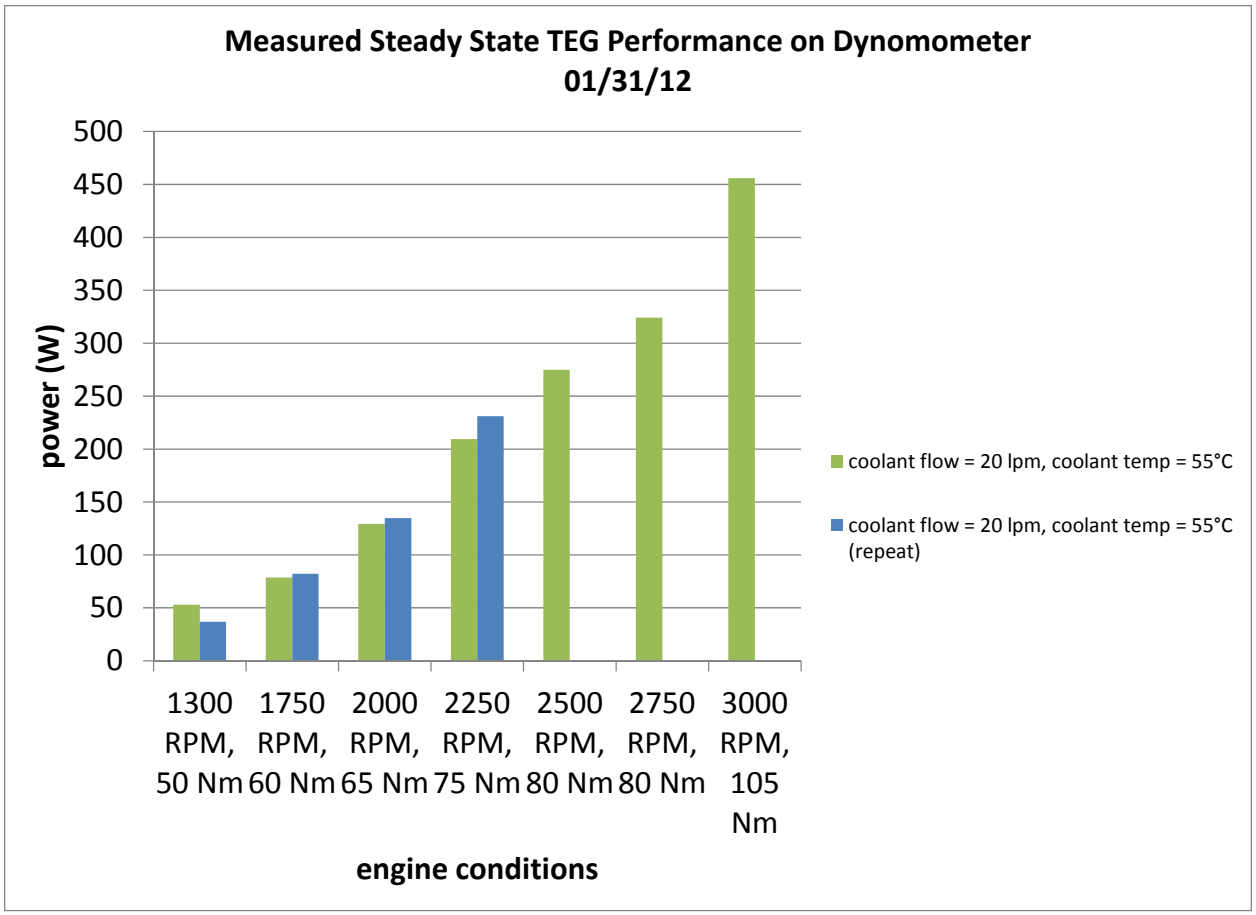

Figure 41: Measured repeatability of steady-state TEG performance on engine dynamometer.

Figure 42 shows the performance of the TEG for the NEDC drive cycle. This is largely a city cycle with a more substantial load at the end of the cycle. Two NEDC cycles were run back to back with a 60 second idle in between. It can be seen from the graph that power output was again repeatable. The slight improvement in performance for the second drive cycle was probably due to the engine being warmer than for the first cycle.

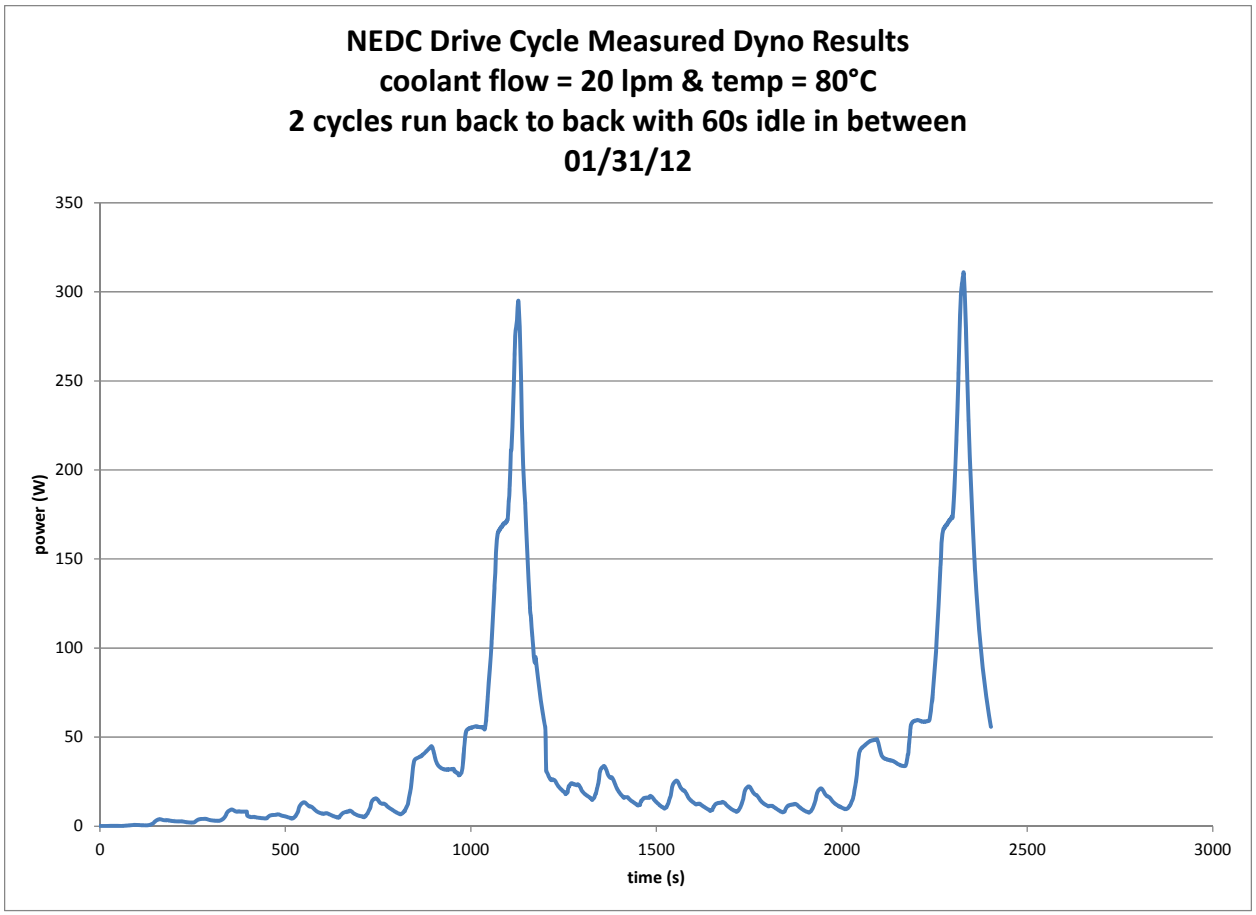

Figure 42: Measured TEG performance on engine dynamometer for NEDC drive cycle. Two drive cycles were run back to back with a 60 second idle in between.

Figure 43-45 show the results of TEG performance during the US06 drive cycle. The US06 drive cycle is a much more aggressive drive cycle than the NEDC. It is more representative of highway driving with more significant accelerations. The result of the more aggressive drive cycle is higher loads on the engine and more waste heat for the TEG to convert to electricity. Again, two cycles were run back to back with a 60 second idle in between. The cycles were run at coolant temperature of 80C and 55C to show what could be a possible benefit of using a lower temperature, auxilary radiator. There was almost a 50 - 100W improvement in power output for many conditions when the coolant was 55C compared to 80C. Figure 43 shows the power output for these tests with a maximum power achieved over 500W. It should be noted that the bypass valve control scheme could not be implemented for these tests. Thus, the bypass could only be either open or closed. Figure 43 also shows the TEG power output with the bypass valve full open or full closed. A throttling bypass valve would be expected to show performance in between the two curves. Figures 45 and 46 show the hot and cold shunt temperatures at 5 different locations along the length of the TEG for the US06 drive cycle with the bypass valve full closed.

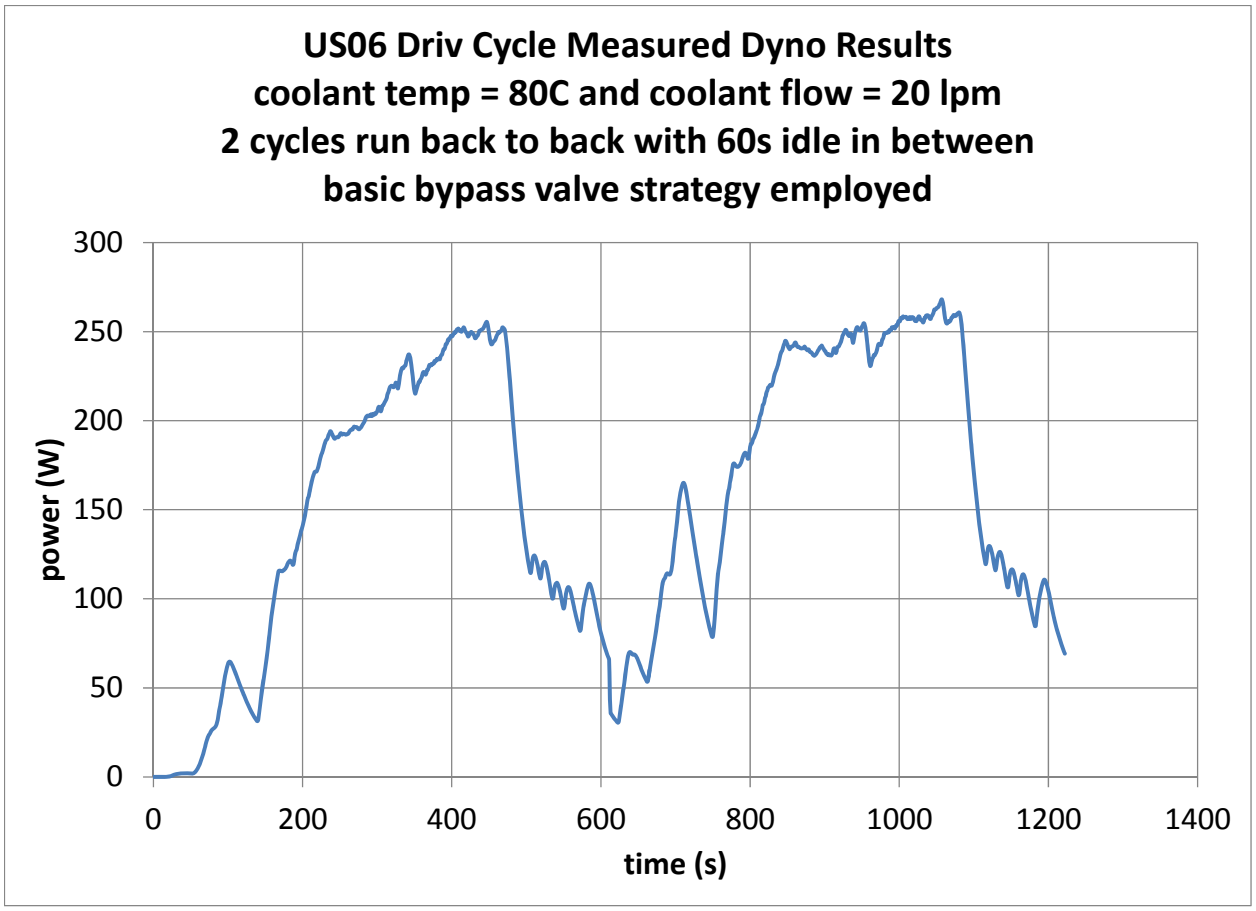
US06 Driv Cycle Measured Dyno Results
coolant temp = 80C and coolant flow = 20 lpm
2 cycles run back to back with 60s idle in between
basic bypass valve strategy employed
power (W)
300
250
200
150
100
50
0
0
200
400
600
800
1000
1200
1400
time (s)

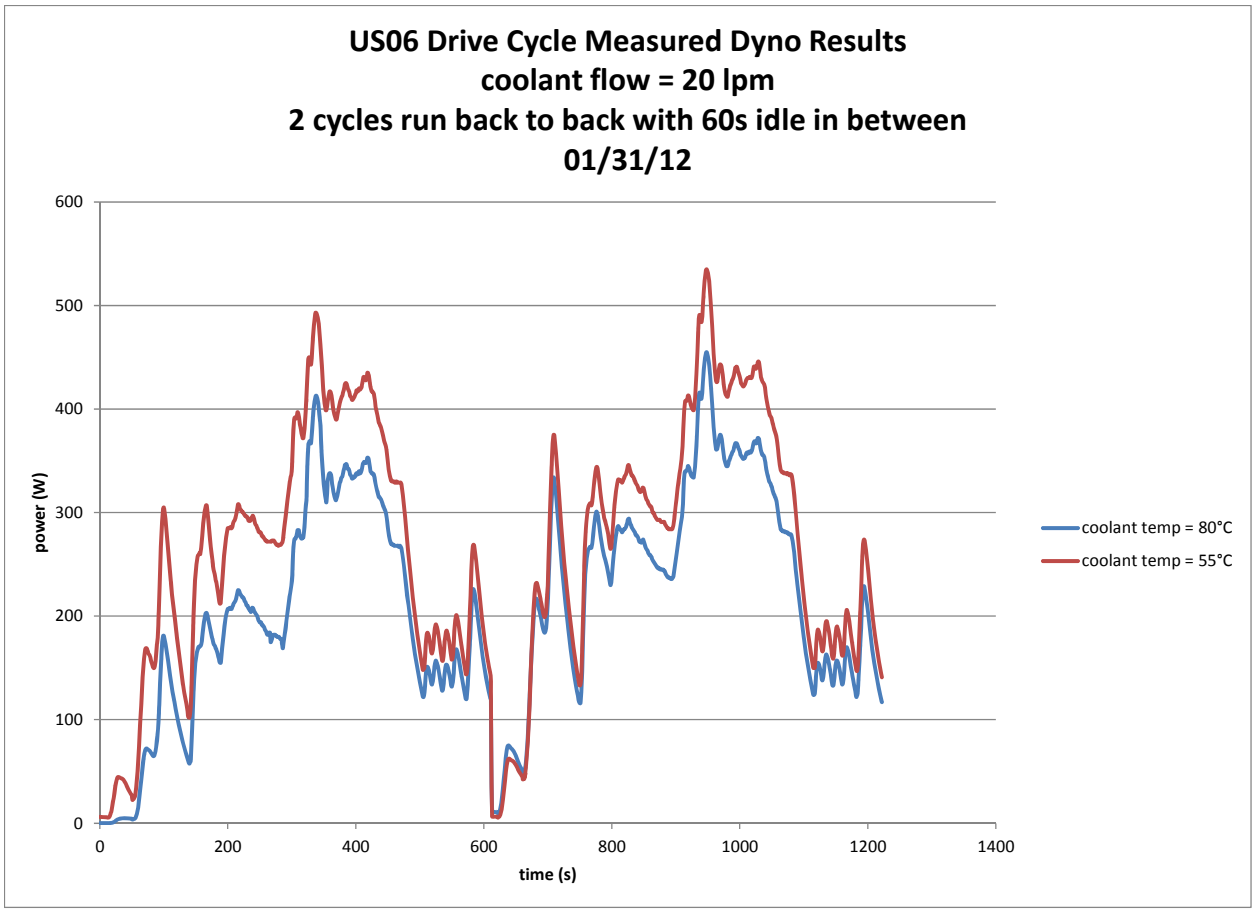

Figure 43: TEG power output for TEG over the US06 drive cycle with bypass valve full closed or with a non-optimal bypass valve strategy.

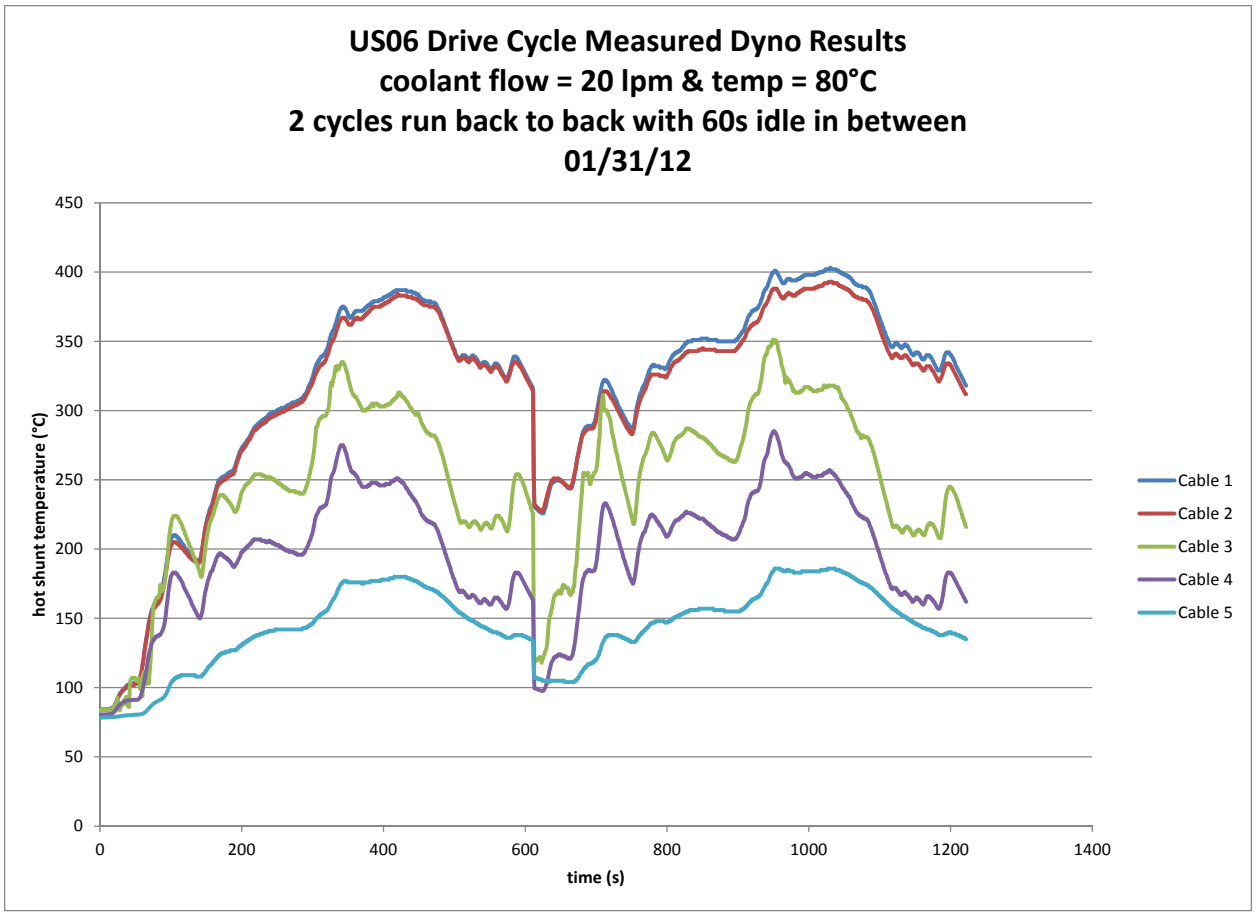

Figure 44: Hot shunt temperatures during the US06 drive cycles with the bypass valve full closed.

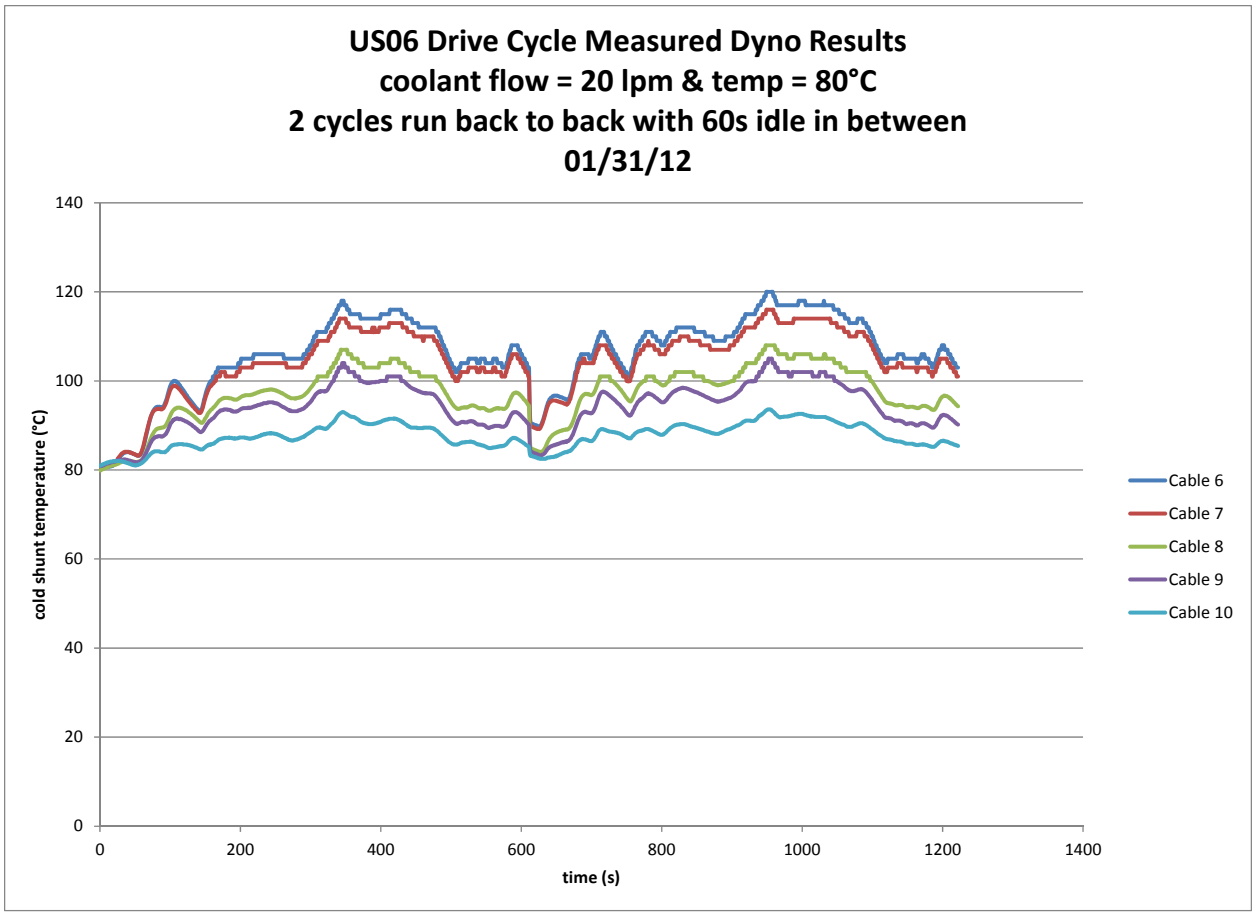

Figure 45: Cold shunt temperatures for the US06 drive cycle with the bypass valve full closed.

BMW vehicle tests

The phase 5 TEG component was integrated into a BMW X6 35i xDrive test vehicle for a final system evaluation in an application-oriented setup. The focus of the system integration was to minimize the negative impact on the regular vehicle components (for example the cooling system, engine performance etc) whilst promoting the most optimal TEG performance.
The first section summarizes the several aspects of the TEG installation while the following parts describe the measurement results for constant and dynamic driving conditions.

TEG system integration into a BMW test vehicle

Instrumentation

The thermoelectric generator has a variety of interfaces and interactions with the surrounding vehicle. In order to analyze the impact of the TEG on the total system performance, numerous temperature, voltage, electric current, differential pressure and volume flow sensors were installed. An A/D signal converter merges all data channels into a digital CAN communication network.
A specific application engine control unit (ECU) provides additional information about engine related values such as the engine speed, load and fuel consumption.
Furthermore an automotive control unit is installed that gathers all measured data and ECU values and processes it by means of a developed control strategy. In particular the exhaust valve and the auxiliary

water pump are controlled in a closed-loop circuit for an optimal utilization of the TEG during dynamic and volatile driving conditions.

Cooling system integration

The generated electric power of the TEG strongly depends on the temperature level of the coolant. Furthermore BMW vehicles have a specific heat-up strategy to reduce fuel consumption and increase passenger comfort. The overall objective was to maintain the lowest coolant temperature for the TEG whilst keeping the engine unaffected from this additional component in the cooling loop. Hence the TEG was installed in parallel to the engine with an auxiliary water pump for the purposes of generating a sufficient coolant flow rate (see Figure 47).

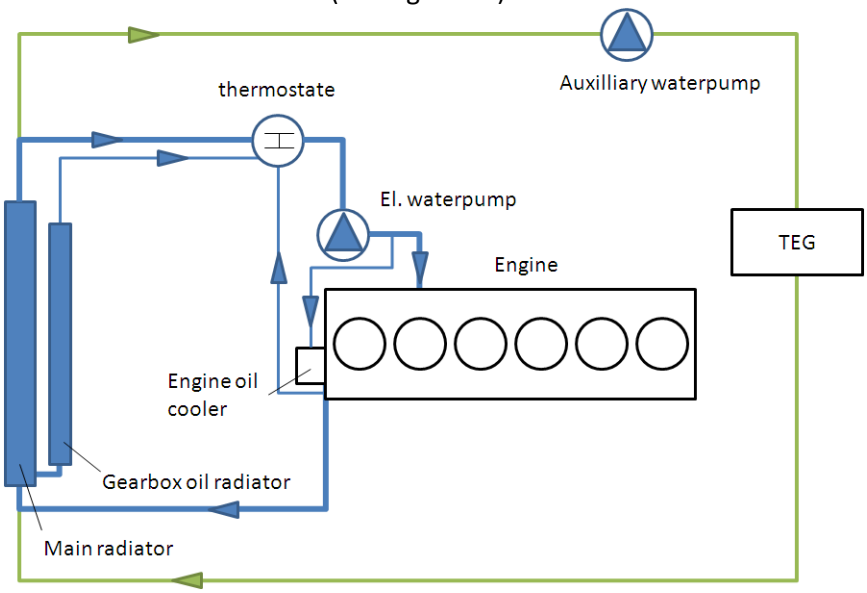

Figure 46: Integration of the TEG into the cooling system of the prototype vehicle

The coolant temperatures are measured at the inlet and outlet port of the TEG in conjunction with the coolant volume flow rate. Based on these values the demand value of the auxiliary water pump is controlled with the goal to minimize the power consumption while ensuring a sufficient cooling power. A non-return valve in the TEG tube prevents fatal damage of the engine in the event of auxiliary water pump failure.

Integration into the power circuit of the vehicle

The TEG component has a high number of parallel current paths and a limited amount of electrical serial TE-elements. Therefore the voltage level of the TEG is too low to use a DC/DC boost converter for a direct integration into the vehicular power circuit, which has a typical voltage of 14V. Hence in this particular prototype vehicle the generated electrical power from the TEG is not utilized to lower the load on the alternator. Rather, a fixed electrical resistor is simulating the electrical load on the TEG and is equipped with voltage and temperature sensors for a precise calculation of the generated power. The impact on fuel consumption is determined by a calculated shift in the engine map based on the TEG power divided by the actual alternator efficiency.

Exhaust system integration

The TEG is installed upstream of the middle muffler roughly 1m behind the main catalyst. In order to maintain the exhaust gas temperature as high as possible at the TEG inlet the exhaust line between the catalyst and the TEG is encapsulated by a thermal insulator (see Figure 47).

Figure 47: TEG integration into the exhaust line of the BMW X6 prototype vehicle

A critical role is assigned to the exhaust valve at the rear end of the TEG. The valve can be opened continuously and splits the total exhaust stream between the outer TEG section and the internal bypass path. This distribution of exhaust between the two paths has a high impact on the exhaust backpressure, the heat rejected to the cooling system and the temperature of the TE elements. The goal of the closed-loop exhaust valve control strategy is to maintain the highest possible power output of the TEG whilst keeping the previously mentioned system values below the allowed limits. This three level strategy is displayed in the following Figure 48.

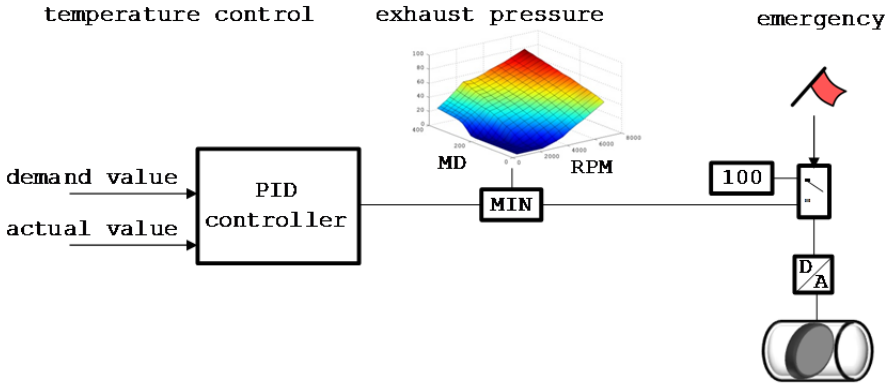

Figure 48: Three level control strategy of the exhaust valve

The first level determines the optimal exhaust valve position with respect to the system temperature. This value is handed over and limited by the second level that takes the engine load and engine speed into consideration. The third and last level requests a fully opened exhaust valve in case of a detected emergency (e.g. temperature limit, pump failure etc).

TEG performance data for stationary driving conditions

The exhaust temperature as well as the exhaust mass flow rate is rising with increased load on the engine. Hence the exhaust enthalpy is strongly dependant on the vehicle speed. However the utilized exhaust stream has to be restricted at higher speeds due to two primary aspects:

- The temperature limits of the thermoelectric material.
- The exhaust backpressure of the TEG results in negative effects on the combustion process.

In summary this leads to a peak in electric power for the so-called design point that was chosen for this specific prototype vehicle at 125 kph (78 mph). Additionally the highest power output is reached for constant driving conditions due to the thermal inertia of the TEG component. The following graph shows the measured power output and the calculated fuel consumption reduction for various vehicle speeds.

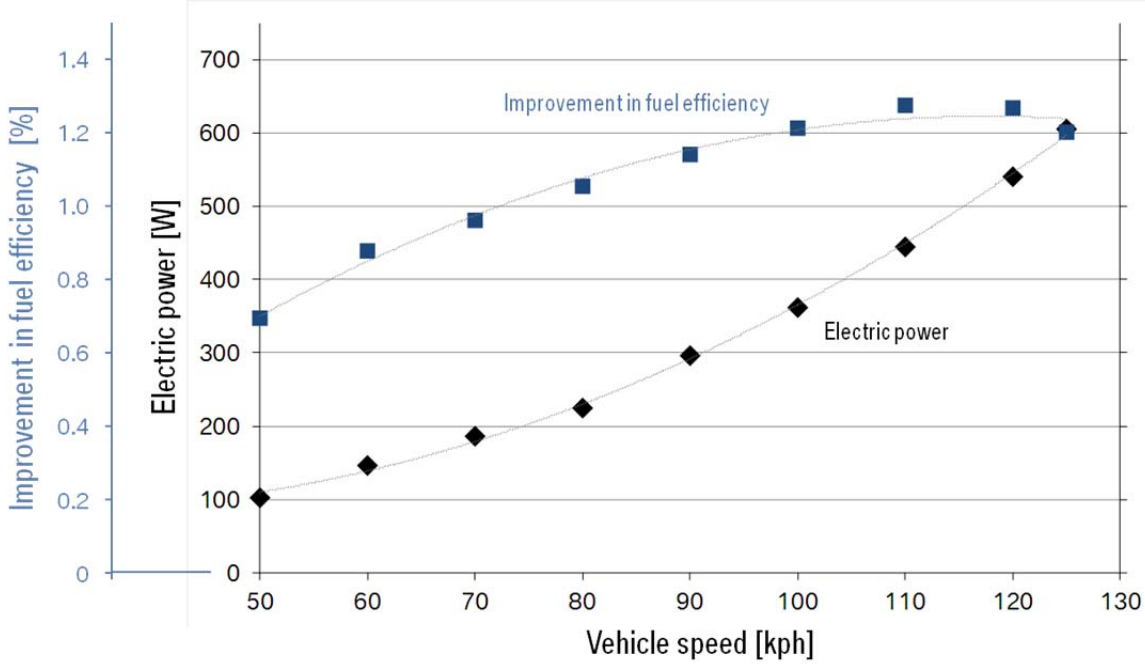

Figure 49: Power output of the TEG and the improvement in fuel efficiency over vehicle speed

The prototype vehicle was tested on a closed track. Each data point represents the final value after several minutes of driving with constant speed. It is evident that the power output increases with speed due to the rising exhaust enthalpy. At the design point a power output of the TEG of 605W was measured. The relative change in fuel efficiency improvement depends on the actual fuel consumption which is rising with increasing vehicle speeds. Therefore the two curves in Figure 49 have different slopes and the relative improvement in fuel efficiency culminates at app. 110kph with a value of over 1.2%.

TEG performance data for dynamic driving conditions

The closed-loop control strategy of the TEG system enables an unaffected driving behavior of the prototype vehicle compared to a regular car. An installed data-logger saves the measured and calculated values during usual and dynamic test drives. The following figure shows a representative use case.

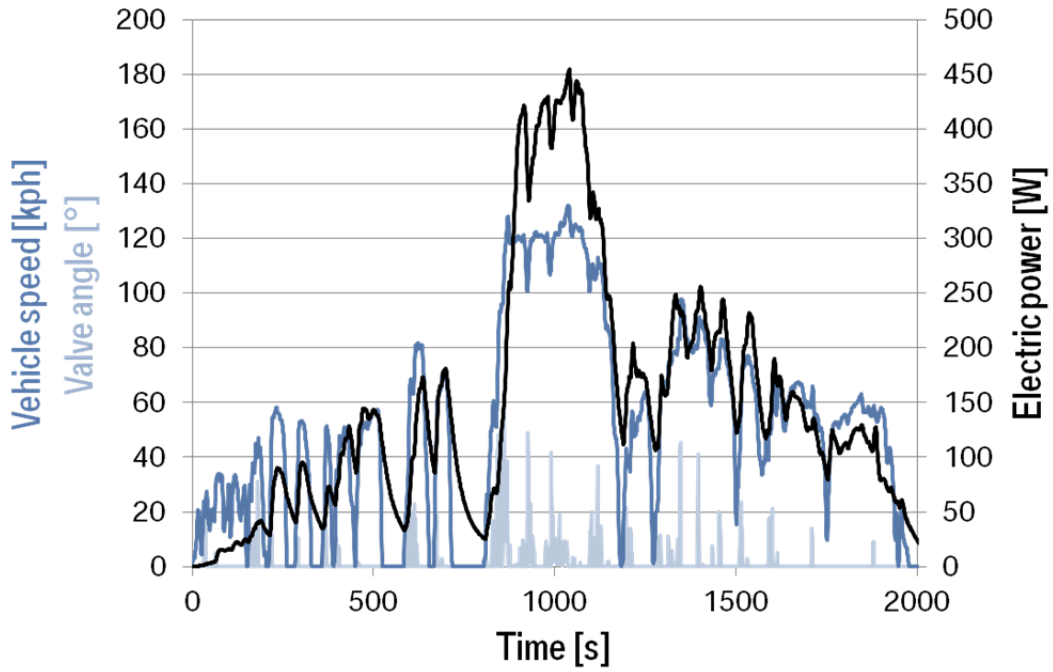

Figure 50: Electric power output, vehicle speed and exhaust valve angle over time for a dynamic test drive

Similar system behavior is observed for constant and dynamic driving conditions as the power output rises with increasing speed. A limiting factor is the need to open the exhaust valve during the acceleration phases (hence a loss of exhaust enthalpy for the heat recovery system) in addition to the thermal inertia of the component.
Therefore the achieved power output is app. 450W for a vehicle speed near the design point in contrast to more than 600W for similar steady-state conditions. Repeated test drives show no degradation in power output of the component for the first few months. The tests will be conducted further as a first indication of the thermo mechanical durability of this component.

Ford Vehicle Testing

A Phase 5 TEG was integrated into a Ford Motor Company vehicle for on-road testing. The vehicle selected for the integration was an all-wheel drive 2011 Lincoln MKT with a 3.5L V-6 Twin-Turbocharged Gasoline Direct-Injection engine and a 6-speed automatic transmission. This vehicle has a rated fuel economy of 16mpg City and 22mpg Highway and the engine is rated at 355 horsepower @ 5700RPM and makes 350 lb-ft of torque at 1500 to 2500 RPM. A picture of the test vehicle used in this study is shown in the figure below.

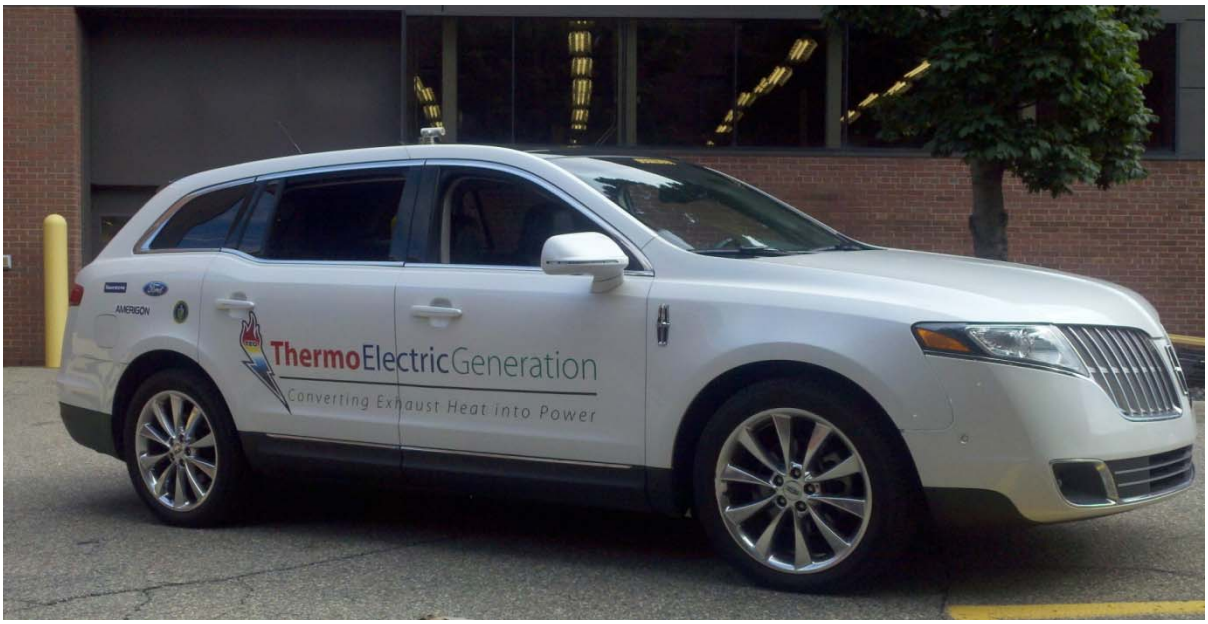

Figure 51: Lincoln MKT test vehicle used for TEG integration and road-test evaluations.

In order to minimize interference with or degradation of vehicle emissions, the TEG was mounted downstream of the light-off and mid-body catalysts. This placed the inlet to the device nearly 2 meters from the outlet of the exhaust flanges. The cooling circuit was integrated directly into the vehicle primary cooling system. Electrical power generated by the TEG was dissipated in a matched load resistor that was mounted in the 2nd row of the vehicle. A photo of the final mounting and integration of the unit is shown in the figure below.

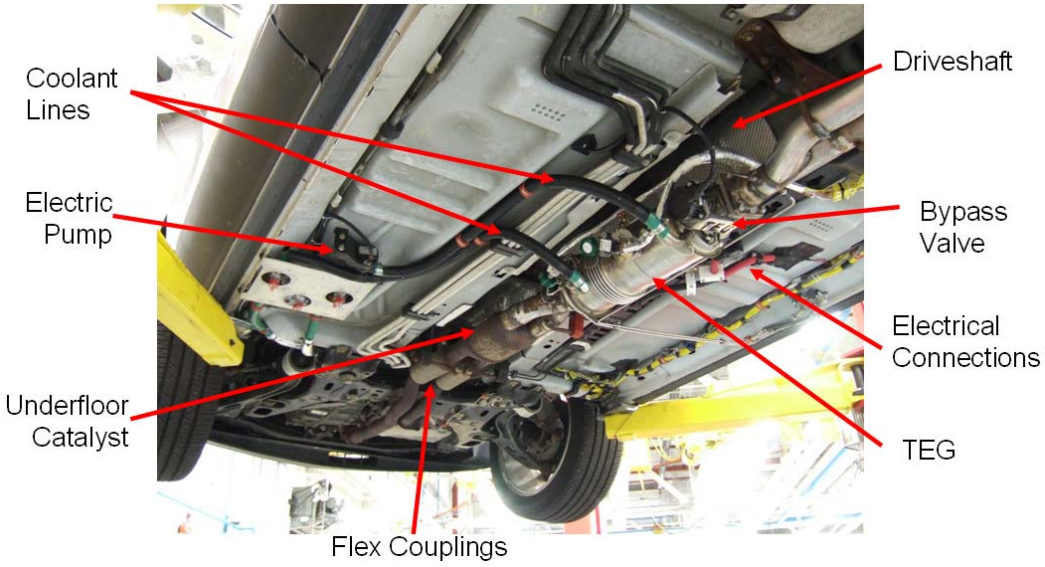

Figure 52: Integration of the TEG into the underfloor of the test vehicle. The front end of the vehicle is at the bottom left of the image.

The testing consisted of over 50 hours of on-road evaluations at various operating parameters. These included cold-start, highway steady speed cruise, and city stop and go driving. An example of each type of drive event is shown in the figures below to provide results typical of the performance measured during the total test evaluation phase.

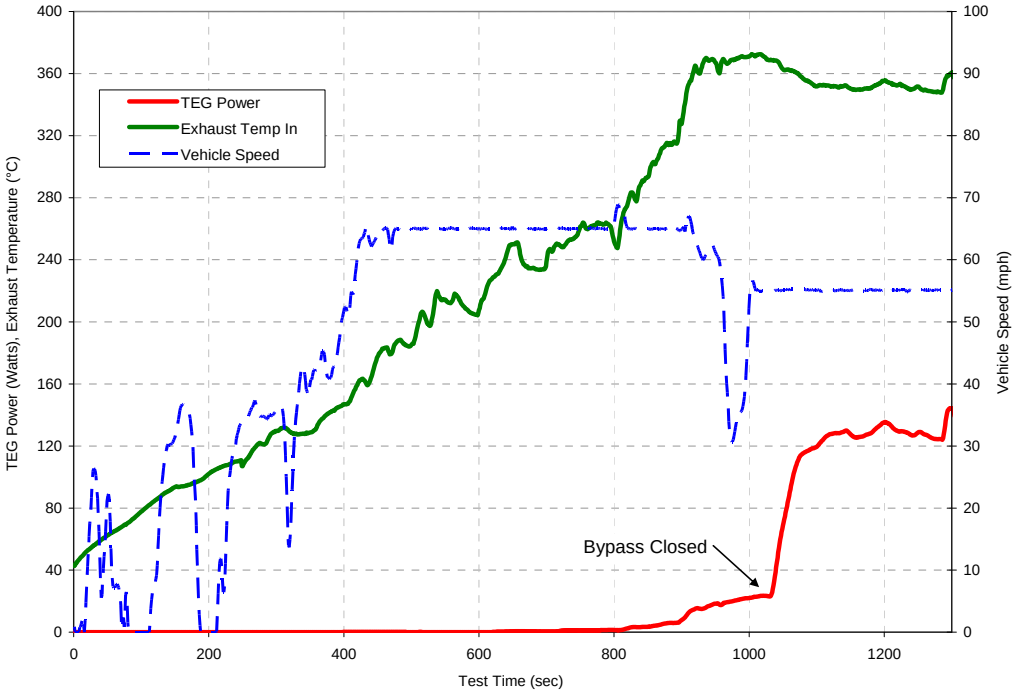

Figure 53: Test data showing cold-start performance of TEG. Bypass valve was closed once vehicle entered 55mph steady cruise portion of test.

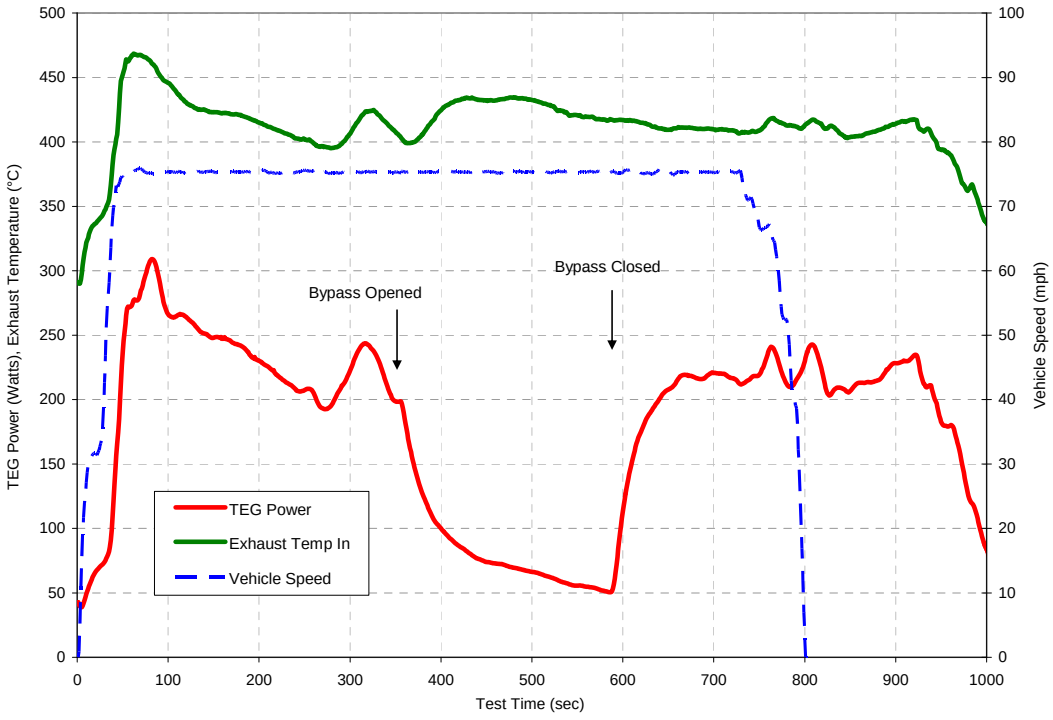

Figure 54: Test data showing typical highway cruise performance of TEG at 75mph. With the exhaust bypass valve closed, the TEG made roughly 225 watts of power.

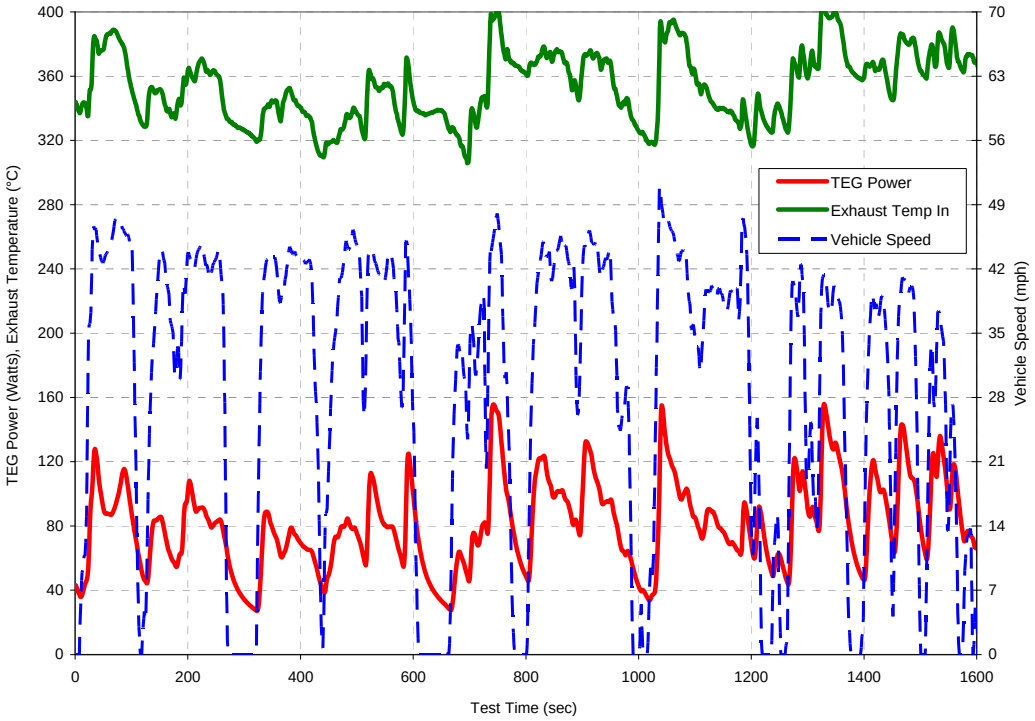

Figure 55: Test data showing typical city driving performance of TEG. With the exhaust bypass valve closed, the TEG made roughly 80 watts of power on average.

4. Products developed

a. Conference Publications

The following publications and presentations were created during the program:

2006

Lon E. Bell, Douglas T. Crane, John W. LaGrandeur, "High Efficiency Waste Energy Recovery System for Vehicle Applications", DEER Conference, August 24 2006

J. W. LaGrandeur, D. T. Crane, B. Mazar, A. Eder, S. Hung, "Exhaust Gas Waste Heat Recovery System Using Segmented High Temperature Materials for Automotive Vehicle Applications", DTEC Conference, August 29, 2006.

D. T. Crane, L. E. Bell, "Maximizing the Performance of a Thermoelectric Power Generator", International Conference on Thermoelectrics (ICT), July 2006.

J. W. LaGrandeur, D.T. Crane, L.E. Bell, "High Efficiency Waste Energy Recovery System for Vehicle Applications", ICT, July 2006.

2007

D. Crane, J. LaGrandeur, L. Bell, "Development of a Scalable 10% Efficient Thermoelectric Generator", DEER Conference, August 15, 2007

2008

J. LaGrandeur, D. Crane, L. Bell, "Development of a 100-Watt High Temperature Thermoelectric Generator", DEER Conference , August 6, 2008

John LaGrandeur, Doug Crane, Lon Bell, " Medium Temperature Range Waste Heat Recovery for Automotive Applications", DTEC Conference, November 2008.

Lon E. Bell, " Addressing the Challenges of Commercializing New Thermoelectric Materials", ICT Conference, August 4, 2008.

D. T. Crane, D. Kossakovski, L. E. Bell, „Modeling the Building Blocks of a 10% Efficient Segmented Thermoelectric Power Generator", ICT Conference, August 4, 2008.

L. Bell, "Accelerating the Commercialization of Promising New Thermoelectric Materials", Material Science and Technology 2008 Conference.

2009

S. Ayres, L. Bell, D. Crane, J. LaGrandeur , "Development of a 500 Watt High Temperature Thermoelectric Generator", DEER Conference, August 5, 2009.

D.T. Crane and J.W. LaGrandeur, "Progress Report on BSST Led, US DOE Automotive Waste Heat Recovery Program", ICT Conference, July 1, 2009.

Lon E. Bell and Douglas T. Crane, "Vehicle Waste Heat Recovery System Design and Characterization", ICT Conference, July 1, 2009.

D.T. Crane and J.W. LaGrandeur, "Automotive Fuel Efficiency Improvement via Exhaust Gas Waste Heat Conversion to Electricity", Thermoelectric Applications Conference, September 30, 2009.

2010

John LaGrandeur, Doug Crane, Lon Bell, "Status of a Cylindrical Waste Heat Power Generator for Vehicles Development Program", DEER Conference, September 29, 2010.

Dr. Lon E. Bell, John LaGrandeur, Dr. Douglas T. Crane, "Progress Report on Vehicular Waste Heat Recovery using a Cylindrical Thermoelectric Generator", IAV Conference, 9 December, 2010.

Lon E. Bell, Douglas Crane, John LaGrandeur, C. Ramesh Koripella, Steven Ayres, "Status of a Thermoelectric Segmented Element Waste Heat Power Generator
for Vehicles, ICT Conference, 31 May, 2010.

Doug Crane, "An introduction to system level steady-state and transient modeling and optimization of high power density thermoelectric generator devices made of segmented thermoelectric elements, ICT Conference, 31 May, 2010.

2011

John LaGrandeur, Doug Crane, "Status of a Cylindrical Waste Heat Power Generator for Vehicles Development Program", DEER Conference, October 5, 2011.

Doug Crane, Ramesh Koripella, Vladimir Jovovic, "Validating Steady-State and Transient Modeling Tools for High Power Density Thermoelectric Generators", ICT/ECT 18 July 2011.

Douglas Crane, John LaGrandeur, Lon E. Bell, "Status of Segmented Element Thermoelectric Generator for Vehicle Waste Heat Recovery", 2011 Thermoelectrics Applications Workshop, January 3, 2011.

John W LaGrandeur, "Thermoelectric Materials and Engines for Automotive and Industrial Waste Heat Conversion to Electricity", M&MT Conference, Pune India, March 8, 2011.

b. Patent applications/awards

BSST has filed 25 invention disclosures with the DOE patent office in Chicago IL and the USPTO. A complete list of the invention disclosures is confidential and may be accessed through Amerigon Inc.

c. Collaborations

Entity	Role and Responsibilities
BMW AG	Vehicle system architecture and FE performance modeling. Economic feasibility analysis and cost/benefit trade study lead.
Ford Motor Company	
Visteon Automotive	Primary heat exchanger design and development (secondary loop architecture). Power conversion and load matching electronics prototype design, build and test.
Faurecia Exhaust Systems	Exhaust system Tier 1 with lead responsibility for TEG integration into BMW and Ford vehicle exhaust systems.
Virginia Polytechnic University	Power conversion and load matching electronics prototype design consulting.
Purdue University	TE materials characterization.
NREL	Engine dynamometer testing (Phase 5) to confirm FE performance using BMW engine.
Caltech and JPL	Characterizing advanced TE materials
OSU	Advanced TE material development

5. Computer modeling summary

A complete description of the Matlab/Simulink model developed and validated within this program can be found within section 3a beginning on page 11. Vehicle models which incorporate the Amerigon TEG model were developed and validated by BMW and Ford and are described in sections 6.c.ii and 6.c.iii respectively.

6. Economic value analysis and commercialization plan

Various combinations of commercially available technologies could reduce fuel consumption in passenger cars, sport-utility vehicles, minivans, and other light-duty vehicles without compromising vehicle performance or safety. *Assessment of Technologies for Improving Light Duty Vehicle Fuel Economy* [14] estimates the potential fuel savings and costs to consumers of available technology combinations for three types of engines: spark-ignition gasoline, compression-ignition diesel, and hybrid. Table 5, reprinted from the referenced report where it appears as Table S.1, shows that a wide variety of technologic approaches are available with many already incorporated in vehicle systems to increase fuel efficiency and to reduce carbon emissions. The table is reprinted below:

This table provides an update to the 2002 National Academy of Sciences CAFÉ standards report cited in our Phase 1 final report and shows the breadth of technology options that are available today. In order for TEG technology to reach the market, it must be on par with respect to the cost benefit of these technologies. At this time, it appears that a system cost of $0.50 to $1.00 per watt produced may be economically viable for the technology in its initial deployment (low volume). The cylindrical architecture appears to be on a path to meet this cost-benefit ratio and activities are underway working towards this goal in a subsequent DOE funded program.

Technologies		Incremental values - A preceding technology must be included								
		4			V6			V8		
Spark Ignition Techs	**Abbr.**	**Low**	**High**	**AVG**	**Low**	**High**	**AVG**	**Low**	**High**	**AVG**
Low Friction Lubricants	LUB	0.5	0.5	0.5	0.5	0.5	0.5	0.5	0.5	0.5
Engine Friction Reduction	EFR	0.5	2.0	1.3	0.5	2.0	1.3	1.0	2.0	1.5
VVT-Coupled Cam Phasing (CCP) SOHC	CCP	1.5	3.0	2.3	1.5	3.5	2.5	2.0	4.0	3.0
Discrete Variable Valve Lift (DVVL) SOHC	DVVL	1.5	3.0	2.3	1.5	3.0	2.3	2.0	3.0	2.5
Cylinder Deactivation SOHC	DEAC	NA	NA	NA	4.0	6.0	5.0	5.0	10.0	7.5
VVT-Intake CAM Phasing (ICP)	ICP	1.0	2.0	1.5	1.0	2.0	1.5	1.5	2.0	1.8
VVT-Dual Cam Phasing (DCP)	DCP	1.5	2.5	2.0	1.5	3.0	2.3	1.5	3.0	2.3
Discrete Variable Valve Lift (DVVL) DOHC	DVVL	1.5	3.0	2.3	1.5	3.5	2.5	2.0	4.0	3.0
Continuous Variable Valve Lift (CVVL)	CVVL	3.5	6.0	4.8	3.5	6.5	5.0	4.0	6.5	5.3
Cylinder Deactivation OHV	DEAC	NA	NA	NA	4.0	6.0	5.0	5.0	10.0	7.5
VVT-Coupled Cam Phasing (CCP) OHV	CCP	1.5	3.0	2.3	1.5	3.5	2.5	2.0	4.0	3.0
Discrete Variable Valve Lift (DVVL) OHV	DVVL	1.5	2.5	2.0	1.5	3.0	2.3	2.0	3.0	2.5
Stoichometric Gasoline Direct Injection	SGDI	1.5	3.0	2.3	1.5	3.0	2.3	1.5	3.0	2.3
Turbocharging and Downsizing	TRBDS	2.0	5.0	3.5	4.0	6.0	5.0	4.0	6.0	5.0
Diesel Techs										
Conversion to Diesel	DSL	15.0	35.0	25.0	15.0	35.0	25.0	NA	NA	NA
Conversion to Advanced Diesel	ADSL	7.0	13.0	10.0	7.0	13.0	10.0	22.0	38.0	30.0
Electrification/Accessory Techs										
Electric Power Steering (EPS)	EPS	1.0	3.0	2.0	1.0	3.0	2.0	1.0	3.0	2.0
Improved Accessories	IACC	0.5	1.5	1.0	0.5	1.5	1.0	0.5	1.5	1.0
Higher Voltage Improved Alternato	HVIA	0.0	0.5	0.3	0.0	0.5	0.3	0.0	0.5	0.3
Transmission Techs										
Continuous Variable Transmission (CVT)	CVT	1.0	7.0	4.0	1.0	7.0	4.0	1.0	7.0	4.0
5-spd Auto Trans. w/Improved Internals		2.0	3.0	2.5	2.0	3.0	2.5	2.0	3.0	2.5
6-spd Auto Trans. w/Improved Internals		1.0	2.0	1.5	1.0	2.0	1.5	1.0	2.0	1.5
7-spd Auto Trans. w/Improved Internals		2.0		2.0	2.0		2.0	2.0		2.0
8-spd Auto Trans. w/Improved Internals		1.0		1.0	1.0		1.0	1.0		1.0
6/7/8-spd Auto Trans. w/Improved	NAUTO	3.0	8.0	5.5	3.0	8.0	5.5	3.0	8.0	5.5
6/7-spd DCT from 4-spd AT	DCT	6.0	9.0	7.5	6.0	9.0	7.5	6.0	9.0	7.5
6/7-spd DCT from 6-spd AT	DCT	3.0	4.0	3.5	3.0	4.0	3.5	3.0	4.0	3.5
Hybrid Techs										
12V BAS Micro-Hybrid	MHEV	2.0	4.0	3.0	2.0	4.0	3.0	2.0	4.0	3.0
Integrated Starter Generator	ISG	29.0	39.0	34.0	29.0	39.0	34.0	29.0	39.0	34.0
Power Split Hybrid	PSHEV	24.0	50.0	37.0	24.0	50.0	37.0	24.0	50.0	37.0
2-Mode Hybrid	2MHEV	25.0	45.0	35.0	25.0	45.0	35.0	25.0	45.0	35.0
Plug-in Hybrid	PHEV	NA	NA	NA	NA	NA	NA	NA	NA	NA
Vehicle Techs										
Mass Reduction - 1%	MR1	0.3		0.3	0.3		0.3	0.3		0.3
Mass Reduction - 2%	MR2	1.4		1.4	1.4		1.4	1.4		1.4
Mass Reduction - 5%	MR5	3.0	3.5	3.3	3.0	3.5	3.3	3.0	3.5	3.3
Mass Reduction - 10%	MR10	6.0	7.0	6.5	6.0	7.0	6.5	6.0	7.0	6.5
Mass Reduction 20%	MR20	11.0	13.0	12.0	11.0	13.0	12.0	11.0	13.0	12.0
Low Rolling Resistance Tires	ROLL	1.0	3.0	2.0	1.0	3.0	2.0	1.0	3.0	2.0
Low Drag Brakes	LDB	1.0		1.0	1.0		1.0	1.0		1.0
Aero Drag Reduction 10%	AERC	1.0	2.0	1.5	1.0	2.0	1.5	1.0	2.0	1.5

Table 5. Assessment of Technologies for Improving Light Duty Vehicle Fuel Economy (numbers shown are percent fuel economy improvement

Over the 5 Phases of the Program, the team worked to evolve a TEG system architecture that provided a balance of cost and performance. In the initial Phase of the Program, Amerigon proposed a secondary loop system that provided several benefits:

- Reduced TEG volume, which helped address hermetic packaging and recycling concerns;
- A means of buffering the dynamic nature of exhaust gas enthalpy as a function of typical driving conditions in the city;
- Providing a closed loop hot fluid to reduce TEG heat exchanger fouling.

Although the proposed architecture provided significant technologic benefit, the requirement for the secondary loop pump and working fluid (He/Xe gas mixture) drove the system cost to an unacceptable high level.

In the third Phase, an inline TEG system was proposed comprising alternating flat hot (exhaust gas) and cold-liquid heat exchangers between which were "sandwiched" thermoelectric engines. This architecture reduced the overall system cost but it was found that the manufacture of the flat plates required extraordinary process control (flatness, parallelism, smoothness) that again drove manufacturing costs higher than desired.

As a result, a cylindrical TEG architecture was developed in Phase 4, which not only had the benefit of simplifying the TEG construction, but also provided a volume reduction for the system by internalizing the exhaust gas bypass within the TEG outer shell. This design was built and tested in vehicles in Phase 5 and confirms the Amerigon stack design engine and cylindrical architecture as a go-forward design concept.

In parallel with the evolution of the TEG and vehicle system architectures, TE material systems were evaluated for economic viability. It was concluded that Tellurium based materials would be cost prohibitive for the application, and as a result a decision to focus on Cobalt Antimonides (Skutterudites or "SKD") was made for future work.

At the time of this publication the maturity of SKD materials and ohmic contact systems are at an appropriate maturity level technically to support their further development. These materials, nor any other thermoelectric power generation materials that operate with a hot side temperature in the range of 500C, are available commercially. While they can be made using industry standard powder metallurgy processes, the necessary manufacturing infrastructures are not in place to support commercialization of automotive TE heat to power. This work is a necessary precursor to implementation of the technology and must be addressed. In order for the TEG cost to meet the market requirements, it is estimated that the TE elements would need to be produced and metalized at a fraction of today's cost, or roughly several cents/die. The industrialization of SKD material is a key component of a follow-on DOE funded TEG program at Amerigon.

7. Graphical Materials List

8. List of Acronyms and Abbreviations

Nomenclature

A	*area (m^2)*
Cp	*specific heat (J/kgK)*
h	*heat transfer coefficient (W/m^2K)*
I	*electrical current (A)*
K	*thermal conductance (W/K)*
m	*mass (kg)*
Q	*heat flow (W)*
R	*electrical resistance (ohm)*
t	*time (s)*
T	*temperature (K)*
u	*reduced current density*
U	*overall heat transfer coefficient (W/m^2K)*

Subscripts

1, 2, 3	*location on the TEG/control volume in the direction of flow*
c	*cold*
cen	*center of*
ch	*channel*
conn	*connector*
cross	*cross sectional*
f	*fluid*
h	*hot*
int	*interfacial*
load	*load*
nat	*natural convection*
s	*surface*
TE	*thermoelectric*

Greek letters

α	*Seebeck coefficient*

Δ, d change in

∞ ambient

9. Appendices (f Necessary)

10. Supplemental Guidelines

NETL cannot release technical reports that include Limited Rights Data (such as trade secret, proprietary or business sensitive information). Thus, if such information is important to technical reporting requirements, it **must** be submitted in a separate appendix to the electronic technical report. This appendix **MUST NOT** be submitted in an electronic format but rather submitted separately in **TWO GOOD QUALITY PAPER COPIES** when the electronic version of the sanitized technical report is submitted. The appendix must not be referenced in or incorporated into the sanitized technical report deliverable under the award. The appendix must be appropriately marked and identified. Only the legend provided in the Rights in Data clause in this award may be placed on the appendix. The appendix must be sent to:

NETL AAD DOCUMENT CONTROL

BUILDING 921

U.S. DEPARTMENT OF ENERGY

NATIONAL ENERGY TECHNOLOGY LABORATORY

P.O. BOX 10940

PITTSBURGH, PA 15236-0940

Further, if this award authorizes the recipient under the provisions of The Energy Policy Act of 1992 (EPAct) to request protection from public disclosure for a limited period of time of certain information developed under this award, the main body of electronic technical reports **MUST NOT** contain such Protected Information. **TWO GOOD QUALITY PAPER COPIES** of such information must be submitted to the address above in a separate appendix to the sanitized electronic version of the technical report. The appendix must not be referenced in or incorporated into, the sanitized technical report deliverable under the award. In accordance with the clause titled "Rights in Data-Programs Covered Under Special Data Statutes," the appendix must be appropriately marked, including the date when the period of protection for the data ends. The EPAct appendix must be appropriately identified with the recipient's name, award number, type of report (final or topical), and reporting period start and end dates.

Company Names and Logos -- Except as indicated above, company names, logos, or similar material should not be incorporated into reports.

Copyrighted Material -- Copyrighted material should not be submitted as part of a report unless written authorization to use such material is received from the copyright

owner and is submitted to DOE with the report.

Measurement Units -- All reports to be delivered under this instrument must use the SI Metric System of Units as the primary units of measure. When reporting units in all reports, primary SI units must be followed by their U.S. Customary Equivalents in parentheses ( ). **The Recipient must insert the text of this clause, including this paragraph, in all subcontracts under this award.** Note: SI is an abbreviation for "Le Systeme International d'Unites."

11. References

1. *Contract number DE-FC26-04NT42279*.
2. *Energy Efficiency Renewable Energy (EERE) High Efficiency Clean Combustion and Waste Heat Recovery for Internal Combustion Engines; Ref. DE-PS26-04NT42099-00, CFDA Number: 81.087 Renewable Energy Research and Development*.
3. Crane, D.T. and L.E. Bell. *Progress Towards Maximizing the Performance of a Thermoelectric Power Generator*. in *25th International Conference on Thermoelectrics*. 2006. Vienna, Austria: IEEE.
4. Crane, D.T., D. Kossakovski, and L.E. Bell, *Modeling the Building Blocks of a 10% Efficient Segmented Thermoelectric Power Generator.* Journal of Electronic Materials, 2009. **38**(7): p. 1382.
5. Snyder, G.J., *Thermoelectric Power Generation: Efficiency and Compatibility*, in *Thermoelectrics Handbook Macro To Nano*, D.M. Rowe, Editor 2006, CRC Press: Boca Raton, FL. p. 9-1 - 9-26.
6. Nolas, G.S., J. Sharp, and H.J. Goldsmid, *Thermoelectrics - Basic Principles and New Materials Developments*2001, Berlin Heidelberg: Springer-Verlag.
7. Rohsenow, W.M., J.P. Hartnett, and Y.I. Cho, eds. *Handbook of Heat Transfer*. 3rd ed. 1998, McGraw-Hill: New York, NY.
8. Crane, D.T. *Modeling High-Power Density Thermoelectric Assemblies Which Use Thermal Isolation*. in *23rd International Conference on Thermoelectrics*. 2004. Adelaide, AU.
9. Faulkner, F., *COLDPLT.exe*, 1999, Thermodynamics Analysis Service: Hobe Sound, FL.
10. Angrist, S.W., *Direct Energy Conversion*. 4th ed1982, Boston: Allyn and Bacon, Inc.
11. Crane, D.T., J.W. LaGrandeur, and L.E. Bell. *Progress Report on BSST Led, US DOE Automotive Waste Heat Recovery Program*. in *International Conference on Thermoelectrics*. 2009. Freiburg, Germany.
12. Crane, D.T. and L.E. Bell, *Design to Maximize Performance of a Thermoelectric Power Generator With a Dynamic Thermal Power Source.* Journal of Energy Resources Technology, 2009. **131**(March 2009): p. 012401-1 - 012401-8.
13. Crane, D.T., *An Introduction to System Level Steady-State and Transient Modeling and Optimization of High Power Density Thermoelectric Generator Devices Made of Segmented Thermoelectric Elements.* Journal of Electronic Materials, 2011. **40**(5): p. 561-569.
14. *Assessment of Fuel Economy Technologies for Light-Duty Vehicles*, 2011, National Research Council of the National Academies.